# MODELING CLEAR CELL SARCOMAGENESIS

by

Krystal M. Straessler

A dissertation submitted to the faculty of
The University of Utah
in partial fulfillment of the requirements for the degree of

Doctor of Philosophy

Department of Human Genetics

The University of Utah

December 2014

**The University of Utah Graduate School**

# STATEMENT OF DISSERTATION APPROVAL

The dissertation of **Krystal M. Straessler**

has been approved by the following supervisory committee members:

| | | |
|---|---|---|
| **Mario R. Capecchi** | , Chair | **3/10/2014** Date Approved |
| **Dean Y. Li** | , Member | **3/10/2014** Date Approved |
| **Anthea Letsou** | , Member | **3/10/2014** Date Approved |
| **Mark M. Metzstein** | , Member | **3/10/2014** Date Approved |
| **Stephen L. Lessnick** | , Member | **3/10/2014** Date Approved |

**Lynn B. Jorde** , Chair/Dean of

the Department/College/School of **Human Genetics**

and by David B. Kieda, Dean of The Graduate School.

# ABSTRACT

Clear cell sarcoma (CCS) is a rare but devastating malignancy with a proclivity for young adults, disturbingly low survivability, and recalcitrance to therapies. Due to the low incidence, it remains difficult to investigate the mechanism behind CCS. By generating an accurate model system that recapitulates human tumor dynamics, there is hope that the molecular mechanisms required for tumor initiation and maintenance can be identified and lead to more directed, successful therapeutic options.

CCS achieves its clinically aggressive phenotype from the expression of a single oncogene, *EWS-ATF1*. This aberrant transcription factor drives clear cell tumorigenesis seemingly from deregulation of ATF1 signaling alone. The impact of CCS on the general population far exceeds its somewhat low prevalence due to its similarities to another aggressive tumor, malignant melanoma. CCS and melanoma resemble one another in morphology, immunohistochemistry, and overall clinical behavior.

A targeted mouse model was developed that conditionally expresses human *EWS-ATF1* cDNA under control of a ubiquitous promoter. Expression of *EWS-ATF1* leads to 100% tumor formation with extraordinary speed, when induced in a permissive cell type. These tumors resembled human CCS in morphology, immunohistochemistry, and gene expression.

Mesenchymal stem cells (MSC) were identified as the main source of traditional

CCS. The *EWS-ATF1* transcript proved capable of driving expression of melanocytic markers within MSCs, inducing the melanoma expression profile. When tumorigenesis was initiated in more differentiated cell types, the tumors did not resemble the traditional CCS phenotype. Therefore, differentiation state of the cell of origin proved critical in shaping tumor phenotype.

It is thought that melanoma and CCS share a cell of origin. To test this, *EWS-ATF1* was expressed within the melanocytic lineage, and gave rise to tumors 1 year post induction, with a low prevalence. These tumors mimic a rare dermal variant of CCS. Due to the long latency between *EWS-ATF1* initiation and tumor formation, it is probable that *EWS-ATF1* alone is not sufficient to drive dermal CCS.

This work has identified *EWS-ATF1* as the driving oncogene behind both clear cell tumor formation and the melanocytic phenotype. This model can be used to investigate novel therapeutics for a more targeted treatment of CCS.

.

This dissertation is dedicated to my husband, Dr. Nicholas Straessler.

TABLE OF CONTENTS

LIST OF TABLES

LIST OF FIGURES

# ACKNOWLEDGEMENTS

I would like to express my most sincere gratitude to my advisor, Professor Mario Capecchi, for giving me the opportunity to earn my PhD in his laboratory. It was an honor and privilege to work under his guidance. Mario allowed me the freedom to explore scientific questions on my own, while still always making himself available for advice and guidance. He instilled in me an enduring love and appreciation of scientific research. I will never forget Mario's advice that "to truly be innovative, you have to work at the edge of science and science fiction." I am forever indebted to Mario for his personal and professional support; I am a better scientist and person for having worked with him.

I would also like to thank my dissertation committee members: Professors Anthea Letsou, Dean Li, Stephen Lessnick, and Mark Metzstein for their help and guidance. They always took the time to listen to my questions and provide their valuable input. I need to extend special thanks to Anthea who not only helped me through my PhD, but also the HHMI Med-to-Grad program. She is a great example of how women in science cannot only be successful, but can excel.

I would like to thank all members of the Capecchi laboratory who have become friends with my family and me. Although challenging at times, I also had a tremendous amount of fun working in this lab and being surrounded by a great group of people with such diverse backgrounds and scientific interests. Dr. Kevin Jones and I collaborated

often on the Sarcoma projects, and I appreciate the guidance and support that he gave to me as my Med-to-Grad advisor and fellow researcher. We have a great support team in Mario's lab, and all of our work would be impossible without the tissue culture and animal care team, as well as our laboratory technicians.

My mother and father have always supported me in everything I have chosen in my life, no matter how difficult it has seemed, and for this I am eternally grateful. They have made it possible for me to follow my dreams, teaching me to never let anything stop me from achieving the goals I set for myself. My mother in particular is a strong, intelligent woman who taught me that if I work hard, I can have a family and a career. She has guided me through with her extraordinary wisdom. My father is an exceptionally hard worker, and I am forever thankful to him for his perpetual support. My curiosity comes from my father who has always taught me to ask big questions to get big answers.

Finally, I want to thank my three children and husband for always supporting me. Connor has been my main motivating force during my entire college and postgraduate careers. Sadie and Easton have brought joy to my life and helped keep me balanced between the rigors of graduate research and home-life. I would not have been successful without the unconditional encouragement of my husband Nick. Not only did he help me at home but was always available as my practice audience, proofreader, and overall biggest advocate.

In the words of Marie Curie:

"I have frequently been questioned, especially by women, of how I could reconcile family life with a scientific career. Well, it has not been easy."

Thank you to Mario, Nick, and all those who made it possible!

# CHAPTER 1

# INTRODUCTION

## Translocation-Based Sarcomas

Sarcomas are a relatively rare group of tumors that arise in mesenchymal tissues such as bone, muscle, and fat. Sarcomas comprise less than 5% of adult cancers but more than 10% of pediatric tumors (Osuna and de Alava, 2009). The etiology of translocation-associated sarcomas in particular is unknown and their high incidence in the pediatric population suggests that relatively few genetic mutations are necessary to complete transformation. Roughly a third of sarcomas fit into this category. The translocations are most often a reciprocal exchange between two heterologous chromosomes. The translocation breakpoint typically occurs within an intron on both chromosomes, which fuses the 5' coding region of one gene to the 3' coding region of another gene on the second translocated chromosome. Each resulting fusion protein associates with a distinct tumor type, leading to the general conclusion that it must contribute both to the oncogenesis and tumor phenotype.

Translocation-based sarcomas generally lack any other signs of genomic instability. Generally, translocation-based tumors arise in young adult populations, but their occurrence can range from pediatric to geriatric populations as well. The presence of a fusion protein is rapidly becoming pivotal to diagnosing specific sarcomas, leading

pathologists to reconsider whether diagnosis should be based primarily on a tumor's genetic makeup or on its morphology. One translocation-based tumor is clear cell sarcoma. Investigation of clear cell sarcoma suggests that a single fusion protein can be sufficient to induce tumor formation and shape tumor phenotype. Clear cell sarcoma provides a strong example of how understanding the genetic anomaly underlying a tumor can reshape the classification criteria of a malignancy.

## Discovery and Characterization of Clear Cell Sarcoma

Clear cell is a rare but aggressive translocation-based sarcoma, initially characterized by Franz M. Enzinger in 1965. He described clear cell as a malignant tumor with relatively benign features that often arose near tendons and aponeuroses. The most striking observations made by Enzinger were the relatively young patients and the aggressive nature of the tumor. The average age of patients in the initial cohort of 21 cases was just 24 (Enzinger, 1965). In more recent, larger, studies of clear cell sarcoma, the average age at diagnosis was 24-30 years of age (Chung and Enzinger, 1983). Enzinger noted that despite the relatively small size of the tumors (average being 4 cm) and apparently benign features, including low mitotic index, these tumors had high rates of local recurrence and, eventually, distant metastasis. Histologically, they varied in morphology but all contained compact nests of cells with cytoplasm that stained lightly eosinophilic and had large, basophilic, prominent nucleoli (Figure 1.1A). It is surprising that this first description of clear cell sarcoma has endured, and the prognosis remains consistent, even with modern fluctuations in the diagnostic criteria (Enzinger, 1965).

Ten years after Enzinger first coined the term clear cell sarcoma, Bearman and colleagues employed electron microscopy to obtain an enhanced view of the cellular

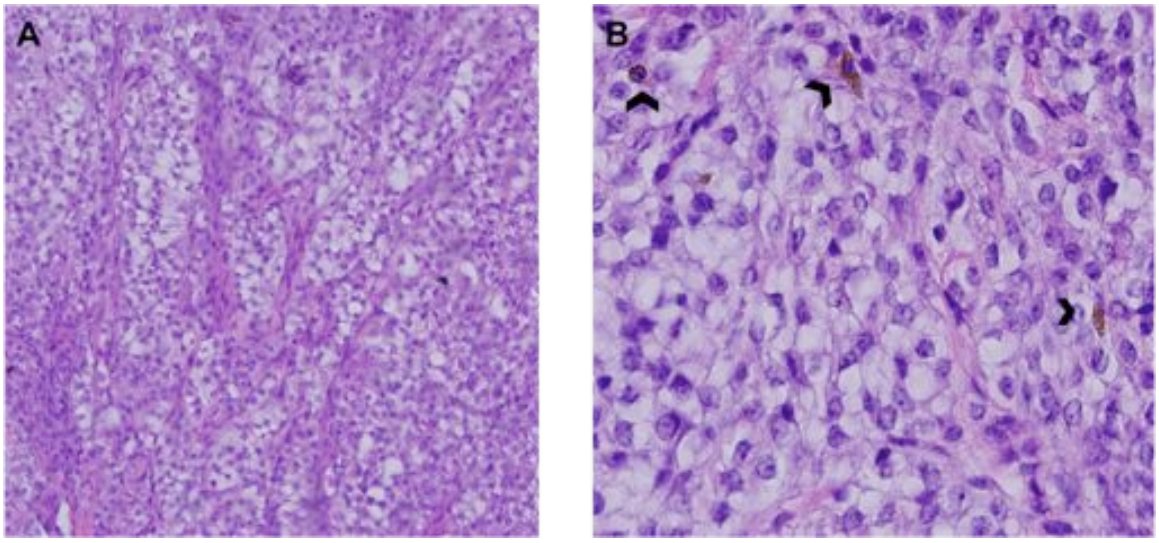


Figure 1.1 Pathology of clear cell sarcoma. A murine clear cell sarcoma A) with fibrous tissue dividing the tumor into defined nests and groups of pale staining tumor cells; B) prominent nucleoli and cytoplasmic melanin pigment (arrowhead).

ultrastructure of the tumors. They were the first to observe that the tumors, though not always visually pigmented, contained cytoplasmic melanin and structures resembling melanosomes (Bearman et al., 1975). This was surprising considering the deep location of the tumors, far from the location of melanocytes. Over the next few years, many case reports noted similar features within the tumors, and the term "malignant melanoma of the soft parts" became synonymous with clear cell sarcoma. The presence of melanin pigment (Figure 1.1B), melanosomes, and various levels of melanocyte differentiation, combined with the counterintuitive location in the deep mesenchyme, have caused dission within the field about the potential cell of origin for these tumors.

With an increase of researchers studying melanoma, a pigmented malignancy arising from melanocytes, immunohistochemical tools were developed to identify melanocyte-specific antigens. Similar to melanoma, clear cell sarcoma was found to express markers of pigmentation as well as other melanocyte-specific antigens. The expression of one marker, melanocytic microphthalmia transcription factor (mMITF), was identified in both melanoma and clear cell sarcoma. Since mMITF is not typically seen in previously described sarcomas, this marker provided a clear diagnostic tool for distinguishing clear cell from other sarcomas. mMITF is a master transcription factor in induction and maintenance of the pigmentation pathway. Clear cell sarcoma and melanoma have also been shown to share expression of other factors in common that are downstream of mMITF, including tyrosinase (TYR) and the tyrosinase-related family of proteins (TRYP1, TRYP2, and DCT1), depending on the degree of melanocyte differentiation found within the tumor (Segal et al., 2003).

Still more parallels between clear cell sarcoma and melanoma have been found as

research progressed. In addition to a common histology and immunohistochemistry, melanoma and clear cell sarcoma share nearly identical gene expression profiles.

Using microarray data to compare clear cell sarcoma to melanoma and various other soft-tissue sarcomas, Segal et al. (2003) demonstrated that clear cell sarcoma not only looks and behaves like melanoma, but Segal et al. demonstrated a hierarchical cluster analysis of 12500 genes classified clear cell as a melanoma subtype. Clear cell sarcoma classifying as Melanoma corroborated the hypothesis that the tumors have a common cell of origin, and further illustrated the challenges in differentiating between the two. As targeted therapeutics advance, failing to accurately diagnose the tumors will become increasingly detrimental to patient outcomes.

In 1990, a recurrent chromosomal aberration in three separate clear cell sarcomas was identified (Bridge et al., 1990). During the same period of time, fluorescence *in situ* hybridization (FISH) techniques became feasible for routine genomic analysis, and identification of possible chromosomal aberrations (Figure 1.2). Using FISH probes to detect translocations within the Ewing's gene (*EWSR1)*, the abnormality was identified as a translocation occurring between the *EWSR1* gene on chromosome 22 and an unknown partner on chromosome 12. Further research demonstrated that this translocation occurred in the vast majority of clear cell sarcomas, but was not present in malignant melanoma samples. It was later determined that the translocation resulted in a unique fusion of the 5' coding region of the *EWSR1* and the 3' coding region of the activating transcription factor 1 (*ATF1*) gene. This translocation is such a recurrent feature of clear cell sarcoma that it immediately became used as the major diagnostic criterion distinguishing clear cell sarcoma from melanoma.

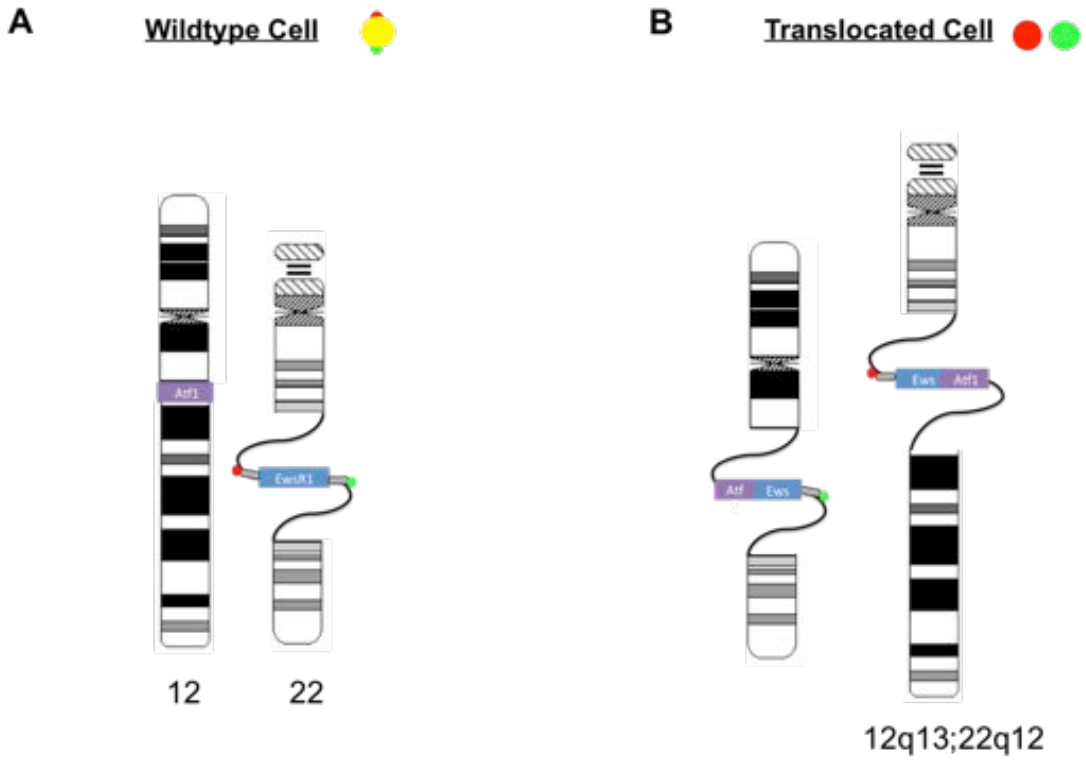


Figure 1.2. EWSR1 fluorescent *in situ* hybridization diagnostic. A) Wildtype chromosomes 12 and 22. Fluorescent probes bind on either side of the EWSR1 gene. When in close proximity, they emit a yellow light. B) In an EWS translocation, the probes are separated onto two nonhomologous chromosomes and each chromosome emits a flourophor red and green, respectively.

For many years, the technology to screen for evidence of the *EWS-ATF1* translocation was not readily available to pathology labs. Although it was known that presence of the fusion could differentiate between the two neoplasms, it was still simpler and more cost effective to differentiate between the two largely based on the location of the tumor. Melanoma was considered to be strictly a cutaneous lesion, while primary tumors found in the deeper extremities attached to the soft-tissue were diagnosed as clear cell sarcoma.

As reverse transcriptase polymerase chain reaction (RT-PCR) protocols provided efficient identification of the fusion gene transcript from a tumor sample, it enabled the reanalysis of old tissue samples embedded in paraffin. Of course, deep, metastatic melanomas from spontaneously regressed primary tumors were a frequent confounder. Many tumors previously diagnosed as metastatic melanoma without a primary lesion were reanalyzed using FISH and/or RT-PCR for evidence of the characteristic translocation and fusion transcript of clear cell sarcoma, respectively. Further, cohorts of malignant melanoma of the gastrointestinal system were found to carry the *EWS-ATF1* translocation characteristic of clear cell sarcoma (Covinsky et al., 2005). A cohort of dermal melanomas gave a similar result (Falconieri et al., 2012; Hantschke et al., 2010). It became obvious that a distinction between clear cell sarcoma and melanoma made on location alone was inadequate. Using the translocation as a diagnostic tool, it is evident that clear cell sarcomas are not relegated to the deep mesenchymal tissues, but can be found in anatomical regions previously thought to be reserved for melanomas. Despite this recognition in the literature, historical practice is difficult to change and location remains the initial step in diagnosing clear cell sarcoma. It remains widely accepted that

clear cell sarcoma is primarily found in the deep mesenchymal tissue; unfortunately, cutaneous lesions are rarely screened for the characteristic translocation.

With the benefit of modern instrumentation and research techniques, more is now known about clear cell sarcoma than when Enzinger first identified these rare tumors. Nonetheless, his 50-year-old description of clear cell sarcoma as a highly aggressive tumor with a predilection for young adults and a generally poor prognosis in spite of its relatively benign appearance, remains accurate.

## Translocations Found in Clear Cell Sarcoma

### EWS-ATF1

The translocation between chromosomes 12 and 22 is one key defining characteristic of clear cell sarcoma. Approximately 90% of clear cell sarcoma tumors harbor the t(12;22)(q13;q12) translocation, resulting in the expression of the EWS-ATF1 fusion protein; the remaining 10% has another translocation partner (t(2;22)(q36;q12)), resulting in the EWS-CREB1 fusion protein (Weiss and Goldblum, 2008). The *EWSR1* gene involved in both translocations was first discovered based on its role in another translocation-based tumor, Ewing sarcoma, where it forms an EWS-FLI1 fusion protein resulting from a t(11;22)(q24;q12) (Delattre et al., 1992). *EWSR1* is a common fusion partner in translocation driven tumors, including Ewing sarcoma, desmoplastic small round cell tumor (Gerald and Haber, 2005), extraskeletal myxoid chondrosarcoma (Brody et al., 1997), and mesothelioma (Panagopoulos et al., 2013). In clear cell sarcoma, EWS-ATF1 is believed to function as an aberrant transcription factor that promotes tumor development through misregulation of ATF1 target genes.

EWSR1 Native Function

The EWSR1 protein is a member of the TET family of RNA binding proteins. The native EWSR1 is known to associate with RNA polymerase transcription factor IID (TFIID) and CREB-binding protein (CBP) in transcription activation (Araya et al., 2003, Bertolotti et al., 1998). The amino terminal domain of the protein contains several serine-tyrosine glycine glutamine-rich repeat sequences that are hypothesized to function as an activation domain (Rossow and Janknecht, 2001, Sankar and Lessnick, 2011). It is this portion of the protein that is conserved in both EWS-ATF1 and EWS-CREB1 clear cell sarcoma fusion proteins, and the other tumors mentioned.

ATF1 Native Function

The most common fusion partner for *EWSR1* in clear cell sarcoma is *ATF1*. ATF1 is a member of the cyclic AMP response element binding protein (CREB) family of transcription factors. *ATF1*, unlike *EWSR1*, is more exclusive to clear cell sarcoma and thought to provide the specificity of the tumor phenotype. The CREB family was one of the first proteins shown to respond to both stress and mitogen signals through phosphorylation-mediated regulation (Mayr and Montminy, 2001). ATF1 contains a DNA binding domain that recognizes cyclic AMP response element (CRE) binding sites in the genome. ATF1 transcriptional stimulation by cAMP occurs through these CRE-containing promoters. ATF1 can also mediate gene expression due to Ca2+ in flux. Activation of ATF1 is mediated through phosphorylation on the Ser63 by phospho kinase A (PKA) and CaM kinases I and II (Liu et al., 1993). Disruption of such a wide range of pathways can explain the large transcriptional misregulation seen in clear cell sarcomas.

ATF1 may also have a more specific role in tumorigenesis through regulation of transcription of the known oncogenes c-jun and c-fos (Gupta and Prywes, 2002; Wang and Prywes, 2000). ATF1 is overexpressed in lymphomas (Hsueh and Lai, 1995), breast cancer (Jones et al., 2012), and metastatic melanoma (Jean et al., 2000). Its role in melanoma is remarkable given the similar characteristics between clear cell sarcoma and melanoma. Overexpression of ATF1 has been shown to increase the survival of melanoma cell lines (Jean et al., 1998), and ATF1 is found to be overexpressed exclusively in metastatic melanoma but not primary melanoma lesions. Expression of an anti-ATF1 antibody within these cell lines as well as in melanoma models has shown to decrease the tumorigenic and metastatic potential of the cells, leading to higher rates of apoptosis (Jean et al., 2000). All fusion protein subtypes of EWS-ATF1 lack the PKA-regulated domain of ATF1, and no longer respond to external signaling (Li and Lee, 1998). A constitutively active EWS-ATF1 transgenic protein strongly misregulates ATF1 target genes (Brown et al., 1995), including mMITF (Davis et al., 2006), when the endogenous PKA domain is swapped for the activation domain of EWS.

*EWS-ATF1* translocations can occur as a result of several different genomic breakpoints in the *EWSR1* and *ATF1* coding regions. Oncogenic translocations typically have breakpoints within intronic regions, and result in transcribed and translated fusion proteins. The *EWSR1* portion of the fusion always includes a minimum of the first seven exons, while only the last exon of *ATF1* is required to generate clear cell sarcoma. Despite these minimal requirements, there are several subtypes of the *EWS-ATF1* fusion gene that include different combinations of exons. The most common subtype is fusion type 1, where the first eight exons of *EWSR1* are fused to the last three exons of the *ATF1*

gene (Figure 1.3). The second most common, subtype 2, includes *EWSR1* exons (1-8) and *ATF1* exons (3-6). To date, four in-frame translocations have been found within tumors confirmed to be clear cell sarcoma (Wang et al., 2009).

EWS-CREB1

A second translocation that gives rise to clear cell sarcoma consists of the same *EWSR1* gene fused to *CREB1*, an *ATF1* family member. CREB1 and ATF1 share homology within highly conserved domains, especially the KID, bZIP, and DNA binding domains (Figure 1.4). When comparing the two different fusions, the *EWSR1* gene is fused to at least the final exon of either *CREB1* or *ATF1*, the exon that encodes the DNA binding domain. *EWS-CREB1* is enriched in clear cell sarcoma arising in the gastrointestinal tract (Antonescu et al., 2006).

Other EWS-ATF1 and EWS-CREB1 Tumors

Notably, due to the ease of FISH screening in tumors containing rearrangements in the *EWSR1* gene, it has become evident that morphologically defined clear cell sarcoma is not the only lesion that contains the *EWS-ATF1* fusion gene. This demonstrates that, although clear cell sarcoma can be diagnosed using *EWS-ATF1*, it remains important to include the standard histological and immunohistochemical analysis to correctly identify clear cell sarcoma. Other *EWS-ATF1* and *EWS-CREB1* expressing tumors are briefly described below. Angiomatoid fibrous histiocytoma (AFH) is a relatively benign mesenchymal neoplasm most commonly occurring in the deep dermis and subcutaneous layers of the extremities, but it can also be found in the trunk, head,

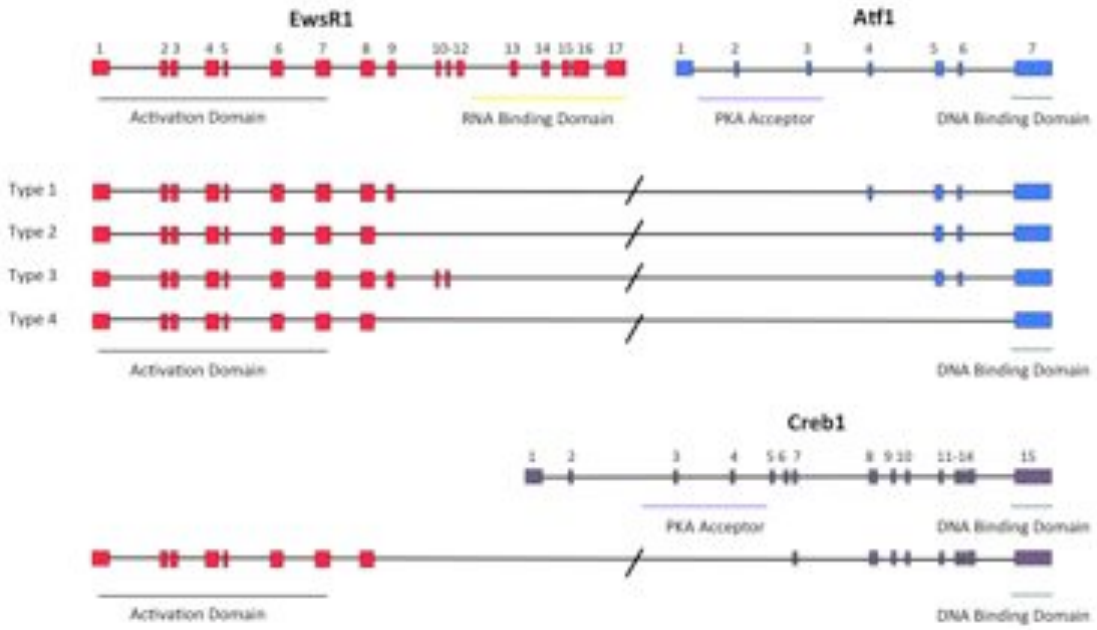


Figure 1.3. *EWS-ATF1* and *EWS-CREB1* genomic variants. *EWSR1* exons (red), *ATF1* exons (blue), and *CREB1* exons (purple). *EWS-ATF1* fusion transcript variants type (1-4) and *EWS-CREB1* all include the activation domain of EWS (black) fused to the DNA binding domain (green) of the ATF/CREB family.

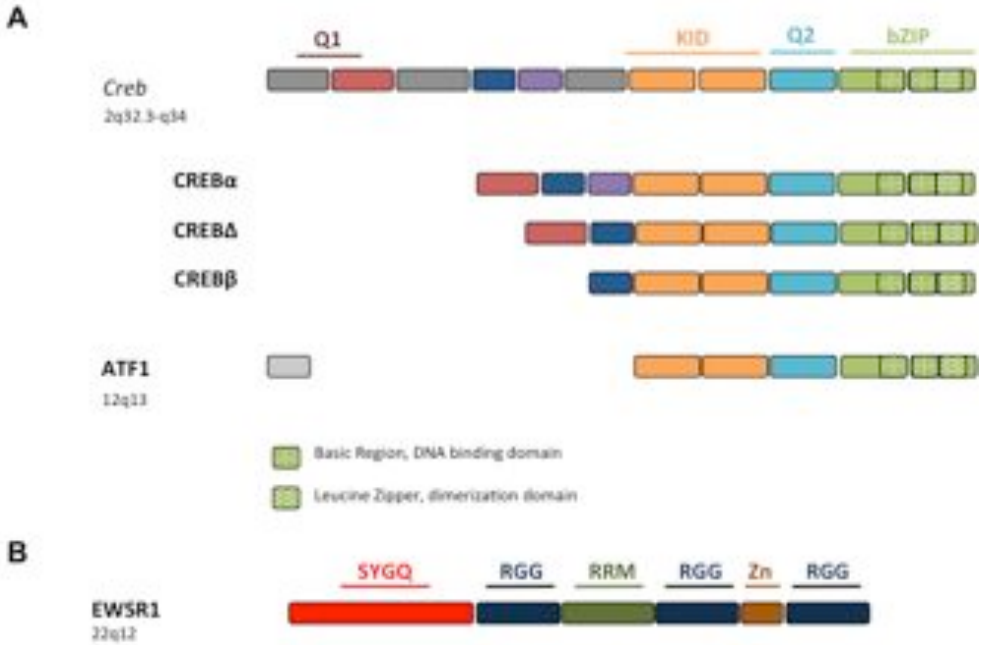


Figure 1.4 EWS, ATF1, CREB protein domains. A) *Creb* genomic region with all protein domains with significant CREB splice variants CREBα, CREBβ, and CREBΔ with shared domains in the same color. Native CREB/ATF1 family members and their shared protein domains in the same color. B) Native EWSR1 protein domains.

and neck regions among other areas (Thway and Fisher, 2012). Similar to clear cell sarcoma, AFH is prevalent in children and young adults but is not restricted to these age groups. AFH is characterized histologically by its distinct nodules of histiocytoid spindle cells surrounded by fibrous psuedocapsules and psuedoangiomatoid spaces (Kao et al., 2014). Originally, AFH was thought to be a more benign variant of malignant fibrous histiocytoma, a formerly popular name for pleomorphic soft-tissue sarcomas that arise primarily in older populations. Recent studies have narrowed the diagnosis and consider AFH a distinct entity. This more benign tumor associates with three different translocations. Both *EWS-ATF1* and *EWS-CREB1* transcripts can be found in AFH samples using RT-PCR, though *EWS-CREB1* is the dominant fusion product. A third translocation t(12;16)(q13;q11) resulting in a *FUS-ATF1* transcript (Chen et al., 2011) has been identified in others. A new entity called primary pulmonary AFH has also recently been identified. Several cases of the endobronchial pulmonary AFH showed rearrangements of *EWS-ATF1* and *EWS-CREB1* (Thway et al., 2012).

Hyalinizing clear cell carcinoma (HCCC) is one of many salivary gland tumors that have recently been identified as translocation-based. Similar to atypical clear cell sarcoma and AFH, HCCCs were identified as harboring an *EWS* translocation by use of the *EWS* FISH probe. Large groups of tumors were screened for *EWS-ATF1* by RT-PCR, and it was found in 100% of typical HCCC tumors. The majority of HCCC tumors have clear glycogen-rich cells surrounded by significant hyalinization. The tumors, which show a slightly higher prevalence in females, arise in the salivary gland and are known to recur and have local metastases and invasions surrounding bone and perineural regions (Weinreb, 2013). HCCC is not a deadly tumor; distant metastasis is extremely rare. So,

although it mimics clear cell sarcoma in its histology and slow growth phenotype, HCCC tumors arise in a distinct cell type and are not as aggressive, leading to a better overall outcome for patients (Thway and Fisher, 2012).

While AFH and HCCC both express the fusion proteins that characterize clear cell sarcoma, the prognosis of patients with AFH and HCCC is not as dire. Furthermore, unlike clear cell sarcoma, AFH and HCCC seem to be benign or restricted to specific tissue types. If indeed transformation requires *EWS-ATF1* expression in all three tumor types, then it is reasonable to hypothesize that the difference between these three neoplasms lies in the cell of origin. If translocations between *EWSR1* and *ATF* family members are this strongly transformative, it will be interesting to discover how many more tumor types carry similar translocation subtypes. In the end, it appears that pathology is not solely determined by fusion protein expression and may ultimately be limited by the inherent capabilities of the cell of origin.

## Cell of Origin of Clear Cell Sarcoma

Sarcomas are notorious for having histopathology that does not reflect the cell of origin. Liposarcomas can arise in regions of the body that do not have adipose tissue while chondrosarcomas can arise in the absence of chondrocytes (Weiss and Goldblum, 2008). Identifying a tumor cell of origin facilitates diagnosis at an early stage and improves patient outcomes. In the clinic, patient treatment plans are prepared based on assumptions made regarding the hypothetical cell of origin. If the cell types responsible for the tumor are identified, targeted and effective treatments can be devised.

The debate over clear cell sarcoma's cell of origin is especially contentious

because of the tumors' deep mesenchymal location despite its melanocytic appearance. The discovery of melanosomes within the tumors led to the initial hypothesis that clear cell sarcoma had a neural crest origin. Tumors expression of s100b, a marker of the neural crest, strength the argument for their neural crest origin (Chung and Enzinger, 1983). Other proposed origins for clear cell sarcoma are; 1) migrating melanocytes that have grown malignant, or 2) mesenchymal stem cells that have differentiated into a melanocyte-mimicking tumor. While these alternatives have two very different cell types, at their foundation, both share potentially overlapping origins in the neural crest.

Neural Crest

Neural crest forms at the dorsal tip of the neural epithelium and gives rise to many different cell types. The neural crest cells of the trunk migrate dorsally and give rise to melanocytes. Others migrate ventrally to give rise to neurons, glial cells, adrenal medulla schwann cells, and melanocytes (Cichorek et al., 2013). In the head and neck, neural crest cells give rise to mesenchymal cells forming cartilage, bone, dermis, adipose, smooth muscle, and also melanocytes. Neural crest-derived cells are widely distributed through the entire adult body and have been shown to contribute to multipotent progenitor populations in adults (Dupin and Sommer, 2012). Both proposed potential cells of origin, melanocytes and mesenchymal progenitors, can be traced back to the neural crest lineage and may even have a common origin in adult tissue.

Melanocyte Biology

Melanocytes are derived from the neural crest and have the ability to produce melanin. The epidermal melanocytes' main purpose is to protect against UV radiation. They do this by producing melanosomes, melanin-producing organelles, and transporting them to the keratinocytes at the surface of the skin. Melanocytes are easily recognized by their distinct morphology, resembling dendritic cells (Cichorek et al., 2013). Melanocytes express TYR, TRYP1, TRYP2, and DCT proteins involved in melanin synthesis, along with mMITF. These are all proteins that are involved in the pigmentation pathway and are important for melanocyte function and survival (Lang et al., 2013). Expression of these melanocyte specific markers within clear cell sarcomas provides a strong case for melanocytes as a cell of origin for clear cell sarcoma.

Currently, there are thought to be two different waves of melanocyte migration and maturation. Traditionally, melanoblasts are believed to migrate from the neural crest to take up residence in the epidermis, hair follicles, and iris along with small populations in the inner ear, nervous system, and heart where they mature into melanocytes. The second hypothesized migration occurs in conjunction with the peripheral nerves. The second wave of melanoblasts is not lineage-restricted but maintains the multipotent ability to differentiate into many neural crest cells *in vitro*. Similar to the earlier wave, their migration is complete before birth. However, it has been shown that these cells maintain their ability to differentiate and repopulate epidermal melanocytes postnatally (Dupin and Sommer, 2012). It has even been hypothesized that this multipotent progenitor cell, which lies along nerve projections within the dermis, may be the true adult melanoblast (Cichorek et al., 2013). This population of cells also represents a

potential cell of origin for dermal clear cell sarcoma. Their location within the deeper tissues makes them a strong candidate as the cells of origin for typical clear cell sarcoma.

Although there is suggestive evidence for a melanocyte cell of origin, there are clear cell sarcomas that express *EWSR1* translocation fusion genes, maintain the standard clear cell sarcoma histology, but do not express melanocyte markers. These clear cell sarcoma subtypes most often arise in the gastrointestinal system (Antonescu et al., 2006) and predominantly express the *EWS-CREB*1 fusion gene. Furthermore, evidence has shown that inducing expression of EWS-ATF1 may in fact induce expression of mMITF. EWS-ATF1 binds to the CRE element in the MITF promoter and promotes transcription of the *MITF* gene (Davis et al., 2006). This indicates that the fusion protein may be sufficient to induce mMITF expression and may induce differentiation into the melanocyte lineage.

Mesenchymal Stem Cell Biology

An alternative cell of origin for clear cell sarcoma is the mesenchymal stem cell. The role of mesenchymal stem cells (MSC) in adult tissue is to respond to damage, and disease states through regeneration and repair. The MSCs can be found in almost all adult tissues, they retain the capacity of self-renewal, and the potential to give rise to osteoblasts, chondroblasts, and adipocytes. MSCs have long been hypothesized to be a potential cell of origin for multiple sarcomas and have given rise to sarcomas through spontaneous and induced transformation (Lin et al., 2011; Matushansky et al., 2007; Rodriguez et al., 2012; Xiao et al., 2013).

The location of the MSC niche has been under debate for many years. These cells

were originally identified within bone marrow in the early 1960s. Friedtein and colleagues demonstrated a subset of bone marrow derived cells were capable of differentiating into bone *in vitro* (Friedtein et al., 1966). MSCs have since been isolated from adipose tissue (Festy et al., 2005), dermis (Haniffa et al., 2007), and periosteum (Chang and Knothe Tate, 2012), among other tissues. The major population of MSCs is now thought to reside in a perivascular niche mixed with, but distinct from, the pericytes (Crisan et al., 2008). This perivascular niche would account for the multiple tissue types from which MSCs can be isolated. The inability to fully characterize the MSC niche is due to the lack of specific markers for this cell type. Currently, the identification of the MSC relies on a combination of markers. Interestingly, MSCs express Nestin, a neuronal marker that is also present in some cases of clear cell sarcoma, but not in melanocytes (Dimas et al., 2008, Mendez-Ferrer et al., 2010). This potential marker for cell of origin, the MSC residing in the deep niche, and the past participation in sarcomagenesis strongly supports the hypothesis that these cells are the starting point for clear cell transformation. There is contradicting evidence for both potential cells of origin and this has only added to the interest in determining which is the true cell from which clear cell arises.

## Model System

The cell of origin for most tumors has remained elusive. Even when examining precancerous lesions, it is difficult to pinpoint the cell type from which the tumors arise. With advances in genetic manipulation of mouse cancer models, it has become possible to induce cancer-causing mutations within a limited lineage of cells, and to determine which cell types are capable of transformation. This is even more important for sarcomas,

which rarely show a precancerous lesion and arise from cells that appear to be displaced. There are several ways to design a model to test the cell of origin of fusion protein driven sarcomas. There are advantages and disadvantages assigned to each model.

The first and most commonly used method for designing mouse models of translocation-based sarcomas is to drive the fusion protein using a ubiquitous promoter. This is accomplished by extracting the fusion gene transcript from human tumors and using RT-PCR to convert the RNA into its complementary DNA (cDNA). The cDNA is placed under the control of an endogenous ubiquitous promoter in the mouse, such as the Rosa26 promoter. A transcriptional stop sequence, often 3-4 polyA sequences, is inserted between the promoter and the cDNA and flanked by LoxP sites. Cre recombinase is used to remove the stop sequence by recombination and allow cDNA expression. This allows for activation of fusion gene expression in multiple cell types while controlling the timing of expression in order to bypass any unfavorable embryonic lethality. One caveat of this method lies with the overexpression of a fusion gene with a strong promoter. If dosage is important, this may adversely influence the results.

A second method uses an endogenous fusion protein promoter to drive expression of the cDNA. This method allows the endogenous promoter to recapitulate tissue specific expression patterns analogous to the endogenous human pattern. The caveat with this method is that it restricts cells that can express the fusion, and thus limits our ability to test all cells. It also limits spatio-temporal control of cDNA expression, and thus we may miss a critical time for fusion expression.

The third method is to recreate the translocation using mouse orthologs. This is accomplished by adding a LoxP site to the intron of each gene at the site where the

breakpoint occurs most of the human orthologs. LoxP sites are arranged so that when Cre recombinase is added to the system, it induces the most common translocation described in human clear cell sarcoma. Much like the first strategy, this method also permits spatio-temporal control through tamoxifen-inducible tissue-specific Cre expression. The pitfalls of this model are the time and cost of making two separate transgenic mouse lines and the increased breeding time needed to combine three separate alleles in the same mouse. Furthermore, use of endogenous mouse genes may not be sufficient to induce clear cell sarcoma. For those reasons, this is the least used strategy, even though it most accurately recapitulates the human dynamic.

All three model building strategies have advantages and disadvantages, but the first is the most commonly used. Expressing the human fusion gene cDNA under the control of a ubiquitous promoter has been shown to efficiently produce tumors that recapitulate human tumor morphology, genetic expression profile, and metastatic potential, making it a powerful model for the study of sarcomagenesis and cell of origin analysis. We will use the first method in this thesis to model clear cell sarcoma.

## Summary

This thesis describes our use of genetic analysis of the role *EWS-ATF1* plays in clear cell sarcomagenesis and, more generally, in tumorigenesis. First, a conditional model was developed that controlled both the temporal and spatial expression of the *EWS-ATF1* human cDNA. Data revealed *EWS-ATF1* to be a potent oncogene that is sufficient to induce tumorigenesis in a shockingly short duration after induction. Second, experiments were performed using specific Cre-drivers to express the *EWS-ATF1* in both

melanocytic and mesenchymal tissue lineages to determine which cells are permissible to clear cell sarcoma formation. From these studies, results demonstrate that melanocytes are not an efficient cell of origin for producing clear cell sarcoma of the tendons and aponeuroses. Instead, findings from this work suggested that mouse mesenchymal stem cells are the cell of origin for classic clear cell sarcoma. Therefore, mesenchymal stem cells can be reprogrammed after expression of the fusion protein to take on a more melanocyte-like state.

## References

Antonescu, C.R., Nafa, K., Segal, N.H., Dal Cin, P., and Ladanyi, M. (2006). EWS-CREB1: a recurrent variant fusion in clear cell sarcoma--association with gastrointestinal location and absence of melanocytic differentiation. Clin Cancer Res *12*, 5356-5362.

Araya, N., Hirota, K., Shimamoto, Y., Miyagishi, M., Yoshida, E., Ishida, J., Kaneko, S., Kaneko, M., Nakajima, T., and Fukamizu, A. (2003). Cooperative interaction of EWS with CREB-binding protein selectively activates hepatocyte nuclear factor 4-mediated transcription. J Biol Chem *278*, 5427-5432.

Bearman, R.M., Noe, J., and Kempson, R.L. (1975). Clear cell sarcoma with melanin pigment. Cancer *36*, 977-984.

Bertolotti, A., Melot, T., Acker, J., Vigneron, M., Delattre, O., and Tora, L. (1998). EWS, but not EWS-FLI-1, is associated with both TFIID and RNA polymerase II: interactions between two members of the TET family, EWS and hTAFII68, and subunits of TFIID and RNA polymerase II complexes. Mol Cell Biol *18*, 1489-1497.

Bridge, J.A., Borek, D.A., Neff, J.R., and Huntrakoon, M. (1990). Chromosomal abnormalities in clear cell sarcoma. Implications for histogenesis. Am J Clin Pathol *93*, 26-31.

Brody, R.I., Ueda, T., Hamelin, A., Jhanwar, S.C., Bridge, J.A., Healey, J.H., Huvos, A.G., Gerald, W.L., and Ladanyi, M. (1997). Molecular analysis of the fusion of EWS to an orphan nuclear receptor gene in extraskeletal myxoid chondrosarcoma. Am J Pathol *150*, 1049-1058.

Brown, A.D., Lopez-Terrada, D., Denny, C., and Lee, K.A. (1995). Promoters containing ATF-binding sites are de-regulated in cells that express the EWS/ATF1 oncogene.

Oncogene *10*, 1749-1756.

Chang, H., and Knothe Tate, M.L. (2012). Concise review: the periosteum: tapping into a reservoir of clinically useful progenitor cells. Stem Cells Transl Med *1*, 480-491.

Chen, G., Folpe, A.L., Colby, T.V., Sittampalam, K., Patey, M., Chen, M.G., and Chan, J.K. (2011). Angiomatoid fibrous histiocytoma: unusual sites and unusual morphology. Mod Pathol *24*, 1560-1570.

Chung, E.B., and Enzinger, F.M. (1983). Malignant melanoma of soft parts. A reassessment of clear cell sarcoma. Am J Surg Pathol *7*, 405-413.

Cichorek, M., Wachulska, M., Stasiewicz, A., and Tyminska, A. (2013). Skin melanocytes: biology and development. Postepy Dermatol Alergol *30*, 30-41.

Covinsky, M., Gong, S., Rajaram, V., Perry, A., and Pfeifer, J. (2005). EWS-ATF1 fusion transcripts in gastrointestinal tumors previously diagnosed as malignant melanoma. Hum Pathol *36*, 74-81.

Crisan, M., Yap, S., Casteilla, L., Chen, C.W., Corselli, M., Park, T.S., Andriolo, G., Sun, B., Zheng, B., Zhang, L.*, et al.* (2008). A perivascular origin for mesenchymal stem cells in multiple human organs. Cell Stem Cell *3*, 301-313.

Davis, I.J., Kim, J.J., Ozsolak, F., Widlund, H.R., Rozenblatt-Rosen, O., Granter, S.R., Du, J., Fletcher, J.A., Denny, C.T., Lessnick, S.L.*, et al.* (2006). Oncogenic MITF dysregulation in clear cell sarcoma: defining the MiT family of human cancers. Cancer Cell *9*, 473-484.

Delattre, O., Zucman, J., Plougastel, B., Desmaze, C., Melot, T., Peter, M., Kovar, H., Joubert, I., de Jong, P., Rouleau, G.*, et al.* (1992). Gene fusion with an ETS DNA-binding domain caused by chromosome translocation in human tumours. Nature *359*, 162-165.

Dimas, K., Tsimplouli, C., Anagnostopoulos, A.K., Mahaira, L., Iliopoulou, E., Perez, S., Vougas, K., and Tsangaris, G.T. (2008). The proteome profile of two cell lines and their xenografts isolated from a patient with clear cell sarcoma (soft-tissue melanoma). Cancer Genomics Proteomics *5*, 175-237.

Dupin, E., and Sommer, L. (2012). Neural crest progenitors and stem cells: from early development to adulthood. Dev Biol *366*, 83-95.

Enzinger, F.M. (1965). CLEAR-CELL SARCOMA OF TENDONS AND APONEUROSES. AN ANALYSIS OF 21 CASES. Cancer *18*, 1163-1174.

Falconieri, G., Bacchi, C.E., and Luzar, B. (2012). Cutaneous clear cell sarcoma: report of three cases of a potentially underestimated mimicker of spindle cell melanoma. Am J

Dermatopathol *34*, 619-625.

Festy, F., Hoareau, L., Bes-Houtmann, S., Pequin, A.M., Gonthier, M.P., Munstun, A., Hoarau, J.J., Cesari, M., and Roche, R. (2005). Surface protein expression between human adipose tissue-derived stromal cells and mature adipocytes. Histochem Cell Biol *124*, 113-121.

Friedtein, A.J., Piatetzky, S., II, and Petrakova, K.V. (1966). Osteogenesis in transplants of bone marrow cells. J Embryol Exp Morphol *16*, 381-390.

Gerald, W.L., and Haber, D.A. (2005). The EWS-WT1 gene fusion in desmoplastic small round cell tumor. Semin Cancer Biol *15*, 197-205.

Gupta, P., and Prywes, R. (2002). ATF1 phosphorylation by the ERK MAPK pathway is required for epidermal growth factor-induced c-jun expression. J Biol Chem *277*, 50550-50556.

Haniffa, M.A., Wang, X.N., Holtick, U., Rae, M., Isaacs, J.D., Dickinson, A.M., Hilk, C.M., and Collin, M.P. (2007). Adult human fibroblasts are potent immunoregulatory cells and functionally equivalent to mesenchymal stem cells. J Immunol *179*, 1595-1604.

Hantschke, M., Mentzel, T., Rutten, A., Palmedo, G., Calonje, E., Lazar, A.J., and Kutzner, H. (2010). Cutaneous clear cell sarcoma: a clinicopathologic, immunohistochemical, and molecular analysis of 12 cases emphasizing its distinction from dermal melanoma. Am J Surg Pathol *34*, 216-222.

Hsueh, Y.P., and Lai, M.Z. (1995). Overexpression of activation transcriptional factor 1 in lymphomas and in activated lymphocytes. J Immunol *154*, 5675-5683.

Jean, D., Harbison, M., McConkey, D.J., Ronai, Z., and Bar-Eli, M. (1998). CREB and its associated proteins act as survival factors for human melanoma cells. J Biol Chem *273*, 24884-24890.

Jean, D., Tellez, C., Huang, S., Davis, D.W., Bruns, C.J., McConkey, D.J., Hinrichs, S.H., and Bar-Eli, M. (2000). Inhibition of tumor growth and metastasis of human melanoma by intracellular anti-ATF-1 single chain Fv fragment. Oncogene *19*, 2721-2730.

Jones, D.T., Lechertier, T., Mitter, R., Herbert, J.M., Bicknell, R., Jones, J.L., Li, J.L., Buffa, F., Harris, A.L., and Hodivala-Dilke, K. (2012). Gene expression analysis in human breast cancer associated blood vessels. PLoS One *7*, e44294.

Kao, Y.C., Lan, J., Tai, H.C., Li, C.F., Liu, K.W., Tsai, J.W., Fang, F.M., Yu, S.C., and Huang, H.Y. (2014). Angiomatoid fibrous histiocytoma: clinicopathological and molecular characterisation with emphasis on variant histomorphology. J Clin Pathol.

Lang, D., Mascarenhas, J.B., and Shea, C.R. (2013). Melanocytes, melanocyte stem cells, and melanoma stem cells. Clin Dermatol *31*, 166-178.

Li, K.K., and Lee, K.A. (1998). MMSP tumor cells expressing the EWS/ATF1 oncogene do not support cAMP-inducible transcription. Oncogene *16*, 1325-1331.

Lin, P.P., Wang, Y., and Lozano, G. (2011). Mesenchymal Stem Cells and the Origin of Ewing's Sarcoma. Sarcoma *2011*.

Liu, F., Thompson, M.A., Wagner, S., Greenberg, M.E., and Green, M.R. (1993). Activating transcription factor-1 can mediate Ca(2+)- and cAMP-inducible transcriptional activation. J Biol Chem *268*, 6714-6720.

Matushansky, I., Hernando, E., Socci, N.D., Mills, J.E., Matos, T.A., Edgar, M.A., Singer, S., Maki, R.G., and Cordon-Cardo, C. (2007). Derivation of sarcomas from mesenchymal stem cells via inactivation of the Wnt pathway. J Clin Invest *117*, 3248-3257.

Mayr, B., and Montminy, M. (2001). Transcriptional regulation by the phosphorylation-dependent factor CREB. Nat Rev Mol Cell Biol *2*, 599-609.

Mendez-Ferrer, S., Michurina, T.V., Ferraro, F., Mazloom, A.R., Macarthur, B.D., Lira, S.A., Scadden, D.T., Ma'ayan, A., Enikolopov, G.N., and Frenette, P.S. (2010). Mesenchymal and haematopoietic stem cells form a unique bone marrow niche. Nature *466*, 829-834.

Osuna, D., and de Alava, E. (2009). Molecular pathology of sarcomas. Rev Recent Clin Trials *4*, 12-26.

Panagopoulos, I., Thorsen, J., Gorunova, L., Micci, F., Haugom, L., Davidson, B., and Heim, S. (2013). RNA sequencing identifies fusion of the EWSR1 and YY1 genes in mesothelioma with t(14;22)(q32;q12). Genes Chromosomes Cancer *52*, 733-740.

Rodriguez, R., Rubio, R., and Menendez, P. (2012). Modeling sarcomagenesis using multipotent mesenchymal stem cells. Cell Res *22*, 62-77.

Rossow, K.L., and Janknecht, R. (2001). The Ewing's sarcoma gene product functions as a transcriptional activator. Cancer Res *61*, 2690-2695.

Sankar, S., and Lessnick, S.L. (2011). Promiscuous partnerships in Ewing's sarcoma. Cancer Genet *204*, 351-365.

Segal, N.H., Pavlidis, P., Noble, W.S., Antonescu, C.R., Viale, A., Wesley, U.V., Busam, K., Gallardo, H., DeSantis, D., Brennan, M.F*., et al.* (2003). Classification of clear-cell sarcoma as a subtype of melanoma by genomic profiling. J Clin Oncol *21*, 1775-1781.

Thway, K., and Fisher, C. (2012). Tumors with EWSR1-CREB1 and EWSR1-ATF1 fusions: the current status. Am J Surg Pathol *36*, e1-e11.

Thway, K., Nicholson, A.G., Wallace, W.A., Al-Nafussi, A., Pilling, J., and Fisher, C. (2012). Endobronchial pulmonary angiomatoid fibrous histiocytoma: two cases with EWSR1-CREB1 and EWSR1-ATF1 fusions. Am J Surg Pathol *36*, 883-888.

Wang, W.L., Mayordomo, E., Zhang, W., Hernandez, V.S., Tuvin, D., Garcia, L., Lev, D.C., Lazar, A.J., and Lopez-Terrada, D. (2009). Detection and characterization of EWSR1/ATF1 and EWSR1/CREB1 chimeric transcripts in clear cell sarcoma (melanoma of soft parts). Mod Pathol *22*, 1201-1209.

Wang, Y., and Prywes, R. (2000). Activation of the c-fos enhancer by the erk MAP kinase pathway through two sequence elements: the c-fos AP-1 and p62TCF sites. Oncogene *19*, 1379-1385.

Weinreb, I. (2013). Translocation-associated salivary gland tumors: a review and update. Adv Anat Pathol *20*, 367-377.

Weiss, S., and Goldblum, J. (2008). Enzinger and Weiss's Soft-tissue Tumors, 5th edn (China: Elsevier).

Xiao, W., Mohseny, A.B., Hogendoorn, P.C., and Cleton-Jansen, A.M. (2013). Mesenchymal stem cell transformation and sarcoma genesis. Clin Sarcoma Res *3*, 10.

# CHAPTER 2

# MODELING CLEAR CELL SARCOMAGENESIS IN THE MOUSE: CELL OF ORIGIN DIFFERENTIATION STATE IMPACTS TUMOR CHARACTERISTICS


## Abstract

Clear cell sarcoma (CCS) of tendons and aponeuroses is a deadly soft-tissue malignancy resembling melanoma. *EWS-ATF1*, the fusion product of a balanced chromosomal translocation between chromosomes 22 and 12, is considered the definitional feature of the tumor. Tumors, developed with 100 percent penetrance through varied means of initiating expression of the fusion oncogene, model human CCS morphologically, immunohistochemically, and by genome-wide expression profiling. We also demonstrate that while fusion oncogene expression in later stages of differentiation can transform mesenchymal progenitor cells and generate tumors resembling CCS generally, expression in cells retaining stem cell markers permits the full melanoma-related phenotype.

## Significance

CCS, a rare soft-tissue malignancy typically arising in the extremities of young adults, closely resembles melanoma. *EWS-ATF1*, a fusion oncogene resulting from a t(12;22) chromosomal translocation, defines the neoplasm. Conditional expression of the human *EWS-ATF1* cDNA in the mouse demonstrates its profound transformational impact. While a number of cell types can be rendered tumorigenic via expression of the fusion oncogene, the undifferentiated cells appear to enable the full melanoma-related phenotype. This model deciphers part of the enigma of the melanoma expression profile of CCS and explains the range of human tumors derived from this powerful translocation product. The mouse model should provide a robust platform for interrogating molecular mechanisms and developing more effective therapies for CCS.

## Introduction

Clear cell sarcoma (CCS) is a soft-tissue neoplasm classically arising in the extremities of young adults near tendons and aponeuroses. Despite their often small size, these tumors have high rates of recurrence and metastasis following standard local therapy, portending a poor general prognosis. CCS was first identified in 1965, then termed “Malignant Melanoma of the Soft Parts” due to its histologic appearance fitting with metastatic melanoma (Enzinger, 1965). In addition, CCS was later found to demonstrate melanocytic differentiation markers, including immunohistochemical positivity for M-MITF, S100B, MelanA, and HMB45 (Granter et al., 2001; Hocar et al., 2012). Until recently, the only means of differentiating CCS from the soft-tissue metastasis of a distant melanoma was its clinical history (i.e., confirmed absence of any

cutaneous melanomas).

In the last decade, recognition of the characteristic t(12;22) (q13;q12) chromosomal translocation and its resultant fusion oncogene *EWSR1-ATF1* (*EWS-ATF1*) has provided a means of defining CCS and distinguishing it from melanoma (Antonescu et al., 2002). Traditional cytogenetics, fluorescent *in situ* hybridization (FISH), and reverse-transcriptase polymerase chain reaction (RT-PCR) have all proven to be diagnostic tools capable of identifying this defining molecular feature of CCS (Wang et al., 2009). The type 1 fusion of *EWS-ATF1*, which includes exons one through eight of *EWSR1* and exons four through seven of *ATF1*, is the most common variant of the described translocation products (Wang et al., 2009).

The EWS-ATF1 fusion protein contains the amino-terminal transcriptional activation domain of the EWSR1 protein joined to the bZIP DNA binding/dimerization domain of activating transcription factor 1 (ATF1). In the fusion protein, the EWSR1 activation domain replaces a protein kinase A phosphoacceptor site that renders endogenous ATF1 activity dependent on the presence of cyclic adenosine monophosphate (Fujimura et al., 2001). As a consequence, EWS-ATF1 is thought to be a constitutive activator of ATF1-regulated genes. A small minority of CCS cases harbor a t(2;22) (q32;q12) translocation and the alternate CREB1 fusion partner replacing ATF1, with which CREB1 shares binding of an identical consus sequence (Wang et al., 2009).

The cell, or cells, of origin for CCS are not known. Traditionally, CCS tumors were characteristically identified near the tendons and aponeuroses of young adults, but have also recently been identified in the gastrointestinal tract (Covinsky et al., 2005; D'Amico et al., 2011; Lyle et al., 2008) and dermis (Falconieri et al., 2012; Hantschke et

al., 2010). The expression of melanocyte-specific markers in CCS tumors has been variably attributed to the effects of the cell of origin or the effects of aberrant *M-Mitf* expression, shown to be driven by EWS-ATF1 in CCS cell lines (Davis et al., 2006). Using *EWS-ATF1* as a diagnostic marker led to the identification of CCSs that do not express melanocytic markers. Further, some histologically distinct neoplasms have also been associated with this fusion oncogene, including angiomatoid fibrous histiocytoma (Somers et al., 2005) and hyalinizing clear cell carcinoma of the salivary gland (Antonescu et al., 2011). The latter tumors do not express *M-Mitf* or other melanocytic markers.

To investigate the role that *EWS-ATF1* plays in clear cell sarcomagenesis and in tumorigenesis more broadly, we developed a mouse model that expresses the human *EWS-ATF1* fusion oncogene complementary DNA (cDNA) in a conditional fashion.

## Results

### Generation of a Targeted Mouse Line Conditionally Expressing the EWS-ATF1 Oncogene

To generate the *EWS-ATF1* cDNA, total RNA was isolated from human CCS tumors, reverse transcribed, and screened by PCR to identify a type 1 *EWS-ATF1* fusion product. The integrity of the *EWS-ATF1* cDNA was confirmed by DNA sequencing. The *EWS-ATF1* cDNA was targeted to the ubiquitously expressed *Rosa26* locus (Mao et al., 1999). Linked to the *EWS-ATF1* cDNA via an internal ribosomal entry site (IRES) was the sequence encoding an enhanced green fluorescent protein (eGFP). To prevent transcription of the fusion gene and eGFP from the *Rosa26* promoter, a neomycin

resistance cassette and poly-adenylation stop signal flanked by *loxP* sites was inserted between the promoter and the *EWS-ATF1-IRES-eGFP* sequence (Figure 2.1A). In the absence of Cre, neither the fusion gene product nor eGFP should be expressed. Temporal, spatial, and tissue-specific control of Cre presence is possible through a variety of techniques for its genetic or protein delivery. Mouse embryonic stem cells confirmed to bear the targeted allele were injected into blastocysts to generate chimeras which were then bred to generate progeny with a germline-transmissible conditional allele of *EWS-ATF1* (designated $Rosa26^{EA1}$).

To confirm inducibility of the *EWS-ATF1* fusion gene and *eGFP* by Cre, embryonic fibroblasts were isolated from E14.5 mouse embryos heterozygous for the $Rosa26^{EA1}$ allele and exposed in culture to purified TAT-Cre protein or vehicle buffer control. TAT-Cre is an engineered Cre protein containing a short peptide sequence

derived from the human immunodeficiency virus that mediates efficient endocytic uptake and nuclear localization of the protein (Joshi et al., 2002). Recombination efficiency *in vitro* exceeds 95 percent as reported previously (Haldar et al., 2009). Without exposure to TAT-Cre, mouse embryonic fibroblasts heterozygous for $Rosa26^{EA1}$ demonstrated no green fluorescence. 24 hr after exposure to TAT-Cre (5 μM), cells began to express eGFP (Figure 2.1B), the percentage of fluorescing cells increased thereafter. The expression of other sarcoma fusion oncogenes from the *Rosa26* locus has proven lethal for mouse embryonic fibroblasts (Haldar et al., 2007). Surprisingly, *EWS-ATF1*-expressing fibroblasts survived beyond the expected crisis and senescence of control fibroblasts that carried the $Rosa26^{EA1}$ allele but were exposed to vehicle rather than TAT-Cre. Expression of *EWS-ATF1* remained strong in the embryonic fibroblasts

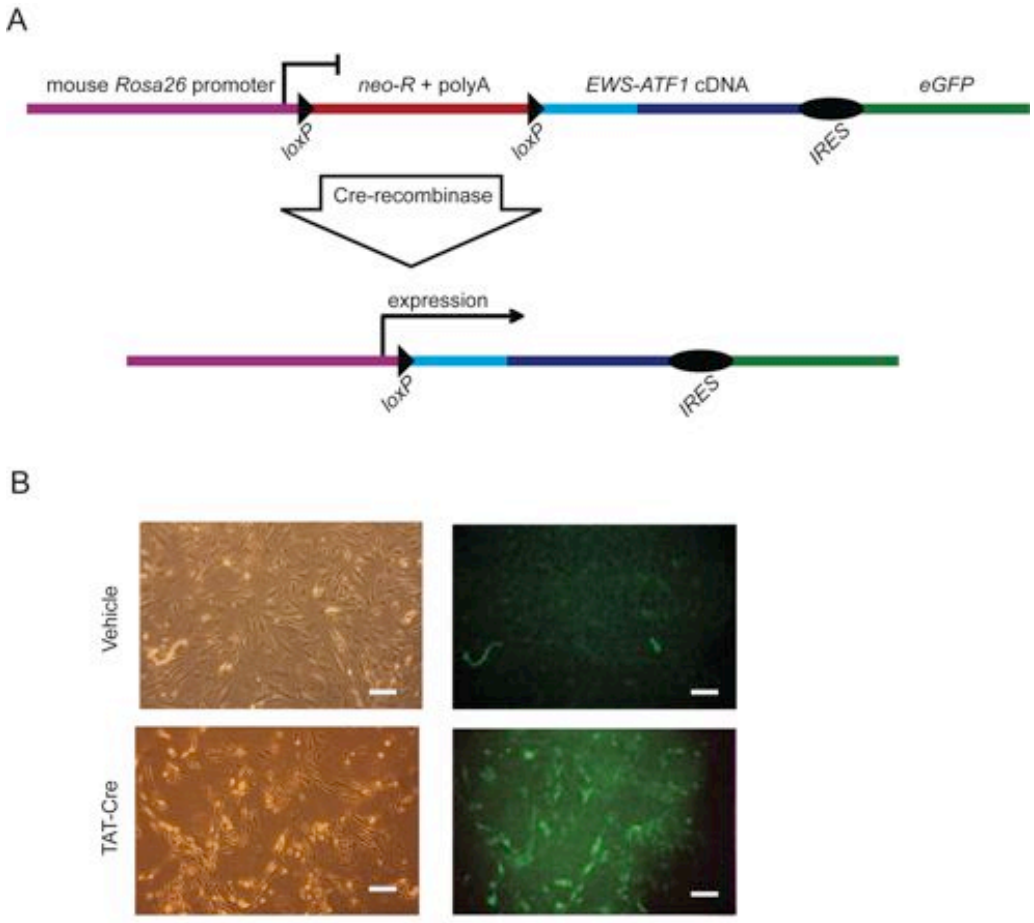


Figure 2.1. Conditional expression of the human clear cell sarcoma fusion oncogene in the mouse (A) Schematic showing the cDNA of the type I variant of EWS-ATF1 isolated from a human tumor and cloned into a vector designed for targeting into the mouse Rosa26 locus. neo-R, neomycin resistance cassette; polyA, polyadenylation stop sequence; IRES, internal ribosome entry site; eGFP, enhanced green fluorescent protein. Cre-mediated recombination excises the stop sequence and initiates expression of the fusion oncogene and eGFP. (B) Embryonic day 14.5 fibroblasts isolated from Rosa26EA1 heterozygous mice were exposed to TAT-Cre protein or vehicle control, and images were collected 24 hr later. The left two panels show light images of fibroblasts, whereas the right two panels show the GFP fluorescence. All scale bars are 50 μm in length.

activated by TAT-Cre, even following long-term passage (data not shown).

Generation of Tumors by *In Vivo* Exposure to TAT-Cre

Because expression of *EWS-ATF1* was so well tolerated *in vitro*, we investigated whether the $Rosa26^{EA1}$ allele might be activated *in vivo* first by injecting TAT-Cre into mice heterozygous for the $Rosa26^{YFP}$ allele. Mice receiving TAT-Cre show YFP expression within 24 hr of injection (Figure 2.S1A). To look at this on a cellular level, mice heterozygous for $Rosa26^{mTmG}$ reporter allele (Muzumdar et al., 2007) were also injected with TAT-Cre. All cells in mice bearing the $Rosa26^{mTmG}$ allele express membrane-bound Tomato fluorescent protein prior to recombination with Cre but express a membrane-bound GFP after Cre-mediated excision of the *mTomato* coding sequence. A single subdermal injection of TAT-Cre resulted in de GFP expression in the surrounding tissue (Figure 2.S1B).

To determine the sufficiency of the *EWS-AFT1* fusion gene to drive clear cell sarcomagenesis *in vivo,* we injected TAT-Cre protein into the anterolateral soft-tissues abutting the tibia and in the distal forelimbs of mice heterozygous for the $Rosa26^{EA1}$ allele. *EWS-ATF1* transcripts were detectable by RT-PCR from tissues harvested within 24 hr of the TAT-Cre injection (Figure 2.S1C). Every injection of TAT-Cre yielded a tumor (Figure 2.2A), tightly localized to the injection site. Control mice, including both uninjected littermates and littermates injected with saline and followed for 15 months, never formed tumors. All mouse tumors derived from the TAT-Cre-activated $Rosa26^{EA1}$ allele demonstrated eGFP fluorescence (Figure 2.2A).

Noting an extremely brief latency to tumorigenesis, the ability to form tumors in a

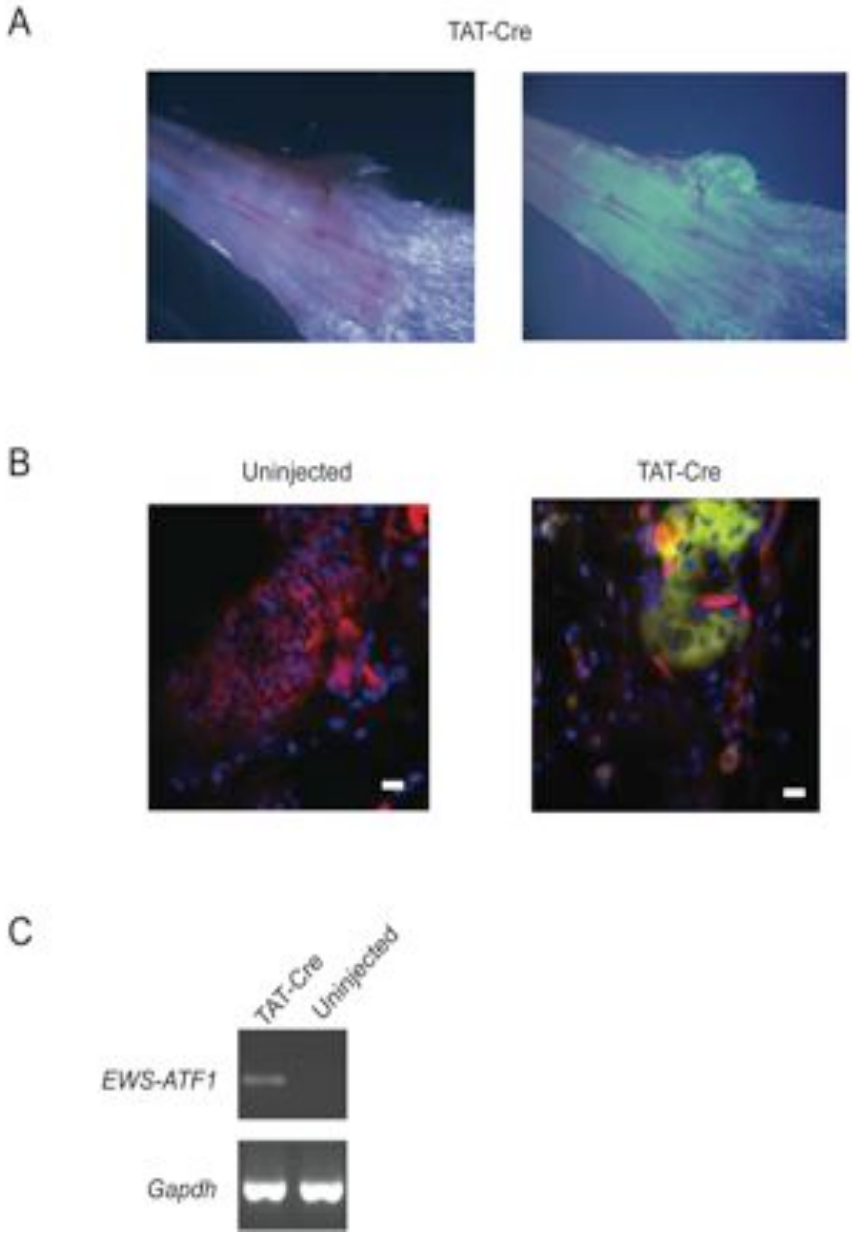


Figure 2.S1. Efficient *in vivo* recombination of LoxP sites after injection of TAT-Cre. (A) Light necroscopy (left) and GFP fluorescence (right) of a *Rosa-YFP* mouse paw injected with TAT-CRE and imaged 24 hr post injection. (B) Expression of membrane-bound Tomato fluorescent protein (red) and GFP (green) in *Rosa-mTmG* mice at baseline (uninjected, left) or 24 hr following subdermal injection of TAT-Cre (injected, right). (C) RT-PCR for the designated transcripts in a TAT-Cre (100 μM) injected and uninjected $Rosa26^{EA1}$ mouse limb 24 hr post injection.

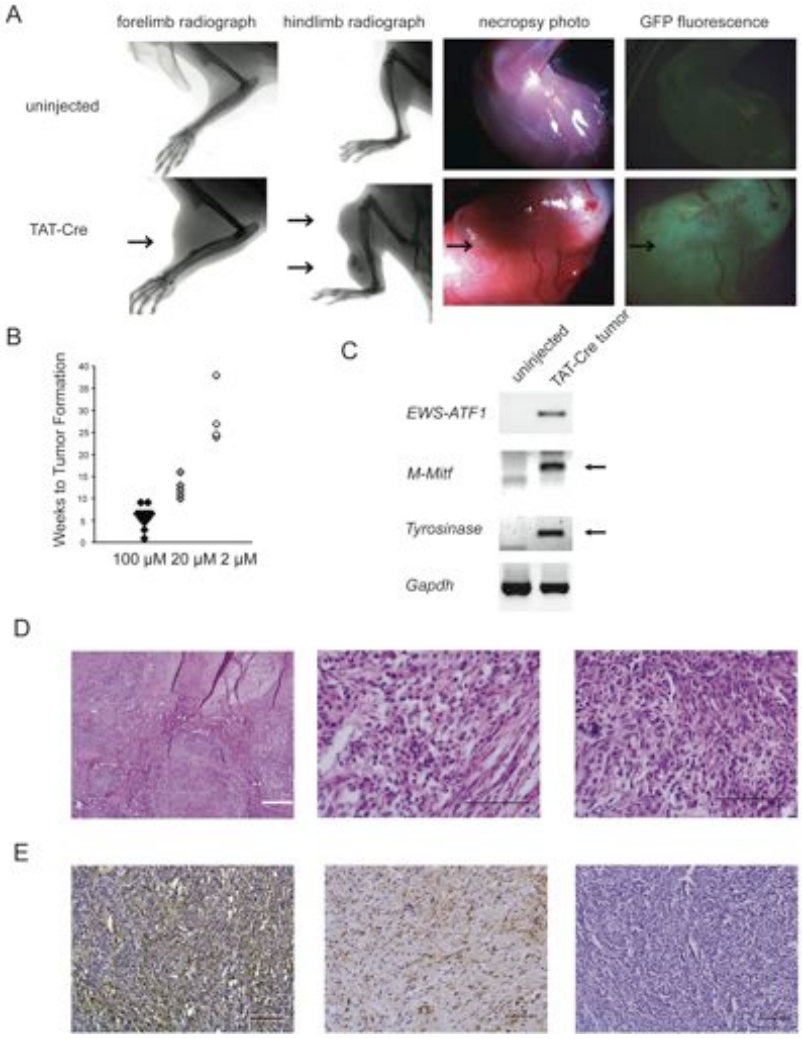


Figure 2.2. TAT-Cre-initiated expression of *EWS-ATF1 in vivo* leads to tumorigenesis. (A) Radiographs of limbs of *Rosa26*$^{EA1}$ heterozygous mice without (top) or with (bottom) injection of TAT-Cre (left two columns). Necroscopy light and GFP fluorescence photo of *Rosa26*$^{EA1}$ limb without injection (top) or of tumor extracted from the TAT-Cre injected *Rosa26*$^{EA1}$ (bottom) (right two columns). Arrows point to individual tumors. (B) Latency to visible tumor formation for *Rosa26*$^{EA1}$ mice injected with 100 µM, 10 µM, and 2 µM solutions of TAT-Cre. (C) RT-PCR analysis of the indicated mRNAs from uninjected control tissues and TAT-Cre-induced tumors. (D) Representative histology of TAT-Cre-induced tumors with H&E stain showing a multinodular tumor at low power (left), figure cells marked by round shape, clear cytoplasm and an open chromatin pattern at higher power (middle), and a tumor having a more spindled cell morphology (right). (E) Immunohistochemical stains for M-MITF (left), S100B (middle), and cytokeratin 5 (right). All black scale bars are 100 µm in length and the white bar is 500 µm.

broad array of tissue locations, and the histological appearance of poly clonality among the first rounds of TAT-Cre-induced tumors, we investigated whether the rapid growth to large tumors might result primarily from a large initial population of induced *EWS-ATF1*-expressing cells. To address this question, we injected limbs of mice heterozygous for the *Rosa26*$^{EA1}$ allele with different concentrations of TAT-Cre and found that the latency to tumor formation correlated with the concentration of TAT-Cre administered (Figure 2.2B).

Injecting 100 μM of TAT-Cre resulted in visible tumors as quickly as 3 weeks post injection, with 100 percent penetrance per injection site by 6 weeks. TAT-Cre at 2 mM still produced tumors with full penetrance, but required a longer latency with visible tumors observed after a period of 6 to 9 months. While TAT-Cre concentration impacted latency to development of a visible tumor, it did not impact the observed rate of tumor growth following visible detection of any specific tumor. Tumors appearing early from concentrated TAT-Cre or after a longer latency from diluted TAT-Cre still grew at a similarly rapid rate after detection.

The tumors that formed following TAT-Cre injection into mice heterozygous for the *Rosa26*$^{EA1}$ allele recapitulated human CCS molecularly, with expression of the fusion oncogene and melanocytic markers *M-Mitf* and *Tyrosinase* (Figure 2.2C). Mouse tumors also matched human tumor histomorphology and immunohistochemical profile. In hematoxylin and eosin (H&E) stained sections, the majority of murine tumors demonstrated nuclear features typical of primitive cell types, with prominent open chromatin patterns as well as abundant clear cytoplasm (the feature for which the tumor is named) (Figure 2.2D). While some tumors had a pseudo-encapsulated, pushing border

with surrounding tissues, others demonstrated clear infiltration into adjacent tissue planes. A minority subset of tumors (20%) demonstrated spindle cell morphology, also observed in some human CCS cases (Figure 2.2D). Consistent with human CCS, the tumors demonstrated immunohistochemical positivity for melanocytic markers (M-MITF and S100B) and lacked staining for cytokeratins (Figure 2.2E).

Unbiased Expression of EWS-ATF1 Also Results in Tumorigenesis, Preferentially in Mesenchyme

Because tumors rapidly invaded surrounding tissues, dissections of the limbs did not clearly indicate from which tissues they arose. In a search for tissues incompatible with transformation, TAT-Cre was injected into subcutaneous adipose, dorsal paw peritendinous, periosteal, intramuscular, and mammary fat pad tissue compartments in mice between 3 weeks and 6 months of age. The latency to tumor appearance varied with age and injection site, but every injection in each of these tissue locations yielded completely penetrant tumorigenesis (Table 2.1). Each of these locations bears some cells of mesenchymal character, but whether these or neighboring cells actually gave rise to tumors remained unclear.

In order to broaden exposure to *EWS-ATF1* fusion protein across multiple cell types and developmental periods, we next utilized $Rosa26^{CreER}$ to express Cre sporadically, in random cell types. While efficient CreER-mediated recombination requires the presence of tamoxifen, a very low level of CreER-mediated recombination is observed even in the absence of tamoxifen (Haldar, et al 2009). Breeding mice bearing the $Rosa26^{CreER}$ allele to mice bearing the $Rosa26^{EA1}$ allele resulted in smaller litters than

Table 2.1

Location and number of tumors resulting from localized TAT-Cre injections

| Injection Location | # of Injections | # of Tumors | Tissue Compartment of Tumor Formation |
|---|---|---|---|
| Limb | 27 | 28 | Periosteal region, within muscle, near tendons on wrist and ankle |
| Subcutaneous | 6 | 7 | dermis at site of injection |
| Mammary fat pad | 19 | 19 | mammary fat pad |
| Intraperitoneal | 7 | 7 | peritoneal wall at site of injection, dermis at sight of injection, salivary gland, mammary fat pad near site of injection |
| Head | 2 | 2 | scalp |

breeding *Rosa26*$^{EA1}$ mice alone, fitting with the previously described early embryonic leakiness of this CreER and suggesting some developmental toxicity of early expression of *EWS-ATF1* (Figure 2.3A).

Among the *Rosa26*$^{CreER/EA1}$ mice that survive embryogenesis, administration of tamoxifen prior to 3 weeks of age results in stunted growth (Figure 2.3B) and death by 12 weeks of age without detectible tumor formation. *Rosa26*$^{CreER/EA1}$ mice receiving tamoxifen after 3 weeks of age form more tumors than those receiving no tamoxifen, but both of these groups demonstrate complete penetrance of tumor formation by 12 weeks of age (Figure 2.3C). The tumors arising in *Rosa26*$^{CreER/EA1}$ mice were histologically similar to the murine TAT-Cre-induced tumors and human clear cell sarcoma (Figure 2.3D). Whether enhanced by later tamoxifen administration or not, tumors arose most often in the extremities, rib cage, and facial tissues of the *Rosa26*$^{CreER/EA1}$ mice, but were also less frequently found in the dermis, liver, and bone (Table 2.2). As following TAT-Cre induction, the preponderance of tumors arose in mesenchymal tissue compartments. A variety of mouse cells are permissive to *EWS-ATF1*-driven transformation, replicating the range of tumor tissue locations observed in molecularly defined human cases of CCS, but preferentially arising in mesenchyme.

EWS-ATF1 Drives an Expression Signature of Transformation

Because the brief latency to tumorigenesis in both models suggested a powerful role for *EWS-ATF1* in driving transformation, we sought to define the expression signature shared by tumors from both means of inducing *EWS-ATF1* expression. To this end, we harvested tumors from each cohort as well as from control mesenchymal tissue,

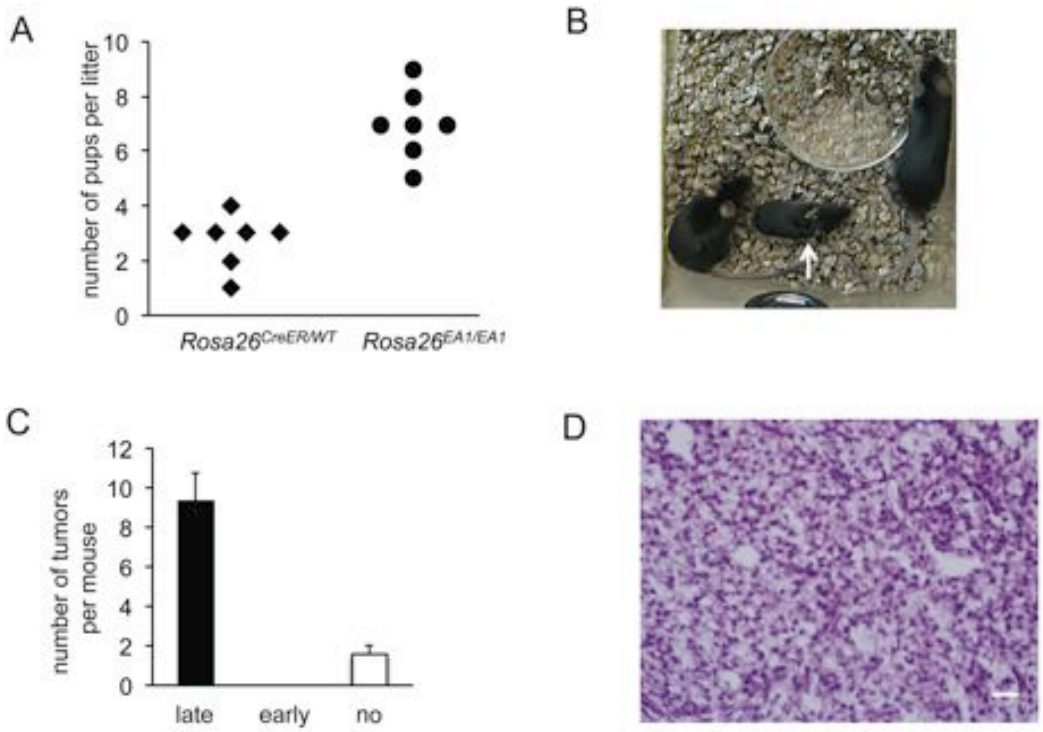


Figure 2.3. Early expression of *EWS-ATF1* in the broad $Rosa26^{CreER}$-lineage renders stunted growth, but later expression drives tumorigenesis. (A) The number of pups per litter of mice heterozygous for the $Rosa26^{CreER}$ allele crossed with mice homozygous for the $Rosa26^{EA1}$ allele compared to that of $Rosa26^{EA1/EA1}$ back-crossed controls. (B) Photograph of a 7-weeks-old male $Rosa26^{EA1/CreER}$ mouse injected with tamoxifen at 10 days (white arrow) and two uninjected female littermates of the same genotype. (C) Chart of the number of tumors per mouse at 12 weeks age among $Rosa26^{EA1/CreER}$ mice injected with tamoxifen after 3 weeks (late, n = 4), before 3 weeks (early, n=3), or not at all (n = 5). Error bars denote standard deviation, t-test $p < 0.05$. (D) H&E stained histopathology demonstrating the classic clear cell morphology apparent in a $Rosa26^{CreER}$ -initiated tumor after late injection of tamoxifen. Scale bar is 20 μm in length.

Table 2.2

Location and number of tumors formed in *Rosa26*$^{CreER/EA1}$ mice.

| Location | # Tumors |
|---|---|
| Ribcage | 7 |
| Limb (muscle) | 11 |
| Limb (near bone) | 10 |
| Face (muscle) | 2 |
| Scapula | 1 |
| ear | 2 |
| Spine | 2 |
| Peritoneal Wall | 3 |
| Liver | 1 |
| dermis | 3 |
| salivary gland | 2 |
| Head (near bone) | 2 |
| Mammary | 2 |

consisting of a portion of the thoracic cage including cartilage, bone, skeletal muscle, and connective tissue, isolated total RNA from each, and performed Illumina sequencing. The samples generated an average of 24.4 ± 3.1 million reads, which aligned to 16,840 ± 778 genes at greater than or equal to 0.1 reads per kilobase per million (RPKM). Clustering analysis demonstrated highly similar expression profiles among tumors induced by either TAT-Cre or *Rosa26*$^{CreER}$, both distinct from control tissues. An unsupervised hierarchical clustering of the samples according to the 200 most differentially expressed genes is shown in Figure 2.4A (Gene lists in Supplemental Table 3). DAVID analysis of the most significantly upregulated genes in the mouse tumors compared to control tissues highlighted several informative KEGG pathways, including cell cycle control, cancer, p53, and extra-cellular matrix pathways (Huang da et al., 2009a; Huang da et al., 2009b) (Figure 2.4B). These data provide insight into the transforming power of *EWS-ATF1*, with consistent alterations in gene expression profiling among different methods of activation.

## Embryonic Expression of EWS-ATF1 in Mesenchymal Tissues and Predecessors Causes Lethality

While experiments with TAT-Cre injections and *Rosa26*$^{CreER}$-initiated *EWS-ATF1* expression suggested that a variety of cell types appear to support a program of transformation, they also suggested that the preferred clear cell sarcomagenesis tissue of origin is mesenchyme. As postnatal mesenchymal tissues derive from both neural crest and mesodermal origins, we investigated the identity of potential cells of origin by breeding mice bearing the *Rosa26*$^{EA1}$ allele to mice bearing *Cre* expressed from

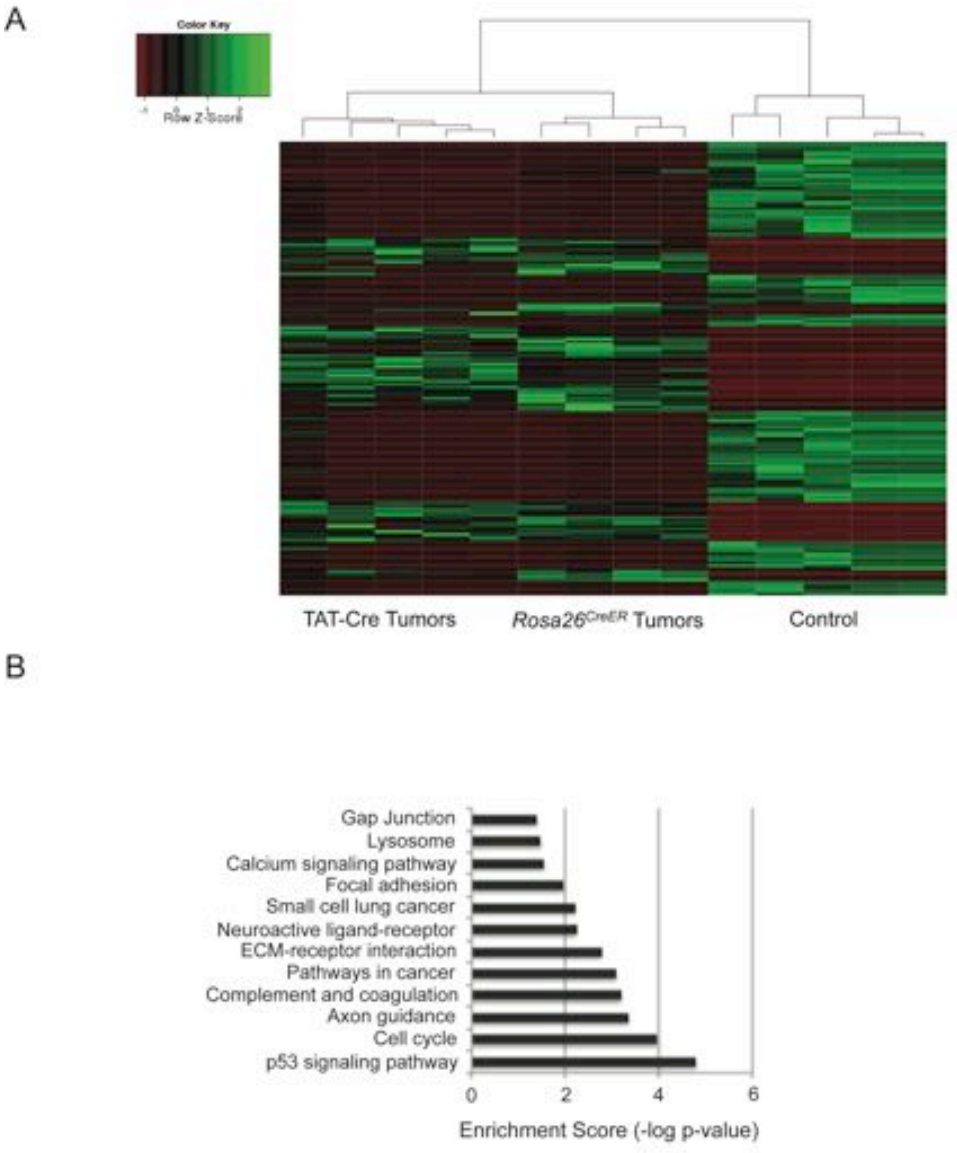


Figure 2.4. The expression signature of *EWS-ATF1*-driven tumors. (A) Heat map depicting the 200-most significantly (p-value < 0.001) differentially expressed genes between TAT-Cre or *Rosa26*$^{CreER}$-initiated tumor and control tissue, as assessed by transcriptome sequencing. (B) DAVID analysis of the most upregulated genes in tumors highlights Kegg pathways known to be involved in transformation.

promoters specific to these lineages. With regard to neural crest, mice bearing the *Rosa26*$^{EA1}$ allele and *Wnt1-Cre* (Danielian et al., 1998) did not complete embryogenesis. Conditional *EWS-ATF1* activated by *Pax3-Cre* (Engleka et al., 2005), *Pax7-Cre* (Keller et al., 2004b), *Tie2-Cre* (Kisanuki et al., 2001), or *Prx1-Cre* (Durland et al., 2008; Logan et al., 2002), all expressed in mesoderm, also resulted in embryonic lethality.

At E13.5, the *Prx1-Cre*-lineage demonstrated GFP fluorescence in *Prx1-Cre;Rosa26*$^{EA1}$ mouse embryos, indicating expression of eGFP from the IRES on the EWS-ATF1 transcript (Figure 2.5A). As late as E14.5, *Prx1-Cre;Rosa26*$^{EA1}$ mouse embryos remained viable, but demonstrated severe limb deformities (Figure 2.5A). It suggests that EWS-ATF1 was toxic to these cells.

*Pax7-Cre; Rosa26*$^{EA1}$ did not produce live progeny but embyros were retrieved as late as E18.5. These embryos showed severe craniofacial deformation with no visible eGFP which suggests that the lineage cannot survive expression of *EWS-ATF1* (Figure 2.S2A).

Mice bearing the *Rosa26*$^{EA1}$ allele and *Myf5-Cre*, which activated the fusion gene expression in myoblasts (Haldar et al., 2007), did not form tumors but demonstrated another phenotype in which *EWS-ATF1* was also apparently toxic to cells. These mice survived to birth and lived to approximately 3 months of age, but were very small in size and severely myopathic, with eGFP expression detectable in the remaining muscle fibers (Figure 2.S2B and 2.S2C).

These data demonstrate that even though the expression of *EWS-ATF1* is tolerated better than the expression of other sarcoma-related fusion oncogenes in mouse embryonic fibroblasts *in vitro* and many tissues *in vivo* when induced after weaning, it is of

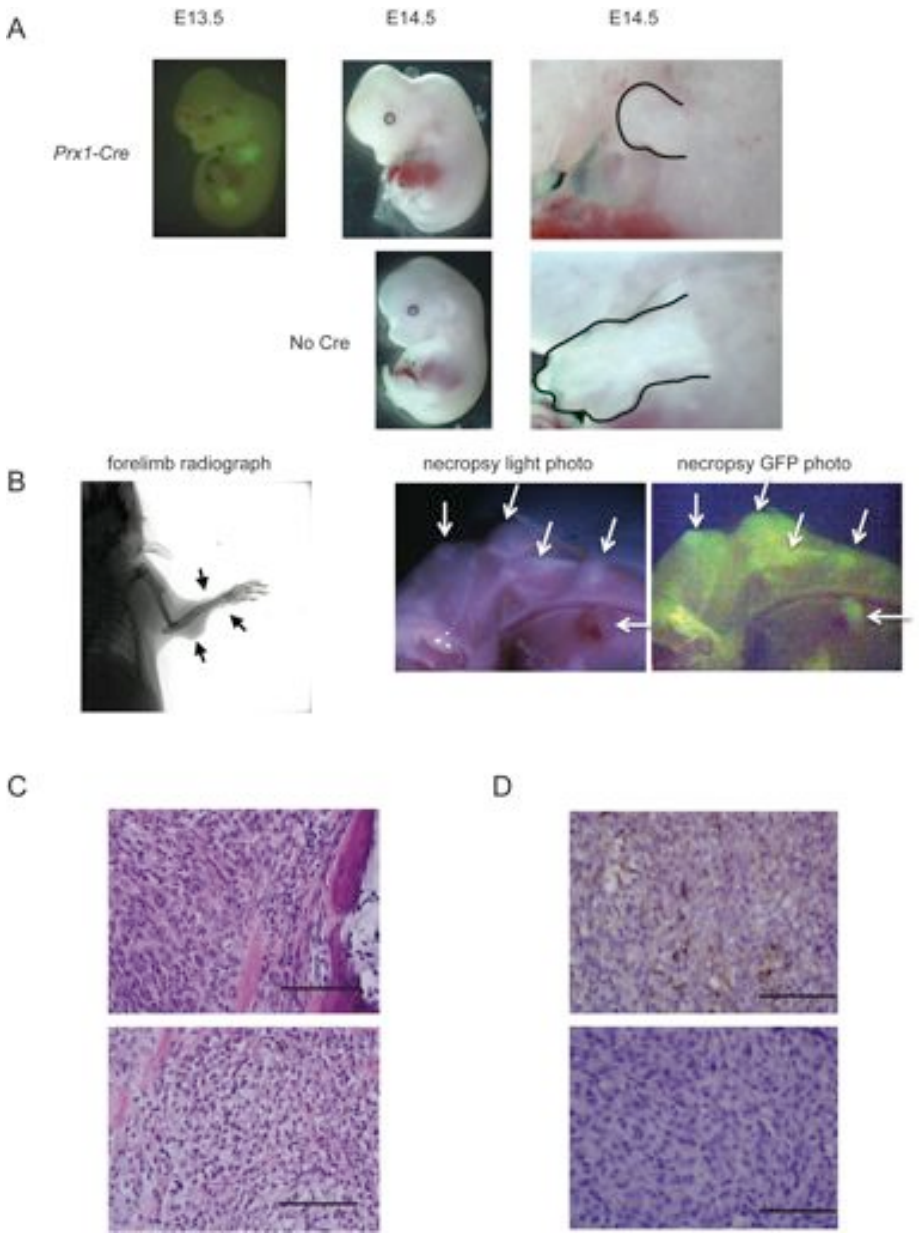


Figure 2.5. *EWS-ATF1* drives apoptosis in the embryonic *Prx1*-lineage and tumorigenesis in the postweaning *Prx1*-lineage. (A) GFP fluorescence image of *Prx1-Cre;Rosa26*$^{EA1}$ embryos at embryonic day 13.5 (far left). *Prx1-Cre;Rosa26*$^{EA1}$ at E14.5 (top middle), compared to littermate controls lacking *Prx1-Cre* (bottom middle), the limbs of mutant and control are enlarged to show difference in size (outlined in right panels) (B) Radiograph of a *Prx1-CreERT2*;*Rosa26*$^{EA1}$ mouse 8 weeks after a single tamoxifen injection at 4 weeks of age (left), gross necropsy photos with halogen light (middle) or GFP fluorescence (right) of *Prx1-CreERT2*;*Rosa26*$^{EA1}$ limb 8 weeks post tamoxifen injection (arrows point to tumors). (C) H&E stained histolopathology of *Prx1-CreERT2*;*Rosa26*$^{EA1}$ tumor immediately adjacent to bone (upper) and tumor exhibiting classic clear cell sarcoma morphology (lower). (D) Immunohistochemistry for M-MITF on *Prx1-CreERT2*;*Rosa26*$^{EA1}$ derived tumors. Scale bars are 100 μm in length.

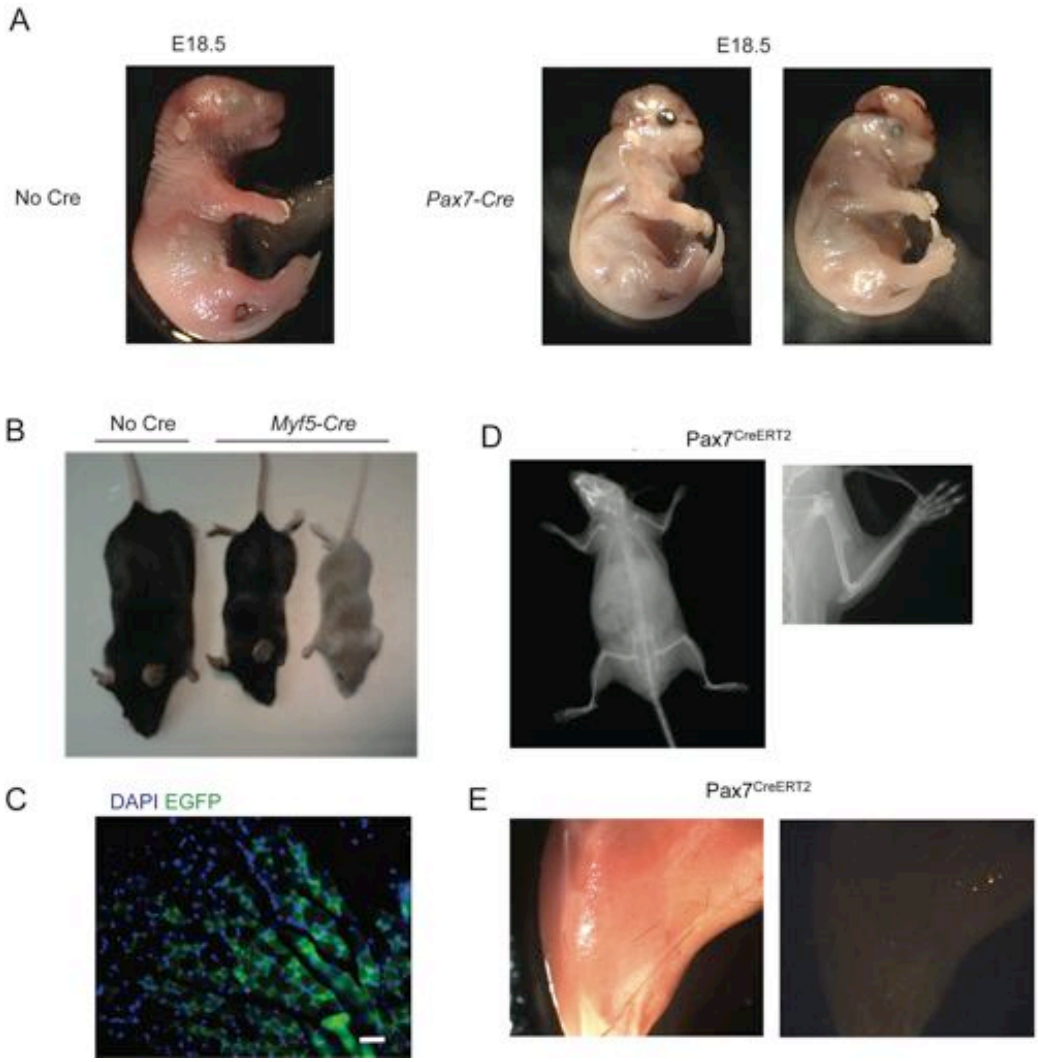


Figure 2.S2. *Pax7* and *Myf5*-lineage is not permissive to transformation during embryonic or postnatal stages. (A) At embryonic day 18.5, *Pax7-Cre;Rosa26*$^{EA1}$ embryos show severe craniofacial defects (middle and right) when compared to littermate controls lacking *Pax7-Cre* (left). **(B)** *Myf5-Cre;Rosa26*$^{EA1}$ mice (middle and far right) and their *Rosa26*$^{EA1}$ littermates who do not express Cre (far left) **(C)** EGFP (green) expression in *Myf5-Cre;Rosa26*$^{EA1}$ myopathic muscle fibers. Blue: DAPI staining. Scale bar is 100 μM. **(D)** Full body (left) and forelimb (right) radiograph of *Pax7*$^{CreERT2}$ ; *Rosa26*$^{EA1}$ mouse 6 months post tamoxifen injection. **(E)** Gross necroscopy (left) and GFP fluorescence (right) show no evidence of tumors formation (GFP) 1 year post tamoxifen injection in *Pax7*$^{CreERT2}$ ; *Rosa26*$^{EA1}$ .

significant toxicity in specific tissue settings during development.

EWS-ATF1 Expression in Postnatal Mesenchymal Progenitors Generates Two CCS Tumor Types

Noting that early tamoxifen administration in *Rosa26*$^{CreER/EA1}$ mice did not result in tumorigenesis but later administration did (Figure 2.3), we hypothesized that the toxicity prompted in the mesenchymal tissues embryonically might be avoided at later stages of development. In order to test this hypothesis, we bred mice bearing the *Rosa26*$^{EA1}$ allele to mice bearing either *Pax7*$^{CreERT2}$ (Murphy et al., 2011) or *Prx1-CreERT2* (Hasson et al., 2007), then administered tamoxifen after 3 weeks of age. By 12 months post tamoxifen, myopathy consistently developed in the *Pax7*$^{CreERT2;}$;*Rosa26*$^{EA1}$ mice but no tumors were observed (Figures 2.S2D, 2.S2E). The absence of tumor formation argues against muscle satellite cells being a potential cell of origin for EWS-ATF1-induced tumors. In the embryo, *Prx1-Cre* is widely expressed in the mesenchyme of the developing mammalian limb and head (Durland et al., 2008), whereas *Prx1-CreERT2* expression is reported to be restricted postnatally to a smaller progenitor cell population in the same anatomic regions, still capable of osteochondrogenic differentiation (Kawanami et al., 2009). *Prx1-CreERT2;Rosa26*$^{EA1}$ mice developed tumors (Figure 2.5B) by 8 weeks post tamoxifen injection with 100% penetrance. Most of these tumors developed in the extremities and head, consistent with the expected anatomic distribution of *Prx1* postnatal expression. The tumors showed GFP fluorescence marking expression of the *EWS-ATF1-IRES-eGFP* transcript (Figure 2.5B). The *Prx1-CreERT2*-induced tumors appeared to arise from the periosteal/perichondrial

layer as well as from within the musculature as judged by gross microscopy and histology (Figure 2.5B and C). The tumors induced in the *Prx1*-lineage demonstrated either the clear cell morphology with lightly stained eosinophilic cytoplasm or spindle cell morphology, both closely resembling tumors induced by TAT-Cre.

Notably, some tumors induced by *Prx1-CreERT2* expressed M-MITF but others did not (Figure 2.5D). CCS in humans often but not always expresses M-MITF (Granter et al., 2001). Thus, it appears that induction of *EWS-ATF*1 expression with *Prx1-CreERT2* generated both subtypes of CCS.

EWS-ATF1 Expression in Postnatal Mesenchymal Stem Cells Generates CCSs with a More Consistent Phenotype

In order to interrogate possible cells of origin in the undifferentiated progenitor cell population that precedes *Prx1* expression postnatally, we bred mice bearing the $Rosa26^{EA1}$ allele to mice bearing $Bmi1^{CreERT2}$ (Sangiorgi and Capecchi, 2008). *Bmi1* is a general marker for stem cells and has been demonstrated to label intestinal, neural, epidermal, and hematopoietic stem cells (Claudinot et al., 2005; Leung et al., 2004; Park et al., 2003; Sangiorgi and Capecchi, 2008). A single peritoneal injection of tamoxifen into $Bmi1^{CreERT2};Rosa26^{EA1}$ mice after 3 weeks of age resulted in fully-penetrant tumorigenesis. Every mouse developed tumors in the deeper mesenchymal tissues of the limb and trunk (Figure 2.6A). Some tumors formed completely within and surrounded by muscle (Figure 2.6B), similar to a subset of the *Prx1*-lineage tumors. A larger portion formed adjacent to bone, arising from the periosteum/perichondrium, also similar to several of the *Prx1*-lineage tumors (Figure 2.6B). The *Bmi1*-lineage tumors consistently

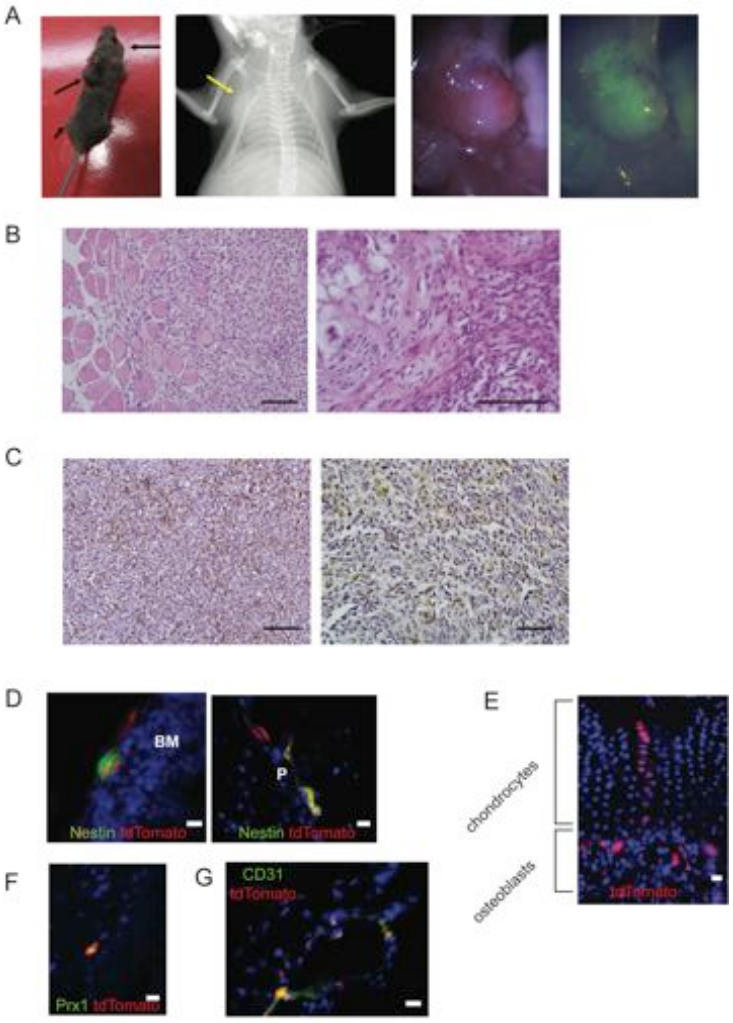


Figure 2.6. The *Bmi1*-lineage, including mesenchymal stem cells, enables more consistent development of clear cell sarcomas with melanocytic features. (A) Living image of *Bmi1*$^{CreERT2}$*;Rosa26*$^{EA1}$ mouse with black arrows indicating tumor formation (far left), radiograph (left), necropsy photo (right), and GFP fluorescence (far right) image of tumor formed in the chest wall (yellow arrow showing location of the tumor). **(B)** H&E stained histopathology of *Bmi1*$^{CreERT2}$-initiated tumors, including both intramuscular (left) and periosteal/perichondrial (right) tumors. **(C)** Immunohistochemistry of *Bmi1*$^{CreERT2}$-initiated tumors stained for M-MITF (left) and S100B (right). **(D)** Immunofluorescence for Nestin (green) and *Bmi1*$^{CreERT2}$-induced expression of tdTomato (red) in *Bmi1*$^{CreERT2}$*; Rosa26tdTomato* mice 30 days after injection of tamoxifen shown in the bone marrow BM (left) and periosteum P (right). **(E)** *Bmi1*-lineage tracing from *Bmi1*$^{CreERT2}$*;Rosa26*$^{tdTomato}$ mouse at 60 days post tamoxifen demonstrates tdTomato fluorescence (red) in osteoblasts and chondrocytes. **(F)** Immunofluorescence against Prx1 (green) and *Bmi1*-lineage defined by tdTomato (red) in *Bmi1*$^{CreERT2}$*;Rosa26*$^{tdTomato}$ mice 30 days post tamoxifen injection. **(G)** Immunofluorescence against CD31 (green) and tdTomato *Bmi1*-lineage cells (red) at 60 days post tamoxifen. All Scale bars are 100 µm in length.

matched the clear cell morphology and immunohistochemical profile of human CCS tumors, uniformly demonstrating M-MITF and S100B (Figure 2.6B and C). Prior reports have suggested a role for *Bmi1* in mesenchymal stem cells based on depletion of the pool of osteochondroprogenitors in mice bearing homozygous disruption of *Bmi1* (Zhang et al., 2010). To follow up these studies and more fully characterize the *Bmi1*-lineage in mesenchyme, mice bearing $Bmi1^{CreERT2}$ were crossed to a robust reporter mouse expressing *tdTomato* conditionally from the *Rosa26* locus. $Bmi1^{CreER};Rosa26^{tdTomato}$ mice were injected with a single dose of tamoxifen at 6 weeks of age and their limb tissues were harvested 1, 2, and 9 months post injection for analysis.

We analyzed the early *Bmi1*-lineage focused on the mesenchymal progenitor population within the bone marrow and endosteum. *Nestin* has recently been shown to be an accurate marker of the multipotent mesenchymal stem cell subpopulation in this location, whereas no specific markers are agreed upon in the periosteum (Mendez-Ferrer et al., 2010). Co-labeling experiments on tissue sections revealed the co-localization of the early *Bmi1*-lineage marker to the *Nestin*-expressing cells both at the endosteal surface in the bone marrow and in periosteum (Figure 2.6D), indicating that *Bmi1* is indeed expressed in this mesenchymal stem cell population. Lineage tracing experiments from tissues harvested 60 days and 9 months following tamoxifen administration revealed that *Bmi1*-expressing cells contribute to both osteoblast and chondrocyte lineages (Figure 2.6E), further affirming *Bmi1* as a marker of very early, stem-like cells in mesenchyme. The previously described *Prx1-CreERT2*-defined lineage marks a similar, but smaller population of these differentiated mesenchymal cells (Kawanami et al., 2009). Using an antibody against Prx1 to locate cells actively expressing the marker, we found a portion

but not all of the cells in the *Bmi1*$^{CreER}$;*Rosa26*$^{tdTomato}$-lineage expressed Prx1, suggesting that differentiating cells from the *Bmi1*-lineage express Prx1 (Figure 2.6F). Lineage tracing with *Prx1-CreERT2* mice and immunofluorescence against Nestin confirmed that a subset of *Prx1*-lineage cells still express Nestin as well (Figure 2.S3A). While mesenchymal stem cell and progenitor populations within and adjacent to the bone explain the location of some tumors arising in both the *Bmi1* and *Prx1*-lineages, other tumors in both groups arose within the muscle compartments. Since it has previously been demonstrated that *Bmi1* is expressed in Pax7-positive satellite cells within muscle (Robson et al., 2011), it is possible that the intramuscular *Bmi1*-lineage tumors could arise from this cell population. However, we already discussed that *Pax7*$^{CreERT2}$; *Rosa26*$^{EA1}$ do not form tumors, arguing against the possibility that satellite cells provide a potential cell of origin for CCS (Figure 2.S2D and E).

Further analysis of the *Bmi1*-lineage within the muscle compartments identified not only satellite cells, but also CD31-expressing endothelial cells (Figure 2.6G). Lineage tracing with *Prx1-CreERT2* mice identified CD31$^{+}$ endothelial cells within its lineage as well (Figure 2.S3B). A perivascular population of cells that has expressed both *Bmi1* and *Prx1*, perhaps at different stages of differentiation, may serve as the originating cells of the CCS tumors that appear within the muscle compartments in these two groups.

## Murine CCS Tumors Fit the Human CCS Expression Profile; Variations Appear to Reflect Different Cells of Origin

In order to determine the impact of these varied potential cells of origin on the resultant tumors, we performed RNA sequencing on a panel of mouse CCS tumors,

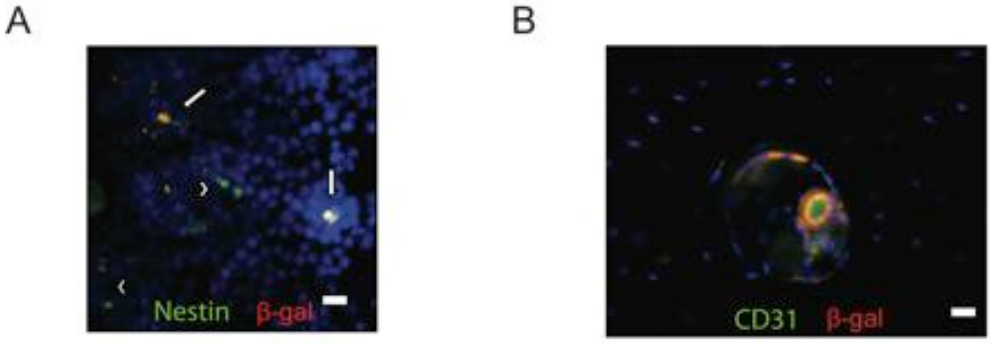


Figure 2.S3, related to Figure 2.6. *Prx1CreERT2*-lineage contributes to the mesenchymal stem cell population followed by the endotheal cell lineage. (A) Expression of β-gal expression (red) and Nestin (Green) in the bone marrow of mice of the β-gal reporter mouse *Rosa26*$^{lacZ}$ crossed to the *Prx1-CreERT2* line . Arrows point to yellow cells and arrowheads point to green cells. **(B)** Immunoflourescence staining for β-gal (red) and the CD31$^{+}$ endothelial cells (green) present 60 days post tamoxifen injection. Scale bars are 100 μm in length.

induced by TAT-Cre, *Rosa26*$^{CreER}$, *Bmi1*$^{CreERT2}$, and *Prx1-CreERT2*. We simultaneously sequenced RNA from mouse synovial sarcomas and osteosarcomas, as well as control mesenchymal tissue. Using Spearman correlation as the distance metric and an average linkage, CCS from all induction methods clustered closely and separately from control tissue and the other two sarcoma types (Figure 2.7A).

To test the extent of molecular similarity between human CCS and the tumors induced by expression of *EWS-ATF1* in mice across the range of tissues of origin, we compared mRNA sequencing expression analysis of mouse CCS tumors to microarray-derived expression data from a panel of related human tumors. A support vector machine (SVM), or supervised machine learning, technique was created to predict the identity of a tumor using a training platform built by human HEEBO microarray data from samples of CCS, melanoma (MEL), solitary fibrous tumor (SFT), leiomyosarcoma (LMS), myxoid liposarcoma (MLS), and synovial sarcoma (SS), all of which except CCS were previously reported (Nielsen et al., 2002). We first filtered the human data by mapping the HEEBO probes to the mm9 mouse reference genome, retaining only the 12,246 probes whose alignments demonstrated at least 80 percent homology across the probe length. The human expression data across this subset of probes were used to train the linear SVM model by creating CCS and non-CCS classes (n = 4 and 25, respectively). The normalized RPKM mouse data were input into the SVM as read depths per probe and classified into one of the two classes. Twelve of 13 murine CCS tumors were predicted to be human CCS, rather than one of the other tumor types (Figure 2.7B). As a control, 0 of 5 RNA sequencing data sets from wildtype mouse mesenchymal tissue controls were identified as human CCS when input into the same SVM. These data confirm that mouse

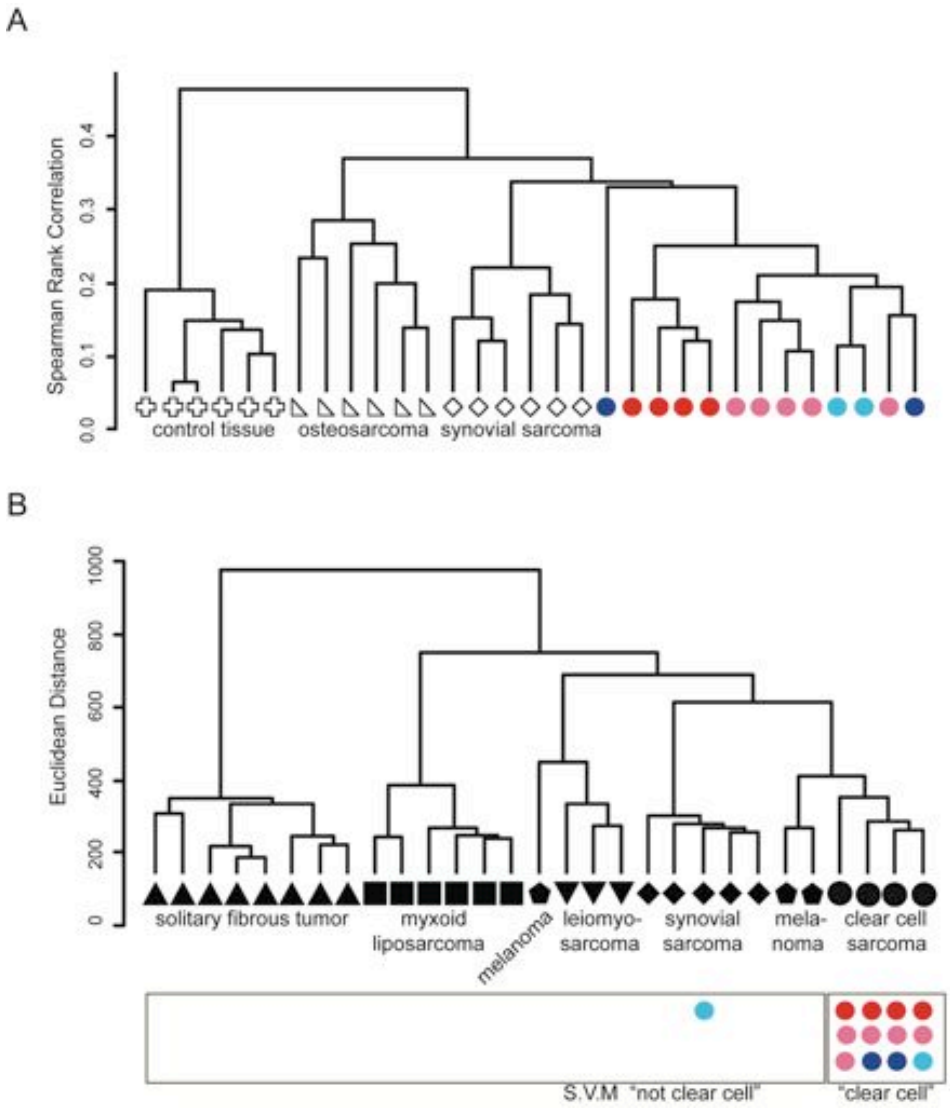


Figure 2.7. Tumors derived from *EWS-ATF1* expression in different cells of origin cluster together according to expression profile and fit human clear cell sarcoma profiles. (A) Unsupervised hierarchical clustering of mouse samples by sequencing-defined transcriptional profiling, osteosarcomas (triangle), synovial sarcomas (diamond), *EWS-ATF1*-driven tumors by TAT-Cre (red circles), *Rosa26*$^{CreER}$ (pink circles), *Bmi1*$^{CreERT2}$ (dark blue circles), and *Prx1-CreERT2* (light blue circles) and control samples from chest-wall mesenchymal tissues (cross). **(B)** Unsupervised hierarchical clustering of human tumors profiled by microarray and used to train the supervised machine-learning module, solitary fibrous tumor (triangle), myxoid liposarcoma (square), melanoma (pentagon), leiomyosarcoma (triangle), synovial sarcoma (diamond), and clear cell sarcoma (circle). The mouse *EWS-ATF1*-driven tumors are placed under the category of human tumors they most identified with on the supervised machine-learning module, TAT-Cre (red circles), *Rosa26*$^{CreER}$ (pink circles), *Bmi1*$^{CreERT2}$ (dark blue circles), and *Prx1-CreERT2* (light blue circles).

tumors derived from conditional expression of *EWS-ATF1* resemble the expression profile of human CCS more closely than the other soft-tissue tumors or melanoma.

Notably, the one mouse CCS that did not cluster closely to the human CCS SVM prediction was a *Prx1-CreERT2*-initiated tumor that did not express *M-Mitf*. In contrast, another *Prx1-CreERT2*-initiated tumor that expressed *M-Mitf* did cluster with human clear cell sarcoma.

Further comparative analysis of the RNA sequencing expression profiles of the two *Prx1*-lineage and the two *Bmi1*-lineage tumors, both sets from the same anatomic locations, identified a number of consistently differentially expressed genes. Three of the top ten genes more highly expressed in *Prx1-CreERT2;Rosa26*$^{EA1}$ were *Crlf1*, which is present in osteoblasts and chondrocytes, along with *Saa1* and *Saa2*, which are upregulated in differentiated compared to undifferentiated mesenchymal stem cells (Clancy et al., 2003; Kovacevic et al., 2008).

To better evaluate the difference between the *Bmi1*$^{CreERT2}$*;Rosa26*$^{EA1}$ and *Prx1-CreERT2;Rosa26*$^{EA1}$ tumors, we performed RT-PCR on a panel of additional samples. This revealed that some *Prx1*-lineage tumors indeed expressed *M-Mitf* and *Tyrosinase*, but not all (Figure 2.8A). All *Bmi1*-lineage tumors expressed these melanocytic markers. Interestingly, the *Prx1*-lineage tumor that did not express *Nestin* also did not express *M-Mitf* or *Tyrosinase*. An additional *Prx1*-lineage tumor failed to express *Tyrosinase* only. This may indicate that between the stem-like state of *Bmi1* expression and the progenitor state of *Prx1* expression *Nestin*, *M-Mitf*, and *Tyrosinase* are epigentically silenced (Figure 2.8B).

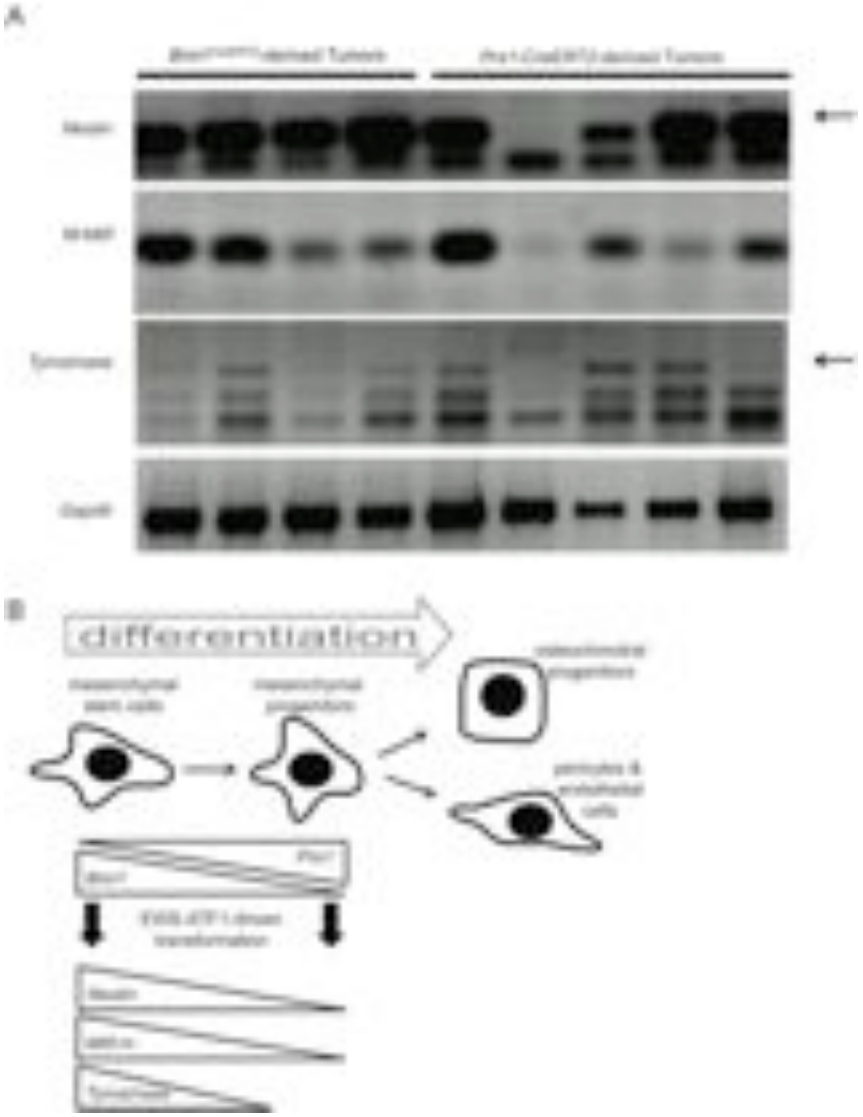


Figure 2.8. Tumors arising from *EWS-ATF1* expression initiated in the *Prx1*- or *Bmi1*-lineage differ by expression profile. (A) RT-PCR analysis of the indicated transcripts on total RNA isolated from *Bmi1*- and *Prx1*-lineage tumors (arrow points to the correct band) (B) Working model of the impact of early differentiation within multipotent mesenchymal progenitors on the possibility of transdifferentiation to express melanocytic markers upon clear cell sarcomagenesis driven by *EWS-ATF1*.

## Discussion

A few mouse genetic models of translocation-associated sarcomas have been expressing *PAX3-FKHR* (Keller et al., 2004a; Keller and Capecchi, 2005; Keller et al., 2004b), myxoid liposarcoma expressing *FUS-CHOP* (Perez-Losada et al., 2000), and synovial sarcoma expressing *SS18-SSX2* (Haldar et al., 2007; Haldar et al., 2009; Haldar et al., 2008). The last of these used means of transcriptional control of the fusion oncogene similar to those used in the current study, with expression in *Cre/loxP* conditional fashion from the *Rosa26* locus. The model of synovial sarcoma also demonstrated fully penetrant tumorigenesis when initiated by $Rosa26^{CreER}$ or Myf5Cre (Haldar et al., 2009). Comparison of the two models highlights the brief latency to tumorigenesis following expression of *EWS-ATF1* initiated by $Rosa26^{CreER}$. The synovial sarcoma model develops tumors after a year, rather than within 3 months. Further, expression of *SS18-SSX2* in most cells, *in vitro* or *in vivo*, was toxic. The very rapid onset of visible tumors in the mouse CCS model relative to synovial sarcoma suggests that fewer additional hits may be required to foster progression of the tumor. This may represent a fundamental difference between the biology of the two fusion oncogenes, as all other aspects of the models are the same.

It has not escaped our notice that the extreme oncogenicity of *EWS-ATF1* in mice contrasts with the rare incidence of formally diagnosed CCS in humans. A potential explanations for this discrepancy is the possibility that EWS-ATF1 involvement in human tumorigenesis remains underappreciated. t(12;22) (q13;q12) chromosomal translocation and resultant fusion oncogenes are identified only when pursued in clinical tumors. The widening range of tumors recently found to bear *EWS-ATF1*, such as

angiomatoid fibrous histiocytoma and clear cell carcinoma of the salivary gland (Antonescu et al., 2011; Chen et al., 2011; Mangham et al., 2010; Ren et al., 2009), suggests that more may yet be identified in the near future. Second, the observed toxicity to embryonic development in the mouse by the early expression of the *EWS-ATF1* fusion gene may greatly limit the acceptable timeframe for the formation of the required t(12;22) chromosomal translocation in humans. Finally, not all balanced chromosomal translocations arise with equal frequency and the formation of the t(12;22) translocation responsible for CCS may be the rate limiting step for this malignancy.

Different cells of origin impacted features of the tumors resulting from *EWS-ATF1* expression. Tumors from both the *Bmi1*- and the *Prx1*- postnatal lineages developed in nearly identical anatomic locations (in the muscle and from the periosteal surface of bones) and fit the histologic appearance of human CCS, but the *Prx1*-lineage tumors did not consistently express the melanocytic markers *M-Mitf*, and *Tyrosinase*. The *M-Mitf*-expressing *Prx1*-lineage tumors fit the general expression signature of human CCS. Those not expressing *M-Mitf* did not. This observation may explain the fact that not all human CCSs clearly express melanoma markers. All four human tumors used for expression profiling were typical, *M-Mitf*-expressing, melanoma-like CCSs. Perhaps the *Prx1*-induced mouse tumor that did not express *M-Mitf* might have fit better with a broader group of human CCSs.

Expression of *Nestin* has previously been reported in human CCS cell lines (Dimas et al., 2008). All *Bmi1*-lineage tumors expressed *Nestin* and the melanocytic markers while variable *Nestin* expression in *Prx1*-lineage tumors predicted expression of the melanocytic markers. *Nestin* has previously been proven to be a marker of stemness

in mesenchyme (Mendez-Ferrer et al., 2010), and overlapped with the *Bmi1*-lineage and partly with the *Prx1*-lineage. This evidence along with the co-labeling experiments showing Prx1 expression within the *Bmi1*-lineage suggests that the differentiation steps between *Bmi1*-expressing cells and *Prx1*-expressing cells include a gradual loss of stemness. The epigenetic state may render the melanocytic markers unavailable for upregulation by ATF constitutive activation alone (Figure 2.8B).

Many have argued in the past about the origin of the melanocytic features of human CCS, variably attributing them to either cell of origin or transformation by *EWS-ATF1*, which also upregulates *M-Mitf*. Although we have not ruled out the possibility that melanocytes or their precursors might also offer sufficient cells of origin, the tumors we have induced in mesenchyme actually bolster both prior arguments. CCS transformation can enable transdifferentiation that includes melanocytic markers, but only from certain cells of origin. Perhaps a cell's reprogrammability, even during aggressive transformation from expression of a powerful fusion oncogene, remains at least partly checked by its antecedent differentiation state.

This mouse model will enable additional dissection of the ATF pathway's impact on oncogenesis *in vivo*. Further, the model is ideally suited to preclinical testing of targeted therapies for this and other CCS pathways. Administration of TAT-Cre produces visible tumors within a few weeks and avoids any pleiotropic developmental effects from toxicity of the fusion oncogene expressed across an entire tissue. These tumors are well-localized, offering a reasonable model for the study of metastasis. Unlike delivery of Cre with a virus, a single molecule of TAT-Cre cannot readily diffuse to a great distance or travel through the blood stream to a distant site and induce recombination, as at least two

molecules of the TAT-Cre protein must enter any given cell to catalyze the recombination event (Joshi et al., 2002).

Due to the low frequency of sarcomas, the most critically scarce resource for developing more effective therapeutic strategies for these malignancies is patients themselves. It is not easy to assemble sufficient numbers of patients for carrying out subtype-specific sarcoma clinical trials. Therapeutic strategies must be optimized and prioritized in the preclinical arena before advancing to clinical trial. Authenticated mouse models could serve this purpose. Genomic sequencing and profiling has vastly increased the ability to test the authenticity of a mouse model's recapitulation of human malignancy. Once established as an excellent facsimile to the human cancer, a mouse model can be used not only to interrogate cancer mechanisms and identify pertinent therapeutic targets, but also as a platform for assessment of drug efficacy. Successful candidate therapeutic strategies could be then moved to human trials with greater assurance of success.

In summary, we have shown that the oncogenic fusion protein that characterizes CCS is sufficient to initiate CCS-like tumors in mice that recapitulate human CCS in terms of cell morphology, immunohistochemistry, and genome-wide expression. This fusion gene generates two distinguishable tumor types in mice that also reflect similar variance in morphology and tissue distribution seen in humans (i.e., principally falling in two classes, those that resemble melanomas because of the expression of *M-Mitf* and its target genes, and those that do not). The apparent difference in cells of origin of these two potential subclasses described herein with mice may provide an explanation of why human CCS commonly, but inconsistently, displays the classical melanocytic features.

## Experimental Procedures

### Targeted Mouse Line Production

Human EWS-ATF1 cDNA was obtained by RT-PCR of total RNA from 8 histologically and immunohistochemically confirmed clear cell sarcoma tumors. The total RNA was obtained as deidentified patient sample through an approved University of Utah Institutional Review Board Protocol. PCR was used to identify tumors that contained the type 1 EWS-ATF1 fusion gene. After screening, the cDNA sample was used to amplify the entire fusion oncogene. The cDNA clone was subcloned into the Rosa26UA plasmid using AscI and Fse1 Sites. This plasmid contained the Loxp-pgk-Neo-tPA-Loxp-AscI-FheI-IRES-EGFP within the *Rosa26* homology arms and the final targeting construct contained Loxp-pgk-Neo-tPA-Loxp-EWS-ATF1-IRES-EGFP. Genotyping protocol and further details on gene targeting used can be found in Supplemental Experimental Procedures.

### Animals, Radiograph, Tissue Preparation, and Immunohistochemistry

All mouse experiments were performed in accordance with humane practices, national and international regulations, and with the approval of the University of Utah Institutional Animal Care and Use committee. Radiographs were obtained post asphyxiation using a Carestream 4000 Pro-Fx instrument (Carestream Molecular Imaging, Woodbridge, Connecticut).

Mouse tumors were extracted after asphyxiation and were fixed overnight in 4% paraformaldehyde prior to embedding in paraffin. Immunostaining and tissue preparation

along with antibodies used are described in the Supplemental Experimental Procedures.

Transcriptome Analysis

A portion of each tumor was snap frozen for delayed total RNA extraction using the Qiagen RNeasy Mini kit (Qiagen, Inc., Valencia, California). RT-PCR was performed with random hexamer primers to generate cDNAs, followed by PCR for specific transcripts (Supplemental Experimental Procedures).

For RNA sequencing, total RNA was prepared using an Illumina TruSeq RNA sample prep kit (Illumina, Inc., San Diego, California) and quality checked with an Agilent Bioanalyzer RNA 6000 chip (Agilent Technologies, Santa Clara, California). mRNAs were captured by oligodT magnetic beads and fragmented. Library quality was then checked by Nanodrop analysis (Thermo Scientific, Wilmington, Delaware), qPCR quantitation using Illumina primers, and another bioanalyzer run. Sequencing was performed on an Illumina HiSeq 2000 machine (Illumina, Inc., San Diego, California) using a 50 cycle single end read. PhiX control library reads were added to each lane for quality assurance. Reads were then aligned with the mm9 mouse genome. Basic clusterings were performed using GeneSifter software (Geospiza, Inc. Seattle, Washington). Method used to classify tumor type using RNA-seq data can be found in the Supplemental Experimental Procedures.

Accession Numbers

The RNA-seq data have been deposited in NCBI's Gene Expression Omnibus (http://www.ncbi.nlm.nih.gov/geo/) and are accessible through the GEO series accession number GSE41293.

Human microarray data have been deposited in NCBI's Gene Expression Omnibus and are accessible through the GEO series accession number GSE43045.

Supplemental Data

The Supplemental Data include Supplemental Experimental Procedures, three supplemental figures, and five supplemental tables.

## Acknowledgements

The authors acknowledge Matt Hockin (University of Utah) for producing the TAT-Cre, Allie Grossmann (University of Utah) for assistance with pathology analysis, Jay S. Wunder and Irene L. Andrulis (University of Toronto) for providing the human CCS samples for isolation of the cDNA, and Brian Dalley and Brett Milash (University of Utah) for assistance with RNA sequencing and analysis. K.M.S. receives graduate student support from the Howard Hughes Med2Grad program. K.B.J. receives career development support from the National Cancer Institute (NIH) K08CA138764K08. This work was partly supported by P30CA042014 from the National Cancer Institute. The content is solely the responsibility of the authors and does not necessarily represent the official views of the National Cancer Institute or the National Institutes of Health.

## References

Antonescu, C. R., Katabi, N., Zhang, L., Sung, Y. S., Seethala, R. R., Jordan, R. C., Perez-Ordonez, B., Have, C., Asa, S. L., Leong, I. T., *et al.* (2011). EWSR1-ATF1 fusion is a novel and consistent finding in hyalinizing clear-cell carcinoma of salivary gland. Genes, chromosomes & cancer *50*, 559-570.

Antonescu, C. R., Tschernyavsky, S. J., Woodruff, J. M., Jungbluth, A. A., Brennan, M.

F., and Ladanyi, M. (2002). Molecular diagnosis of clear cell sarcoma: detection of EWS-ATF1 and M-MITF transcripts and histopathological and ultrastructural analysis of 12 cases. The Journal of molecular diagnostics : JMD *4*, 44-52.

Chen, G., Folpe, A. L., Colby, T. V., Sittampalam, K., Patey, M., Chen, M. G., and Chan, J. K. (2011). Angiomatoid fibrous histiocytoma: unusual sites and unusual morphology. Modern pathology : an official journal of the United States and Canadian Academy of Pathology, Inc *24*, 1560-1570.

Clancy, B. M., Johnson, J. D., Lambert, A. J., Rezvankhah, S., Wong, A., Resmini, C., Feldman, J. L., Leppanen, S., and Pittman, D. D. (2003). A gene expression profile for endochondral bone formation: oligonucleotide microarrays establish novel connections between known genes and BMP-2-induced bone formation in mouse quadriceps. Bone *33*, 46-63.

Claudinot, S., Nicolas, M., Oshima, H., Rochat, A., and Barrandon, Y. (2005). Long-term renewal of hair follicles from clonogenic multipotent stem cells. Proceedings of the National Academy of Sciences of the United States of America *102*, 14677-14682.

Covinsky, M., Gong, S., Rajaram, V., Perry, A., and Pfeifer, J. (2005). EWS-ATF1 fusion transcripts in gastrointestinal tumors previously diagnosed as malignant melanoma. Human pathology *36*, 74-81.

D'Amico, F. E., Ruffolo, C., Romeo, S., Massani, M., Dei Tos, A. P., and Bassi, N. (2011). Clear Cell Sarcoma of the Ileum: Report of a Case and Review of the Literature. International journal of surgical pathology.

Danielian, P. S., Muccino, D., Rowitch, D. H., Michael, S. K., and McMahon, A. P. (1998). Modification of gene activity in mouse embryos in utero by a tamoxifen-inducible form of Cre recombinase. Curr Biol *8*, 1323-1326.

Davis, I. J., Kim, J. J., Ozsolak, F., Widlund, H. R., Rozenblatt-Rosen, O., Granter, S. R., Du, J., Fletcher, J. A., Denny, C. T., Lessnick, S. L.*, et al.* (2006). Oncogenic MITF dysregulation in clear cell sarcoma: defining the MiT family of human cancers. Cancer cell *9*, 473-484.

Dimas, K., Tsimplouli, C., Anagnostopoulos, A. K., Mahaira, L., Iliopoulou, E., Perez, S., Vougas, K., and Tsangaris, G. T. (2008). The proteome profile of two cell lines and their xenografts isolated from a patient with clear cell sarcoma (soft-tissue melanoma). Cancer genomics & proteomics *5*, 175-237.

Durland, J. L., Sferlazzo, M., Logan, M., and Burke, A. C. (2008). Visualizing the lateral somitic frontier in the Prx1Cre transgenic mouse. Journal of anatomy *212*, 590-602.

Engleka, K. A., Gitler, A. D., Zhang, M., Zhou, D. D., High, F. A., and Epstein, J. A. (2005). Insertion of Cre into the Pax3 locus creates a new allele of Splotch and identifies

unexpected Pax3 derivatives. Dev Biol *280*, 396-406.

Enzinger, F. M. (1965). CLEAR-CELL SARCOMA OF TENDONS AND APONEUROSES. AN ANALYSIS OF 21 CASES. Cancer *18*, 1163-1174.

Falconieri, G., Bacchi, C. E., and Luzar, B. (2012). Cutaneous Clear Cell Sarcoma: Report of Three Cases of a Potentially Underestimated Mimicker of Spindle Cell Melanoma. The American Journal of dermatopathology.

Fujimura, Y., Siddique, H., Lee, L., Rao, V. N., and Reddy, E. S. (2001). EWS-ATF-1 chimeric protein in soft-tissue clear cell sarcoma associates with CREB-binding protein and interferes with p53-mediated trans-activation function. Oncogene *20*, 6653-6659.

Granter, S. R., Weilbaecher, K. N., Quigley, C., Fletcher, C. D., and Fisher, D. E. (2001). Clear cell sarcoma shows immunoreactivity for microphthalmia transcription factor: further evidence for melanocytic differentiation. Modern pathology : an official journal of the United States and Canadian Academy of Pathology, Inc *14*, 6-9.

Haldar, M., Hancock, J. D., Coffin, C. M., Lessnick, S. L., and Capecchi, M. R. (2007). A conditional mouse model of synovial sarcoma: insights into a myogenic origin. Cancer Cell *11*, 375-388.

Haldar, M., Hedberg, M. L., Hockin, M. F., and Capecchi, M. R. (2009). A CreER-based random induction strategy for modeling translocation-associated sarcomas in mice. Cancer Res *69*, 3657-3664.

Haldar, M., Randall, R. L., and Capecchi, M. R. (2008). Synovial sarcoma: from genetics to genetic-based animal modeling. Clinical orthopaedics and related research *466*, 2156-2167.

Hantschke, M., Mentzel, T., Rutten, A., Palmedo, G., Calonje, E., Lazar, A. J., and Kutzner, H. (2010). Cutaneous clear cell sarcoma: a clinicopathologic, immunohistochemical, and molecular analysis of 12 cases emphasizing its distinction from dermal melanoma. The American journal of surgical pathology *34*, 216-222.

Hasson, P., Del Buono, J., and Logan, M. P. (2007). Tbx5 is dispable for forelimb outgrowth. Development *134*, 85-92.

Hocar, O., Le Cesne, A., Berissi, S., Terrier, P., Bonvalot, S., Vanel, D., Auperin, A., Le Pechoux, C., Bui, B., Coindre, J. M., and Robert, C. (2012). Clear cell sarcoma (malignant melanoma) of soft parts: a clinicopathologic study of 52 cases. Dermatology research and practice *2012*, 984096.

Huang da, W., Sherman, B. T., and Lempicki, R. A. (2009a). Bioinformatics enrichment tools: paths toward the comprehive functional analysis of large gene lists. Nucleic acids research *37*, 1-13.

Huang da, W., Sherman, B. T., and Lempicki, R. A. (2009b). Systematic and integrative analysis of large gene lists using DAVID bioinformatics resources. Nature protocols *4*, 44-57.

Joshi, S. K., Hashimoto, K., and Koni, P. A. (2002). Induced DNA recombination by Cre recombinase protein transduction. Genesis *33*, 48-54.

Kawanami, A., Matsushita, T., Chan, Y. Y., and Murakami, S. (2009). Mice expressing GFP and CreER in osteochondro progenitor cells in the periosteum. Biochemical and biophysical research communications *386*, 477-482.

Keller, C., Arenkiel, B. R., Coffin, C. M., El-Bardeesy, N., DePinho, R. A., and Capecchi, M. R. (2004a). Alveolar rhabdomyosarcomas in conditional Pax3:Fkhr mice: cooperativity of Ink4a/ARF and Trp53 loss of function. Genes & development *18*, 2614-2626.

Keller, C., and Capecchi, M. R. (2005). New genetic tactics to model alveolar rhabdomyosarcoma in the mouse. Cancer research *65*, 7530-7532.

Keller, C., Hansen, M. S., Coffin, C. M., and Capecchi, M. R. (2004b). Pax3:Fkhr interferes with embryonic Pax3 and Pax7 function: implications for alveolar rhabdomyosarcoma cell of origin. Genes & development *18*, 2608-2613.

Kisanuki, Y. Y., Hammer, R. E., Miyazaki, J., Williams, S. C., Richardson, J. A., and Yanagisawa, M. (2001). Tie2-Cre transgenic mice: a new model for endothelial cell-lineage analysis in vivo. Dev Biol *230*, 230-242.

Kovacevic, A., Hammer, A., Stadelmeyer, E., Windischhofer, W., Sundl, M., Ray, A., Schweighofer, N., Friedl, G., Windhager, R., Sattler, W., and Malle, E. (2008). Expression of serum amyloid A transcripts in human bone tissues, differentiated osteoblast-like stem cells and human osteosarcoma cell lines. Journal of cellular biochemistry *103*, 994-1004.

Leung, C., Lingbeek, M., Shakhova, O., Liu, J., Tanger, E., Saremaslani, P., Van Lohuizen, M., and Marino, S. (2004). Bmi1 is essential for cerebellar development and is overexpressed in human medulloblastomas. Nature *428*, 337-341.

Logan, M., Martin, J. F., Nagy, A., Lobe, C., Olson, E. N., and Tabin, C. J. (2002). Expression of Cre Recombinase in the developing mouse limb bud driven by a Prxl enhancer. Genesis *33*, 77-80.

Lyle, P. L., Amato, C. M., Fitzpatrick, J. E., and Robinson, W. A. (2008). Gastrointestinal melanoma or clear cell sarcoma? Molecular evaluation of 7 cases previously diagnosed as malignant melanoma. The American journal of surgical pathology *32*, 858-866.

Mangham, D. C., Williams, A., Lalam, R. K., Brundler, M. A., Leahy, M. G., and Cool, W. P. (2010). Angiomatoid fibrous histiocytoma of bone: a calcifying sclerosing variant mimicking osteosarcoma. The American journal of surgical pathology *34*, 279-285.

Mao, X., Fujiwara, Y., and Orkin, S. H. (1999). Improved reporter strain for monitoring Cre recombinase-mediated DNA excisions in mice. Proceedings of the National Academy of Sciences of the United States of America *96*, 5037-5042.

Mendez-Ferrer, S., Michurina, T. V., Ferraro, F., Mazloom, A. R., Macarthur, B. D., Lira, S. A., Scadden, D. T., Ma'ayan, A., Enikolopov, G. N., and Frenette, P. S. (2010). Mesenchymal and haematopoietic stem cells form a unique bone marrow niche. Nature *466*, 829-834.

Murphy, M. M., Lawson, J. A., Mathew, S. J., Hutcheson, D. A., and Kardon, G. (2011). Satellite cells, connective tissue fibroblasts and their interactions are crucial for muscle regeneration. Development (Cambridge, England) *138*, 3625-3637.

Muzumdar, M. D., Tasic, B., Miyamichi, K., Li, L., and Luo, L. (2007). A global double-fluorescent Cre reporter mouse. Genesis *45*, 593-605.

Nielsen, T. O., West, R. B., Linn, S. C., Alter, O., Knowling, M. A., O'Connell, J. X., Zhu, S., Fero, M., Sherlock, G., Pollack, J. R.*, et al.* (2002). Molecular characterisation of soft-tissue tumours: a gene expression study. Lancet *359*, 1301-1307.

Park, I. K., Qian, D., Kiel, M., Becker, M. W., Pihalja, M., Weissman, I. L., Morrison, S. J., and Clarke, M. F. (2003). Bmi-1 is required for maintenance of adult self-renewing haematopoietic stem cells. Nature *423*, 302-305.

Perez-Losada, J., Pintado, B., Gutierrez-Adan, A., Flores, T., Banares-Gonzalez, B., del Campo, J. C., Martin-Martin, J. F., Battaner, E., and Sanchez-Garcia, I. (2000). The chimeric FUS/TLS-CHOP fusion protein specifically induces liposarcomas in transgenic mice. Oncogene *19*, 2413-2422.

Ren, L., Guo, S. P., Zhou, X. G., and Chan, J. K. (2009). Angiomatoid fibrous histiocytoma: first report of primary pulmonary origin. The American journal of surgical pathology *33*, 1570-1574.

Robson, L. G., Di Foggia, V., Radunovic, A., Bird, K., Zhang, X., and Marino, S. (2011). Bmi1 is expressed in postnatal myogenic satellite cells, controls their maintenance and plays an essential role in repeated muscle regeneration. PloS one *6*, e27116.

Sangiorgi, E., and Capecchi, M. R. (2008). Bmi1 is expressed in vivo in intestinal stem cells. Nature genetics *40*, 915-920.

Somers, G. R., Viero, S., Nathan, P. C., Teshima, I., Pereira, C., and Zielka, M. (2005). Association of the t(12;22)(q13;q12) EWS/ATF1 rearrangement with polyphenotypic

round cell sarcoma of bone: a case report. The American journal of surgical pathology *29*, 1673-1679.

Wang, W. L., Mayordomo, E., Zhang, W., Hernandez, V. S., Tuvin, D., Garcia, L., Lev, D. C., Lazar, A. J., and Lopez-Terrada, D. (2009). Detection and characterization of EWSR1/ATF1 and EWSR1/CREB1 chimeric transcripts in clear cell sarcoma (melanoma of soft parts). Modern pathology : an official journal of the United States and Canadian Academy of Pathology, Inc *22*, 1201-1209.

Zhang, H. W., Ding, J., Jin, J. L., Guo, J., Liu, J. N., Karaplis, A., Goltzman, D., and Miao, D. (2010). Defects in mesenchymal stem cell self-renewal and cell fate determination lead to an osteopenic phenotype in Bmi-1 null mice. Journal of bone and mineral research : the official journal of the American Society for Bone and Mineral Research *25*, 640-652.

Supplemental Material

Supplemental Table 1

Dysregulated genes from *RosaCreER* tumors to control mesenchyme

| #DisplayName | Name | Chr | BH_FDR_VarOutFilt | Log2Ratio |
|---|---|---|---|---|
| MUSG00000048636 | A730049H | chr6 | 487.5802 | 8.508934 |
| MUSG00000020000 | Moxd1 | chr10 | 480.18414 | 8.048805 |
| MUSG00000026247 | Ecel1 | chr1 | 380.29922 | 7.308377 |
| MUSG00000044951 | Mylk4 | chr13 | 370.76764 | -6.3523226 |
| MUSG00000033717 | Adra2a | chr19 | 358.08832 | 6.593305 |
| MUSG00000033350 | Chst2 | chr9 | 351.956 | 6.4737024 |
| MUSG00000022296 | Baalc | chr15 | 336.02307 | 6.6612577 |
| MUSG00000054934 | Kcnmb4 | chr10 | 325.54507 | 6.8758116 |
| MUSG00000041737 | Tmem45b | chr9 | 323.50125 | -7.281594 |
| MUSG00000015981 | Stk32c | chr7 | 320.8254 | 6.0321503 |
| MUSG00000024011 | Pi16 | chr17 | 320.15665 | 5.3523307 |
| MUSG00000028072 | Ntrk1 | chr3 | 320.15665 | 6.1623497 |
| MUSG00000073375 | Lrrc30 | chr17 | 320.15665 | -5.0029926 |
| MUSG00000030546 | Plin1 | chr7 | 319.28293 | -6.5906067 |
| MUSG00000021700 | Rab3c | chr13 | 311.0993 | 8.106302 |
| MUSG00000003279 | Dlgap1 | chr17 | 304.06097 | 5.8167896 |
| MUSG00000031489 | Adrb3 | chr8 | 301.8349 | -5.755275 |
| MUSG00000031538 | Plat | chr8 | 298.72815 | 6.020567 |
| MUSG00000074264 | Amy1 | chr3 | 293.43936 | -5.1407065 |
| MUSG00000001510 | Dlx3 | chr11 | 288.179 | 6.729669 |
| MUSG00000019539 | Rcn3 | chr7 | 286.569 | 5.237727 |
| MUSG00000027470 | Mylk2 | chr2 | 286.40793 | -5.069202 |
| MUSG00000021508 | Cxcl14 | chr13 | 284.1306 | 5.5428596 |
| MUSG00000021898 | Asb14 | chr14 | 282.11258 | -5.181327 |
| MUSG00000030730 | Atp2a1 | chr7 | 277.18924 | -3.869698 |
| MUSG00000031382 | Asb11 | chrX | 275.66095 | -4.224964 |
| MUSG00000049134 | Nrap | chr19 | 275.43213 | 7277577 |
| MUSG00000029544 | Cabp1 | chr5 | 274.6313 | 4.9407372 |

Supplemental Table 1 Continued

| #DisplayName | Name | Chr | BH_FDR_VarOutFilt | Log2Ratio |
|---|---|---|---|---|
| MUSG00000047746 | Fbxo40 | chr16 | 271.91275 | -4.0054646 |
| MUSG00000034981 | Parm1 | chr5 | 268.62863 | 4.9151974 |
| MUSG00000056632 | Dsg3 | chr18 | 268.5755 | 6.257076 |
| MUSG00000081683 | Fzd10 | chr5 | 267.09747 | 5.270862 |
| MUSG00000028396 | 2310002L09Rik | chr4 | 266.60492 | -4.3342896 |
| MUSG00000020067 | Mypn | chr10 | 264.77475 | -4.107181 |
| MUSG00000006457 | Actn3 | chr19 | 264.77475 | -4.239534 |
| MUSG00000070561 | Kcnj11 | chr7 | 262.76276 | -5.192804 |
| MUSG00000025089 | Gfra1 | chr19 | 260.2715 | 4.7128496 |
| MUSG00000073530 | Pappa2 | chr1 | 256.12085 | 6.1933675 |
| MUSG00000033595 | Lgi3 | chr14 | 256.12085 | 5.1362867 |
| MUSG00000053279 | Aldh1a1 | chr19 | 256.12085 | -3.799156 |
| MUSG00000031519 | Asb5 | chr8 | 255.83704 | -3.4651434 |
| MUSG00000027513 | Pck1 | chr2 | 255.41393 | -7.378881 |
| MUSG00000062077 | Trim54 | chr5 | 254.98772 | -3.8898075 |
| MUSG00000026418 | Tnni1 | chr1 | 253.77046 | -4.4820924 |
| MUSG00000032495 | Lrrc2 | chr9 | 253.3548 | -3.8658276 |
| MUSG00000044918 | AC122466.1 | chr5 | 252.4963 | -3.8131616 |
| MUSG00000005237 | Dnahc2 | chr11 | 252.17702 | 5.0860724 |
| MUSG00000024471 | Myot | chr18 | 251.83801 | -3.637672 |
| MUSG00000042638 | Gucy2c | chr6 | 251.61998 | 6.048879 |
| MUSG00000032717 | Mdfi | chr17 | 250.79628 | 4.907887 |
| MUSG00000022490 | Ppp1r1a | chr15 | 249.76688 | -3.1289558 |
| MUSG00000032648 | Pygm | chr19 | 249.26892 | -3.7824817 |
| MUSG00000030399 | Ckm | chr7 | 247.59552 | -3.5535975 |
| MUSG00000034472 | Rasd2 | chr8 | 247.47748 | -5.5839987 |
| MUSG00000072720 | Myo18b | chr5 | 246.99503 | -6.4021235 |
| MUSG00000007097 | Atp1a2 | chr1 | 246.64458 | -3.4054813 |
| MUSG00000034164 | Emid1 | chr11 | 245.89084 | 5.1213684 |
| MUSG00000059741 | Myl3 | chr9 | 245.89084 | -3.577375 |
| MUSG00000025279 | Dnase1l3 | chr14 | 242.90636 | 6.589141 |
| MUSG00000023484 | Prph | chr15 | 240.10432 | 4.615322 |
| MUSG00000063434 | Sorcs3 | chr19 | 239.5735 | 7.672165 |
| MUSG00000020007 | Il20ra | chr10 | 237.1167 | 6.1824985 |

Supplemental Table 1 Continued

| #DisplayName | Name | Chr | BH_FDR_VarOut Filt | Log2Ratio |
|---|---|---|---|---|
| MUSG00000022440 | C1qtnf6 | chr15 | 236.69069 | 4.137205 |
| MUSG00000016349 | Eef1a2 | chr2 | 235.40964 | -3.4299123 |
| MUSG00000020871 | Dlx4 | chr11 | 235.23553 | 5.0911536 |
| MUSG00000008658 | A2bp1 | chr16 | 235.23553 | -4.17637 |
| MUSG00000027932 | Slc27a3 | chr3 | 234.68805 | 4.7569885 |
| MUSG00000011148 | Adssl1 | chr12 | 233.4765 | -3.8315296 |
| MUSG00000029683 | Lmod2 | chr6 | 233.38545 | -3.1519678 |
| MUSG00000043122 | A530016L24Rik | chr12 | 232.52924 | -4.6765566 |
| MUSG00000078815 | Cacng6 | chr7 | 230.2141 | -3.6743655 |
| MUSG00000066687 | Zbtb16 | chr9 | 229.9002 | -4.9372206 |
| MUSG00000013936 | Myl2 | chr5 | 228.52686 | -3.3076627 |
| MUSG00000029658 | 4930434E21Rik | chr5 | 226.77449 | 4.8859544 |
| MUSG00000001508 | Sgca | chr11 | 226.6507 | -3.6371195 |
| MUSG00000021909 | Tnnc1 | chr14 | 226.54567 | -4.385018 |
| MUSG00000045731 | Pnoc | chr14 | 225.96626 | 7.9276757 |
| MUSG00000067653 | Ankrd23 | chr1 | 225.62358 | -3.5831268 |
| MUSG00000033182 | Klhdc6 | chr6 | 225.0529 | -4.489414 |
| MUSG00000031465 | Angpt2 | chr8 | 224.64398 | 5.1902056 |
| MUSG00000039883 | Lrrc17 | chr5 | 224.24094 | 4.1970134 |
| MUSG00000040740 | Slc25a34 | chr4 | 224.05902 | -3.9280937 |
| MUSG00000075307 | Kbtbd10 | chr2 | 223.45564 | -3.2167172 |
| MUSG00000028773 | Fabp3 | chr4 | 223.23387 | -3.7450953 |
| MUSG00000000938 | Hoxa10 | chr6 | 223.23387 | 4.2750225 |
| MUSG00000056366 | AC152453.2 | chr10 | 223.05965 | -3.907881 |
| MUSG00000002588 | Pon1 | chr6 | 218.91219 | -5.7318826 |
| MUSG00000053675 | Tgm5 | chr2 | 218.56955 | 6.6077943 |
| MUSG00000070577 | RP23-331P21.1 | chr4 | 217.84714 | -4.160675 |
| MUSG00000001555 | Fkbp10 | chr11 | 217.75108 | 4.3323402 |
| MUSG00000033998 | Kcnk1 | chr8 | 217.43677 | 6.337978 |
| MUSG00000024972 | Lgals12 | chr19 | 216.70924 | -4.6357517 |
| MUSG00000056900 | Usp13 | chr3 | 216.4425 | -3.6007102 |
| MUSG00000021573 | Tppp | chr13 | 215.90805 | -4.384508 |
| MUSG00000018796 | Acsl1 | chr8 | 215.42184 | -3.6346068 |
| MUSG00000028348 | Murc | chr4 | 187.42012 | -3.5817485 |
| MUSG00000024049 | Myom1 | chr17 | 179.63863 | -3.8796365 |

Supplemental Table 1 Continued

| #DisplayName | Name | Chr | BH_FDR_VarOut Filt | Log2Ratio |
|---|---|---|---|---|
| MUSG00000036298 | Slc2a13 | chr15 | 213.87697 | 4.625506 |
| MUSG00000022510 | Trp63 | chr16 | 213.8185 | -4.1744146 |
| MUSG00000079662 | Ntn3 | chr17 | 213.8122 | 4.435866 |
| MUSG00000030087 | Klf15 | chr6 | 213.57721 | -3.9553843 |
| MUSG00000085888 | AL596127.1 | chr11 | 213.57721 | -3.9765482 |
| MUSG00000024424 | Ttc39c | chr18 | 213.57721 | 4.509438 |
| MUSG00000035963 | Odf3l2 | chr10 | 212.5474 | -3.3703911 |
| MUSG00000031791 | Tmem38a | chr8 | 212.5052 | -3.6412983 |
| MUSG00000040705 | A930016O22 | chr7 | 209.94919 | -3.0145135 |
| MUSG00000035923 | Myf6 | chr10 | 209.69392 | -2.986141 |
| MUSG00000061723 | Tnnt3 | chr7 | 209.51656 | -3.008223 |
| MUSG00000015568 | Lpl | chr8 | 209.29007 | -4.4366355 |
| MUSG00000029552 | Tes | chr6 | 208.41597 | 4.0548263 |
| MUSG00000025592 | Dach2 | chrX | 208.38301 | -5.1109314 |
| MUSG00000034310 | Tmem132d | chr5 | 207.74046 | 5.243197 |
| MUSG00000022844 | Pdia5 | chr16 | 207.61292 | 4.7393265 |
| MUSG00000028427 | Aqp7 | chr4 | 207.30656 | -3.879792 |
| MUSG00000022237 | Ankrd33b | chr15 | 207.24948 | -3.6740572 |
| MUSG00000024909 | Efemp2 | chr19 | 207.2182 | 3.8995125 |
| MUSG00000022357 | Klhl38 | chr15 | 207.0389 | -4.933534 |
| MUSG00000032431 | Crtap | chr9 | 206.87576 | 4.4756474 |
| MUSG00000053194 | Cib4 | chr5 | 205.4891 | 4.94893 |
| MUSG00000006800 | Sulf2 | chr2 | 205.4891 | 4.217456 |
| MUSG00000025911 | Adhfe1 | chr1 | 204.19116 | -4.492567 |
| MUSG00000024747 | Aldh1a7 | chr19 | 204.19116 | -4.481659 |
| MUSG00000031204 | Asb12 | chrX | 203.92229 | -3.503943 |
| MUSG00000046585 | Ccdc147 | chr19 | 203.46303 | 4.9554834 |
| MUSG00000001281 | Itgb7 | chr15 | 203.12039 | 4.7575765 |
| MUSG00000085493 | AC109608.1 | chr5 | 201.82484 | -3.073761 |
| MUSG00000034591 | Slc41a2 | chr10 | 201.79552 | 4.814822 |
| MUSG00000001131 | Timp1 | chrX | 201.4039 | 3.7572412 |
| MUSG00000036040 | Adamtsl2 | chr2 | 201.05252 | 4.029011 |
| MUSG00000021579 | Lrrc14b | chr13 | 200.99107 | -4.881723 |
| MUSG00000022790 | Igsf11 | chr16 | 200.94711 | 4.724098 |
| MUSG00000086298 | AL645687.1 | chr11 | 200.81288 | -3.215664 |

Supplemental Table 1 Continued

| #DisplayName | Name | Chr | BH_FDR_VarOut Filt | Log2Ratio |
|---|---|---|---|---|
| MUSG00000010492 | AL844529.1 | chr2 | 200.60922 | -4.1871786 |
| MUSG00000031097 | Tnni2 | chr7 | 200.5983 | -2.902014 |
| MUSG00000004885 | Crabp2 | chr3 | 199.9851 | 6.0561423 |
| MUSG00000032262 | Elovl4 | chr9 | 199.39642 | 4.4088526 |
| MUSG00000061780 | Cfd | chr10 | 198.03387 | -6.721265 |
| MUSG00000007107 | Atp1a4 | chr1 | 197.93828 | -3.5941033 |
| MUSG00000044499 | Hs3st5 | chr10 | 197.14946 | -4.0188565 |
| MUSG00000053199 | Arhgap20 | chr9 | 196.36145 | -3.8054554 |
| MUSG00000001333 | Sync | chr4 | 195.88353 | -4.2720866 |
| MUSG00000028116 | Myoz2 | chr3 | 195.88353 | -2.504497 |
| MUSG00000034127 | Tspan8 | chr10 | 195.64609 | -3.7243423 |
| MUSG00000042895 | Abra | chr15 | 195.4459 | -2.5107687 |
| MUSG00000041476 | Smpx | chrX | 195.36908 | -2.8672905 |
| MUSG00000021238 | Aldh6a1 | chr12 | 194.95695 | -2.9864573 |
| MUSG00000039323 | Igfbp2 | chr1 | 194.49142 | 6.337668 |
| MUSG00000006221 | Hspb7 | chr4 | 194.29236 | -2.7313786 |
| MUSG00000030672 | Mylpf | chr7 | 194.12343 | -2.5271173 |
| MUSG00000033576 | Apol6 | chr15 | 194.12343 | -3.4293156 |
| MUSG00000026208 | Des | chr1 | 194.06015 | -2.789014 |
| MUSG00000020593 | Lpin1 | chr12 | 193.75479 | -3.404712 |
| MUSG00000085779 | AC155932.2 | chr10 | 193.5945 | -3.4852865 |
| MUSG00000043639 | Rbm20 | chr19 | 193.3198 | -4.1965566 |
| MUSG00000026489 | Cabc1 | chr1 | 193.20584 | -3.7354646 |
| MUSG00000031952 | Chst5 | chr8 | 193.14217 | 4.8222823 |
| MUSG00000026564 | Dusp27 | chr1 | 191.1846 | -3.0644398 |
| MUSG00000039891 | Txlnb | chr10 | 190.79266 | -4.5875497 |
| MUSG00000075707 | Dio3 | chr12 | 190.5655 | 5.216036 |
| MUSG00000038670 | Mybpc2 | chr7 | 190.42168 | -3.726841 |
| MUSG00000019852 | D10Bwg1379 | chr10 | 190.13094 | 5.5388694 |
| MUSG00000066113 | Adamtsl1 | chr4 | 189.67055 | 3.846046 |
| MUSG00000056973 | Ces3 | chr8 | 189.54007 | -6.525118 |
| MUSG00000070436 | Serpinh1 | chr7 | 189.26395 | 3.622658 |
| MUSG00000038763 | Alpk3 | chr7 | 188.64099 | -4.4072165 |
| MUSG00000004558 | Ndrg2 | chr14 | 188.6355 | -3.2423582 |
| MUSG00000079434 | Neu2 | chr1 | 188.32147 | -2.9948566 |

Supplemental Table 1 Continued

| #DisplayName | Name | Chr | BH_FDR_VarOut Filt | Log2Ratio |
|---|---|---|---|---|
| MUSG00000022098 | Bmp1 | chr14 | 185.8586 | 3.6008914 |
| MUSG00000073600 | Gm1614 | chr18 | 185.57263 | -3.5751438 |
| MUSG00000061877 | BC048679 | chr7 | 185.23454 | -4.8752084 |
| MUSG00000020695 | Mrc2 | chr11 | 185.23454 | 3.448641 |
| MUSG00000071540 | CT009541.1 | chr14 | 185.19316 | -4.2355247 |
| MUSG00000032719 | Gm106 | chr1 | 184.7214 | 4.3092384 |
| MUSG00000030317 | Timp4 | chr6 | 184.66367 | -1.85609 |
| MUSG00000027895 | Kcnc4 | chr3 | 184.51306 | -3.279609 |
| MUSG00000059974 | Ntm | chr9 | 184.51306 | 4.387507 |
| MUSG00000022747 | St3gal6 | chr16 | 184.10413 | -3.295076 |
| MUSG00000030495 | Slc7a10 | chr7 | 183.44142 | -3.9611976 |
| MUSG00000054162 | Spock3 | chr8 | 183.34132 | 4.145957 |
| MUSG00000023191 | Leprel2 | chr6 | 183.16028 | 3.6686528 |
| MUSG00000039579 | Grin3a | chr4 | 182.8071 | 5.1591344 |
| MUSG00000054314 | AC135017.1 | chr1 | 182.73393 | -4.170439 |
| MUSG00000085837 | AC139376.3 | chr10 | 182.45853 | 4.2495193 |
| MUSG00000038552 | Fndc4 | chr5 | 182.11572 | 3.8219244 |
| MUSG00000025932 | Eya1 | chr1 | 181.89449 | -4.001165 |
| MUSG00000071547 | Nt5dc2 | chr14 | 180.6342 | 3.6890478 |

Supplemental Table 2

Top 200 dysregulated genes from TAT-Cre to control mesenchyme

| #DisplayName | Name | Chr | BH_FDR_VarOutFilt | Log2Ratio |
|---|---|---|---|---|
| MUSG00000039728 | Slc6a5 | chr7 | 695.32056 | 9.748271 |
| MUSG00000033717 | Adra2a | chr19 | 501.55576 | 7.923036 |
| MUSG00000029544 | Cabp1 | chr5 | 487.98743 | 7.388971 |
| MUSG00000031489 | Adrb3 | chr8 | 463.02866 | -5.952426 |
| MUSG00000041737 | Tmem45b | chr9 | 419.05856 | -5.7590013 |
| MUSG00000054934 | Kcnmb4 | chr10 | 418.05173 | 6.8791113 |
| MUSG00000046321 | Hs3st2 | chr7 | 398.83743 | 8.735553 |
| MUSG00000035963 | Odf3l2 | chr10 | 374.50806 | -5.636129 |
| MUSG00000020264 | Slc36a2 | chr11 | 345.07883 | -3.982498 |
| MUSG00000042717 | Ppp1r3a | chr6 | 339.90778 | -3.2681649 |
| MUSG00000074264 | Amy1 | chr3 | 335.79572 | -3.474454 |
| MUSG00000024972 | Lgals12 | chr19 | 335.25778 | -3.9306924 |
| MUSG00000068697 | Myoz1 | chr14 | 335.0342 | -3.1408453 |
| MUSG00000028396 | 2310002L09Rik | chr4 | 331.21973 | -3.2354274 |
| MUSG00000031382 | Asb11 | chrX | 329.85007 | -2.7583697 |
| MUSG00000044951 | Mylk4 | chr13 | 327.7272 | -2.5913801 |
| MUSG00000030546 | Plin1 | chr7 | 325.90692 | -4.323547 |
| MUSG00000021456 | Fbp2 | chr13 | 325.90692 | -3.057298 |
| MUSG00000031097 | Tnni2 | chr7 | 319.28357 | -2.8845527 |
| MUSG00000041046 | Ramp3 | chr11 | 313.1104 | 6.740988 |
| MUSG00000022296 | Baalc | chr15 | 308.18652 | 5.8349915 |
| MUSG00000027513 | Pck1 | chr2 | 306.77353 | -6.080129 |
| MUSG00000061723 | Tnnt3 | chr7 | 305.761 | -2.733902 |
| MUSG00000027792 | Bche | chr3 | 303.31223 | -3.874257 |
| MUSG00000020000 | Moxd1 | chr10 | 298.25275 | 8.371794 |
| MUSG00000041592 | Sdk2 | chr11 | 298.25275 | 6.731137 |
| MUSG00000078234 | Klhdc7a | chr4 | 298.25275 | -4.297958 |
| MUSG00000022490 | Ppp1r1a | chr15 | 294.59436 | -1.9532316 |
| MUSG00000073375 | Lrrc30 | chr17 | 291.04276 | -2.137593 |
| MUSG00000035095 | Fam167a | chr14 | 289.75995 | 5.426114 |
| MUSG00000031284 | Pak3 | chrX | 289.22336 | 4.618136 |
| MUSG00000053279 | Aldh1a1 | chr19 | 287.717 | -2.4878745 |
| MUSG00000021448 | Shc3 | chr13 | 287.38525 | 5.8656516 |

Supplemental Table 2 Continued

| #DisplayName | Name | Chr | BH_FDR_VarOutFilt | Log2Ratio |
|---|---|---|---|---|
| MUSG00000034127 | Tspan8 | chr10 | 276.24612 | -2.7089212 |
| MUSG00000022747 | St3gal6 | chr16 | 273.5672 | -2.733389 |
| MUSG00000025089 | Gfra1 | chr19 | 270.04758 | 4.5787997 |
| MUSG00000018796 | Acsl1 | chr8 | 265.40552 | -2.3866332 |
| MUSG00000009097 | Tbx1 | chr16 | 265.37695 | -3.7160244 |
| MUSG00000043122 | A530016L24Rik | chr12 | 265.37695 | -3.7926533 |
| MUSG00000028464 | Tpm2 | chr4 | 264.9648 | -2.1793914 |
| MUSG00000006800 | Sulf2 | chr2 | 264.24286 | 4.75812 |
| MUSG00000020164 | 1700058G18Rik | chr10 | 262.26566 | 5.176994 |
| MUSG00000002588 | Pon1 | chr6 | 262.13806 | -5.70244 |
| MUSG00000023191 | Leprel2 | chr6 | 258.44067 | 4.3983436 |
| MUSG00000000567 | Sox9 | chr11 | 258.2816 | 4.6242256 |
| MUSG00000022235 | Cmbl | chr15 | 257.44235 | -3.4317958 |
| MUSG00000040181 | Fmo1 | chr1 | 255.56738 | -1.9216794 |
| MUSG00000030399 | Ckm | chr7 | 252.44913 | -2.3285868 |
| MUSG00000031204 | Asb12 | chrX | 252.40158 | -2.7090862 |
| MUSG00000032648 | Pygm | chr19 | 251.49156 | -2.6745157 |
| MUSG00000055125 | C2cd4b | chr9 | 251.14946 | 5.6696815 |
| MUSG00000032640 | Chsy1 | chr7 | 250.93301 | 5.142914 |
| MUSG00000033350 | Chst2 | chr9 | 250.49149 | 6.249664 |
| MUSG00000062329 | Cytl1 | chr5 | 247.75082 | -3.2811992 |
| MUSG00000028427 | Aqp7 | chr4 | 247.54716 | -2.7005918 |
| MUSG00000033900 | Mtap9 | chr3 | 246.99413 | 5.091521 |
| MUSG00000086429 | AC155722.2 | chr6 | 246.8797 | -3.6064801 |
| MUSG00000033576 | Apol6 | chr15 | 246.49896 | -2.517058 |
| MUSG00000024471 | Myot | chr18 | 244.4173 | -2.5417118 |
| MUSG00000024747 | Aldh1a7 | chr19 | 243.12596 | -3.303781 |
| MUSG00000021573 | Tppp | chr13 | 241.50938 | -3.7290323 |
| MUSG00000054863 | AC123925.1 | chr15 | 241.08868 | 4.91942 |
| MUSG00000026688 | Mgst3 | chr1 | 240.5575 | -2.1721818 |
| MUSG00000055421 | Pcdh9 | chr14 | 238.92775 | 5.6450276 |
| MUSG00000020774 | Aspa | chr11 | 237.70683 | -3.417474 |
| MUSG00000002997 | Prkar2b | chr12 | 235.99165 | -3.0752368 |
| MUSG00000028572 | Hook1 | chr4 | 235.91614 | -1.5910404 |
| MUSG00000022237 | Ankrd33b | chr15 | 162.66501 | -1.4590746 |
| MUSG00000011148 | Adssl1 | chr12 | 234.64519 | -2.3008068 |

Supplemental Table 2 Continued

| #DisplayName | Name | Chr | BH_FDR_VarOutFil | Log2Ratio |
|---|---|---|---|---|
| MUSG00000040740 | Slc25a34 | chr4 | 233.72208 | -2.8050847 |
| MUSG00000032845 | Alpk2 | chr18 | 232.1026 | -3.027931 |
| MUSG00000086373 | AL603787.4 | chr11 | 231.42502 | 7.3561726 |
| MUSG00000028773 | Fabp3 | chr4 | 231.42502 | -2.693085 |
| MUSG00000030730 | Atp2a1 | chr7 | 230.86472 | -1.5225446 |
| MUSG00000078815 | Cacng6 | chr7 | 230.45076 | -1.9623677 |
| MUSG00000056366 | AC152453.2 | chr10 | 230.2809 | -2.7704766 |
| MUSG00000007097 | Atp1a2 | chr1 | 229.03056 | -1.4771129 |
| MUSG00000086552 | AL645850.2 | chr11 | 228.26184 | 5.573143 |
| MUSG00000044499 | Hs3st5 | chr10 | 225.4451 | -3.1350167 |
| MUSG00000021898 | Asb14 | chr14 | 224.94147 | -2.2751503 |
| MUSG00000056973 | Ces3 | chr8 | 224.68773 | -5.56713 |
| MUSG00000086298 | AL645687.1 | chr11 | 224.60306 | -1.8817327 |
| MUSG00000041476 | Smpx | chrX | 224.54385 | -2.5846179 |
| MUSG00000046186 | Cd109 | chr9 | 224.32643 | 4.649976 |
| MUSG00000047250 | Ptgs1 | chr2 | 223.09773 | 4.2215476 |
| MUSG00000015568 | Lpl | chr8 | 222.59981 | -2.8926902 |
| MUSG00000024085 | Man2a1 | chr17 | 221.98627 | 4.1042943 |
| MUSG00000030317 | Timp4 | chr6 | 221.97661 | -1.6823303 |
| MUSG00000030672 | Mylpf | chr7 | 221.61629 | -2.1738992 |
| MUSG00000011305 | Plin5 | chr17 | 219.9586 | -3.1480775 |
| MUSG00000025271 | Pfkfb1 | chrX | 219.32445 | -4.1595488 |
| MUSG00000016349 | Eef1a2 | chr2 | 218.61314 | -1.5615479 |
| MUSG00000025592 | Dach2 | chrX | 217.89972 | -3.2607534 |
| MUSG00000061780 | Cfd | chr10 | 217.87999 | -4.640636 |
| MUSG00000032431 | Crtap | chr9 | 215.98528 | 3.917808 |
| MUSG00000040147 | Maob | chrX | 215.94095 | -2.4914267 |
| MUSG00000042821 | Snai1 | chr2 | 215.259 | 3.7567198 |
| MUSG00000079434 | Neu2 | chr1 | 213.71864 | -2.960282 |
| MUSG00000085888 | AL596127.1 | chr11 | 213.20375 | -2.2937524 |
| MUSG00000031791 | Tmem38a | chr8 | 212.8889 | -2.1893082 |
| MUSG00000030996 | Art1 | chr7 | 211.89856 | -1.4201736 |
| MUSG00000062077 | Trim54 | chr5 | 210.84435 | -1.4394009 |
| MUSG00000027932 | Slc27a3 | chr3 | 210.5749 | 4.2861753 |
| MUSG00000032717 | Mdfi | chr17 | 210.22195 | 4.3752823 |
| MUSG00000027470 | Mylk2 | chr2 | 209.63853 | -2.053392 |
| MUSG00000020592 | Sdc1 | chr12 | 207.80847 | 4.6079664 |

Supplemental Table 2 Continued

| #DisplayName | Name | Chr | BH_FDR_VarOutFil | Log2Ratio |
|---|---|---|---|---|
| MUSG00000021622 | Ckmt2 | chr13 | 206.79471 | -4.0985365 |
| MUSG00000028518 | Prkaa2 | chr4 | 206.66533 | -1.773984 |
| MUSG00000085837 | AC139376.3 | chr10 | 206.66533 | 3.8732312 |
| MUSG00000020067 | Mypn | chr10 | 206.40132 | -1.4293271 |
| MUSG00000067786 | Nnat | chr2 | 205.45538 | -2.7891822 |
| MUSG00000033722 | BC034090 | chr1 | 204.53076 | 3.2816439 |
| MUSG00000019852 | D10Bwg1379e | chr10 | 204.13742 | 6.109788 |
| MUSG00000038028 | 9630033F20Rik | chr6 | 204.13742 | -2.3092434 |
| MUSG00000056900 | Usp13 | chr3 | 203.67804 | -1.7349612 |
| MUSG00000070577 | RP23-331P21.1 | chr4 | 203.03082 | -2.0056293 |
| MUSG00000001508 | Sgca | chr11 | 202.74736 | -1.5935688 |
| MUSG00000029683 | Lmod2 | chr6 | 202.25873 | -1.2874486 |
| MUSG00000020007 | Il20ra | chr10 | 202.25873 | 4.647301 |
| MUSG00000026051 | 1500015O10Rik | chr1 | 201.98192 | 6.4777293 |
| MUSG00000010830 | Kdelr3 | chr15 | 201.17287 | 3.4136984 |
| MUSG00000029499 | Pxmp2 | chr5 | 200.23778 | -2.2399957 |
| MUSG00000045954 | Sdpr | chr1 | 198.63828 | -2.713705 |
| MUSG00000040705 | A930016O22Rik | chr7 | 198.49203 | -2.0283363 |
| MUSG00000056313 | 1810011O10Rik | chr8 | 198.42921 | 3.9972613 |
| MUSG00000034842 | Art3 | chr5 | 198.1167 | -1.6239358 |
| MUSG00000008658 | A2bp1 | chr16 | 197.09831 | -1.6316038 |
| MUSG00000021792 | 5730469M10Rik | chr14 | 194.49963 | -2.469864 |
| MUSG00000075307 | Kbtbd10 | chr2 | 194.4392 | -1.2455858 |
| MUSG00000033065 | Pfkm | chr15 | 194.37672 | -1.7576139 |
| MUSG00000032017 | Grik4 | chr9 | 194.37498 | 5.298998 |
| MUSG00000030785 | Cox6a2 | chr7 | 193.09462 | -2.1431155 |
| MUSG00000036298 | Slc2a13 | chr15 | 192.08948 | 4.665283 |
| MUSG00000007107 | Atp1a4 | chr1 | 191.58116 | -1.2880176 |
| MUSG00000061877 | BC048679 | chr7 | 190.78339 | -3.032414 |
| MUSG00000042109 | Csdc2 | chr15 | 190.33357 | 3.5787375 |
| MUSG00000020620 | Abca8b | chr11 | 189.55467 | -2.120869 |
| MUSG00000030701 | Plekhb1 | chr7 | 187.73755 | -1.8986708 |
| MUSG00000039747 | Orai2 | chr5 | 187.70735 | 3.094277 |
| MUSG00000053199 | Arhgap20 | chr9 | 186.74031 | -1.5194192 |
| MUSG00000032643 | Fhl3 | chr4 | 186.74031 | -2.9612942 |
| MUSG00000021579 | Lrrc14b | chr13 | 185.87445 | -2.3634498 |
| MUSG00000066113 | Adamtsl1 | chr4 | 185.77455 | 4.8028965 |

Supplemental Table 2 Continued

| #DisplayName | Name | Chr | BH_FDR_VarOutFil | Log2Ratio |
|---|---|---|---|---|
| MUSG00000032495 | Lrrc2 | chr9 | 185.76541 | -1.449477 |
| MUSG00000048636 | A730049H05Rik | chr6 | 185.39844 | 6.6403923 |
| MUSG00000061013 | Mkx | chr18 | 184.13673 | 4.376296 |
| MUSG00000022861 | Dgkg | chr16 | 183.88383 | 5.486276 |
| MUSG00000020871 | Dlx4 | chr11 | 183.74213 | 5.112527 |
| MUSG00000007877 | Tcap | chr11 | 181.43417 | -1.3892876 |
| MUSG00000036611 | Eepd1 | chr9 | 181.33263 | -1.9433873 |
| MUSG00000037375 | Hhat | chr1 | 181.33263 | 3.9299035 |
| MUSG00000030401 | Rtn2 | chr7 | 181.23526 | -1.8412994 |
| MUSG00000040732 | Erg | chr16 | 180.68834 | 3.991934 |
| MUSG00000030972 | Acsm5 | chr7 | 180.42287 | -3.8022199 |
| MUSG00000047746 | Fbxo40 | chr16 | 180.16908 | -1.4047076 |
| MUSG00000037035 | Inhbb | chr1 | 178.48047 | 3.5832784 |
| MUSG00000041540 | Sox5 | chr6 | 178.44637 | 3.2899435 |
| MUSG00000001555 | Fkbp10 | chr11 | 178.08107 | 3.7104278 |
| MUSG00000031562 | Dctd | chr8 | 177.29805 | 4.580376 |
| MUSG00000027386 | Fbln7 | chr2 | 177.27371 | 4.3263416 |
| MUSG00000025203 | Scd2 | chr19 | 176.82832 | 3.6767373 |
| MUSG00000029086 | Prom1 | chr5 | 176.2153 | 6.091686 |
| MUSG00000085596 | AL589870.1 | chr2 | 176.02875 | 4.573597 |
| MUSG00000017300 | Tnnc2 | chr2 | 174.23633 | -2.6310127 |
| MUSG00000048416 | Mlf1 | chr3 | 174.1692 | -4.109269 |
| MUSG00000003123 | Lipe | chr7 | 173.90735 | -2.4999354 |
| MUSG00000026473 | Glul | chr1 | 173.037 | -2.1305416 |
| MUSG00000028116 | Myoz2 | chr3 | 173.00778 | -0.9958694 |
| MUSG00000023828 | Slc22a3 | chr17 | 172.10063 | -2.6783168 |
| MUSG00000026826 | Nr4a2 | chr2 | 172.07404 | 4.534403 |
| MUSG00000025007 | Aldh18a1 | chr19 | 171.54446 | 3.5386472 |
| MUSG00000006457 | Actn3 | chr19 | 170.7221 | -1.3629844 |
| MUSG00000002944 | Cd36 | chr5 | 170.70049 | -1.8729578 |
| MUSG00000025268 | Maged2 | chrX | 170.52975 | 3.179602 |
| MUSG00000027661 | Slc2a10 | chr2 | 170.52975 | 3.738658 |
| MUSG00000079588 | Tmem182 | chr1 | 170.18378 | -1.8083715 |
| MUSG00000082100 | AL646043.3 | chr11 | 169.38046 | -2.5842943 |
| MUSG00000010803 | Gabra1 | chr11 | 168.54994 | 5.9549494 |
| MUSG00000023959 | Clic5 | chr17 | 168.22551 | -1.86824 |
| MUSG00000035923 | Myf6 | chr10 | 167.95686 | -0.8380006 |

Supplemental Table 2 Continued

| #DisplayName | Name | Chr | BH_FDR_VarOutFil | Log2Ratio |
|---|---|---|---|---|
| MUSG00000020098 | Pcbd1 | chr10 | 167.86977 | 4.1033087 |
| MUSG00000085779 | AC155932.2 | chr10 | 166.81633 | -1.7934469 |
| MUSG00000033256 | Shf | chr2 | 166.1581 | 3.2989743 |
| MUSG00000025488 | Cox8b | chr7 | 166.14236 | -2.6872952 |
| MUSG00000030087 | Klf15 | chr6 | 165.59212 | -2.1438282 |
| MUSG00000026335 | Pam | chr1 | 165.30537 | 3.285277 |
| MUSG00000024210 | Ip6k3 | chr17 | 165.30537 | -1.514169 |
| MUSG00000005628 | Tmod4 | chr3 | 164.60292 | -1.7199639 |
| MUSG00000071347 | C1qtnf9 | chr14 | 163.56107 | -1.3000892 |
| MUSG00000024526 | Cidea | chr18 | 163.39284 | -1.5838745 |
| MUSG00000080115 | AC134329.1 | chr10 | 163.36519 | 4.061877 |
| MUSG00000045875 | Adra1a | chr14 | 163.15768 | -3.0558121 |
| MUSG00000035279 | A430110N23Rik | chr7 | 162.78282 | 3.786073 |
| MUSG00000027239 | Mdk | chr2 | 162.66501 | 3.2920961 |
| MUSG00000057606 | Colq | chr14 | 162.66501 | -1.3473989 |
| MUSG00000030727 | Rabep2 | chr7 | 162.51932 | -1.5217919 |

Supplemental Table 3

Top 160 shared genes between TAT-Cre and *Rosa26CreER* tumors compared to control mesenchyme

| Gene Name |
|---|
| Pcdh9 |
| Hs3st2 |
| Rab3c |
| Sdk2 |
| Lgals12 |
| Zbtb16 |
| Myot |
| Ckm |
| Tspan8 |
| Chst2 |
| Asb14 |
| Fbxo40 |
| AL645850.2 |
| Adssl1 |
| Lpl |
| Timp4 |
| Sgca |
| Neu2 |
| Plin1 |
| Prkar2b |
| Aspa |
| Mtap9 |
| Smpx |
| Ppp1r3a |
| 1700058G18Rik |
| Plin5 |
| Stk32c |
| Aldh1a7 |
| Cmbl |
| Bche |
| Lrrc2 |
| Mylpf |

Supplemental Table 3 Continued

| Gene Name |
|---|
| Ptgs1 |
| Prph |
| Ecel1 |
| Baalc |
| Fabp3 |
| Atp1a2 |
| Myl2 |
| Mgst3 |
| Man2a1 |
| Amy1 |
| Pak3 |
| Dlx4 |
| C1qtnf6 |
| Mylk2 |
| Ntrk1 |
| Kbtbd10 |
| Ankrd23 |
| Actn3 |
| Rcn3 |
| Tbx1 |
| 4930434E21Rik |
| Myo18b |
| Maob |
| Parm1 |
| Kcnmb4 |
| Dlx3 |
| Aldh1a1 |
| Dsg3 |
| Tmem45b |
| Emid1 |
| AC152453.2 |
| Snai1 |
| Ces3 |
| Myoz1 |
| Pi16 |
| Pygm |
| Dnase1l3 |

Supplemental Table 3 Continued

| Gene Name |
|---|
| Odf3l2 |
| Slc6a5 |
| Hs3st5 |
| Lrrc17 |
| Alpk2 |
| Rasd2 |
| Myl3 |
| Slc25a34 |
| AC122466.1 |
| Chsy1 |
| Dlgap1 |
| Nrap |
| Mdfi |
| Tnnt3 |
| Tnni1 |
| Fkbp10 |
| Slc27a3 |
| Adra2a |
| C2cd4b |
| A730049H05Rik |
| Usp13 |
| Tnni2 |
| Plat |
| Fmo1 |
| Il20ra |
| Pfkfb1 |
| Ramp3 |
| Adrb3 |
| Asb11 |
| Hoxa10 |
| Apol6 |
| Gfra1 |
| Eef1a2 |
| Fbp2 |
| Pck1 |
| Dnahc2 |
| Fam167a |

Supplemental Table 3 Continued

| Gene Name |
|---|
| Kcnk1 |
| Tppp |
| Mypn |
| Asb12 |
| Sox9 |
| Cytl1 |
| Klhdc6 |
| Cacng6 |
| 2310002L09Rik |
| Fzd10 |
| Ppp1r1a |
| Asb5 |
| Lmod2 |
| Angpt2 |
| Tnnc1 |
| AL603787.4 |
| St3gal6 |
| Mylk4 |
| Shc3 |
| Acsl1 |
| AC123925.1 |
| Crtap |
| Tgm5 |
| Art1 |
| AL645687.1 |
| Cxcl14 |
| Prkcq |
| Dach2 |
| Gucy2c |
| Kcnj11 |
| Sorcs3 |
| RP23-331P21.1 |
| AC155722.2 |
| Atp2a1 |
| Trim54 |
| Pnoc |
| Klhdc7a |

Supplemental Table 3 Continued

| Gene Name |
|---|
| Cabp1 |
| Abca8a |
| Pappa2 |
| Sulf2 |
| Cd109 |
| Lgi3 |
| Cfd |
| Aqp7 |
| Lrrc30 |
| Hook1 |
| A530016L24Rik |
| Leprel2 |
| Tpm2 |
| Slc36a2 |
| Moxd1 |
| A2bp1 |
| Pon1 |

## Supplemental Experimental Procedures

### Targeted Mouse Line Production and Genotyping

Primers used to identify the type 1 fusion were CGCCTAGAGGGAAAGCGAG AGG for forward and AAATGACCTCAAGGAAGCTACGGGC for reverse. This final targeting construct contained Loxp-pgk-Neo-tPA-Loxp-EWS-ATF1-IRES-EGFP was electroporated into mouse embryonic stem cells and the clones were screened by long-range PCR for the correct 5' and 3' insertion. The correct clones were then subjected to Southern blot analysis to identify insertion number and size. Cells from one clone with a confirmed target were microinjected into C57BL/6 blastocysts to generate chimeric mice. The chimeric mice were mated to C57BL/6 females and their agouti offspring were tested by PCR to confirm germ-line transmission of the conditional allele.

The *Rosa26*$^{EA1}$ mice were genotyped with the following primers using tail-tip-derived DNA:

Forward-WT: GTTATCAGTAAGGGAGCTGCAGTGG,

Reverse-targeted: AAGACCGCGAAGAGTTTGTCCTC

Reverse – WT: GGCGGATCACAAGCAATAATAACC.

These primers yield a 300 base pair band for the targeted locus and a 415 base pair band for wildtype locus. The PCR conditions were set to 95°C for 30 seconds, 59°C for 45 seconds, and 72°C for 30 seconds, for 30 cycles.

The generation of each of the other mouse lines used has been previously described, including the *Rosa26*$^{CreER}$ (Badea et al., 2003), *Wnt1-Cre* (Danielian et al., 1998), *Pax3-Cre* (Engleka et al., 2005), *Pax7-Cre* (Keller et al., 2004b), *Pax7-CreERT2* (Murphy et al., 2011), *Prx1-Cre* (Logan et al., 2002), *Prx1-CreERT2* (Hasson et al.,

2007), *Bmi1*$^{CreERT2}$ (Sangiorgi and Capecchi, 2008), *Myf5-Cre* (Haldar et al., 2007), and *Rosa26*$^{mTmG}$ (Muzumdar et al., 2007).

PCR primers for specific transcripts:

| Target Gene | Primer | Sequence |
|---|---|---|
| *Nestin* | forward | CCAAGAGAAGCCTGGGAACT |
| | reverse | AGATCGCTCAGATCCTGGAA |
| *M-Mitf* | forward | TACAGAAAGTAGAGGGAGGACTAAG |
| | reverse | CCTGGTGCCTCTGAGCTTGCTGTATGTGGTAC |
| *Tyrosinase* | forward | GAGCGGTATGAAAGGAACCA |
| | reverse | CCAACGATCCCATTTTTCTT |
| *Gapdh* | forward | ACCACAGTCCATGCCATCAC |
| | reverse | TCCACCACCCTGTTGCTGTA |
| EWS-ATF1 | forward | ATCGTGGAGGCATGAGCA |
| | reverse | ACTCCATCTGTGCCTGGACT |

Tamoxifen Administration

Tamoxifen (Sigma) was dissolved directly in corn oil (Sigma) at a final concentration of 20 mg/ml, and was injected intraperitoneally in adult mice at a concentration of 4 mg per 40 g body weight. *Rosa*$^{CreER/EA1}$, *Bmi*$^{CreERT2}$;*Rosa*$^{EA1}$ and *Prx1-CreERT2* mice were injected at approximately 6 weeks postnatal with a single intraperitoneal injection of tamoxifen. Rosa$^{CreER/EA1}$ mice were also injected at postnatal

day 4.

Histology and Immunohistochemistry

Specimen containing bone were decalcified in 14 percent EDTA prior to embedding. Six to eight micron sections were cut and mounted on slides for standard H&E staining or immunohistochemistry. For fluorescence-based detection, immunohistochemistry was performed on 8 μm frozen sections of samples fixed in 4% paraformaldehyde at 4°C for 5 hr and dehydrated in a sucrose gradient before embedding in optimum cutting temperature media.

Antibodies used for immunohistochemistry included anti-Nestin (Aves Labs,Tigard, Oregon), anti-CD31 (BD-Biosciences, San Jose, California), anti-Prx1 (Lifespan Biosciences, Seattle, Washington), anti-Keratin5 (Covance, Princeton, New Jersey), anti-M-Mitf (Millipore, Billerica, Massachusetts), and anti-s100B (Sigma-Aldrich, St. Louis, Missouri).

Tumor Type Classifications Using RNA-seq Data and Supervised Machine Learning Model

In order to validate that at transcription level, the tumor tissues of the mouse mutants indeed resembles human clear cell sarcoma tissues, we used Support Vector Machine (SVM), a supervised machine learning technique, to classify mouse tumors and normal chest tissues. In order to reduce the impact of the platform differences between microarray human data and RNA-sequencing mouse data, we filtered the original probe set of the HEEBO microarray used to generate a high-confidence (HC) probe set that is

highly homologous between human and mouse. We first mapped all HEEBO probes to the mouse reference genome (mm9) using the BLAST algorithm (Altschul et al., 1990) and parameter set <M=1 N=-1 Q=3 R=2 W=9 wordmask=seg lcmask E=1e-5>. We then retained alignments with at least 80% identity over the probe length. This procedure removed 73% of the total probes from the original HEEBO microarray; 12,246 probes remained. The transcription level of these HC probes in human and the corresponding mouse genomic regions was used for the following analysis.

For each HC probe sequence, we calculated the coverage from RNA-sequencing reads in each mouse library, normalized by the average coverage depth of control libraries. Similarly, for each human tumor type genotyped by HEEBO microarray (Nielsen et al., 2002), we calculated the expression level ratio between tumor samples and normal-tissue controls over each HC probe. The SVM analysis was performed using the svm module in the e1071 R package (www.CRAN.R-project.org/package=e1071).

Differential Expression Analysis

For each library, the RNA-seq reads were aligned to the reference mouse genome and splice junction library, as previously described. We then used the OverdispersedRegionScanSeqs script in the USeq package (Nix et al., 2008) to calculate the expression levels of annotated EMBL gene in RPKM values (Reads Per Kilobase of transcript per Million mapped reads). USeq also discovers differentially expressed genes between two RNA-seq libraries by calling the DESeq R package (Anders and Huber, 2010). Internally, the DESeq algorithm uses a negative binomial distribution to model the read coverage, which is robust to the between-libraries variations of RNA-seq data by

using biological replicate data.

## Supplemental References

Altschul, S. F., Gish, W., Miller, W., Myers, E. W., and Lipman, D. J. (1990). Basic local alignment search tool. J Mol Biol *215*, 403-410.

Anders, S., and Huber, W. (2010). Differential expression analysis for sequence count data. Genome Biol *11*, R106.

Badea, T. C., Wang, Y., and Nathans, J. (2003). A noninvasive genetic/pharmacologic strategy for visualizing cell morphology and clonal relationships in the mouse. J Neurosci *23*, 2314-2322.

Nix, D. A., Courdy, S. J., and Boucher, K. M. (2008). Empirical methods for controlling false positives and estimating confidence in ChIP-Seq peaks. BMC Bioinformatics *9*, 523.

# CHAPTER 3

# MELANOBLASTS A POTENTIAL SOURCE FOR DERMAL CLEAR CELL SARCOMA


## Abstract

Clear cell sarcoma or "malignant melanoma of the soft parts" is a rare mesenchymal tumor that shares a close clinical and histological similarity to melanoma. Clear cell sarcoma and melanoma exhibit nearly identical gene expression profiles and consequently shares a poor general prognosis. Although highly similar, they are two distinct entities and where clear cell sarcoma has a predilection for the extremities of young adults, melanoma prefers cutaneous layers of an elderly population. The two lesions can also be distinguished genetically by a translocation occurring between chromosomes 12 and 22 that resides in clear cell sarcoma and is absent in melanoma. This translocation produces a fusion oncogene *EWS-ATF1* that has been shown previously to drive clear cell tumorigenesis. *EWS-ATF1* expression in the dermis of a mouse model was sufficient to induce dermal clear cell sarcoma in this model but the cells of origin for these tumors were not identified. This is in conjunction with new clinical data showing clear cell sarcoma is not limited to the deep extremities but can be found within dermal layers (Hantschke et al., 2010) begs the question if melanoma and clear cell sarcoma share a common cell of origin. To test the ability for melanocytes, the

cell from which melanoma arises, to form clear cell sarcoma in the dermis or epidermis, the *EWS-ATF1* human fusion gene was expressed in mouse melanocytes. Tumors did form 1 year after expression of *EWS-ATF1* concluding that while melanocytes are capable of transformation with *EWS-ATF1* expression, they are not efficient cells of origin compared to the mesenchymal stem cells in more common deep mesenchymal clear cell sarcoma.

## Introduction

Clear cell sarcoma is a mesenchymal tumor that has often been compared to malignant melanoma (Segal et al., 2003). Clear cell sarcoma demonstrates a high frequency of lymphnode metastasis, presence of melanin, ultrastructural evidence of melanosomes, and immunohistochemical staining for S-100, HMB-45, mMITF, and TYR, all characteristics of melanoma (Antonescu et al., 2002). They also share a poor prognosis stemming from a high resistance to standard chemotherapies. The one clear difference between the two is the presence of a t(12;22) producing the chimeric *EWS-ATF1* oncogene (Coindre et al., 2006). Previous reports have shown that *EWS-ATF1* is sufficient to drive clear cell tumorigenesis (Straessler et al., 2013; Yamada et al., 2013). Our lab has also shown that when expressed within a progenitor or mesenchymal stem cell, *EWS-ATF1* can reprogram the cell to express melanocytic markers and resemble a melanoma expression profile. This can explain the majority of clear cells that arise in the deep mesenchymal tissues but resemble melanoctyes, but it cannot fully explain the variants of clear cell found within the dermis and other locations (Hantschke et al., 2010). These tumors may still share a common cell of origin with melanoma.

Melanocytes are a group of cells principally residing in the epidermis that produce

melanin. Melanocytes can also be found sparsely in the inner ear, eye, and heart (Cichorek et al., 2013). Melanocytes contain melanosomes, melanin producing organelles, and express genes important for pigment production such as the melanocytic master transcription factor (MITF) and its downstream pigment proteins tyrosinase (TYR) and Tyrosinase like proteins (DCT, TRYP1, and TRYP2) . Melanocytes have a long life span but recently, a progenitor population has been proven to repopulate the melanocyte niche (Davids et al., 2009). These melanoblasts reside in the dermis although the exact location remains controversial (Gleason et al., 2008). Melanoblasts express MITF but lack some of the downstream pigmentation factors such as TYR, DCT, and TRYP (Cichorek et al., 2013). Melanocytes are the cell of origin for melanoma and have often been hypothesized to be a cell of origin for clear cells sarcoma.

Tissue-specific Cre drivers allow us to test whether melanocytes are indeed a cell of origin for clear cell sarcoma. *EWS-ATF1* cDNA expression was initiated postnatally in the cells expressing tyrosinase to test whether melanocytes were a cell of origin for clear cell sarcoma.

## Results

### TAT-CRE Injections into the Dermal Layer of Rosa$^{EA1}$ Mice Lead to Clear Cell Sarcoma Tumorigenesis

Rosa$^{EA1}$ mice containing a LoxP stop LoxP followed by the *EWS-ATF1* human cDNA were previously described (Straessler et al., 2013). With the expression of Cre recombinase in a cell, the LoxP sites recombine to excise the stop and lead to expression of the *EWS-ATF1*. To test the ability for the Rosa$^{EA1}$ mice to form dermal tumors, an engineered Cre protein containing the TAT peptide sequence derived from the human

immunodeficiency virus was used. The TAT sequence allows the protein to be released from endocytic uptake and localized to the nuclease. The TAT-Cre protein was delivered to the dermis through cutaneous injections.

When TAT-Cre recombinase is injected into the dermal layer of the mouse, tumors arise in the dermis and subcutaneous layers within several weeks post injection. These tumors grow quickly and mimic tumors seen in the dermis of human patients. When sections of the tumors are stained using haematoxlin and eosin (H&E), they show the standard large bloated cytoplasm with a slightly eosinophilic stain (Figure 3.1). These tumors expressed the *EWS-ATF1* gene along with other melanocytic markers. While it became clear that the $Rosa^{EA1}$ mouse was capable of recapitulating the dermal clear cell sarcoma, it remained unclear from what cell type these tumors arose. It became necessary to use tissue specific Cre drivers to narrow down the potential cell of origin for the dermal subtype of clear cell sarcoma.

## Expression of *EWS-ATF1* Within the Cutaneous Melanocyte Lineage Does Not Lead to Tumor Formation

To target expression of *EWS-ATF1* within the melanocyte specific lineage, the $Rosa^{EA1}$ mice were crossed to the transgenic Tyr-CreERT2 mice (Bosenberg et al., 2006). Tyr-CreERT2 mice express an inactive form of the Cre recombinase under the tyrosinase promoter. It is not until tamoxifen is added that a conformational change within the Cre protein converts the enzyme into its active form. At this time, the Cre will recombine the LoxP sites removing the polyA STOP sequence and allow expression of *EWS-ATF1* in any cell that currently expresses Tyrosinase. To efficiently express *EWS-ATF1* within

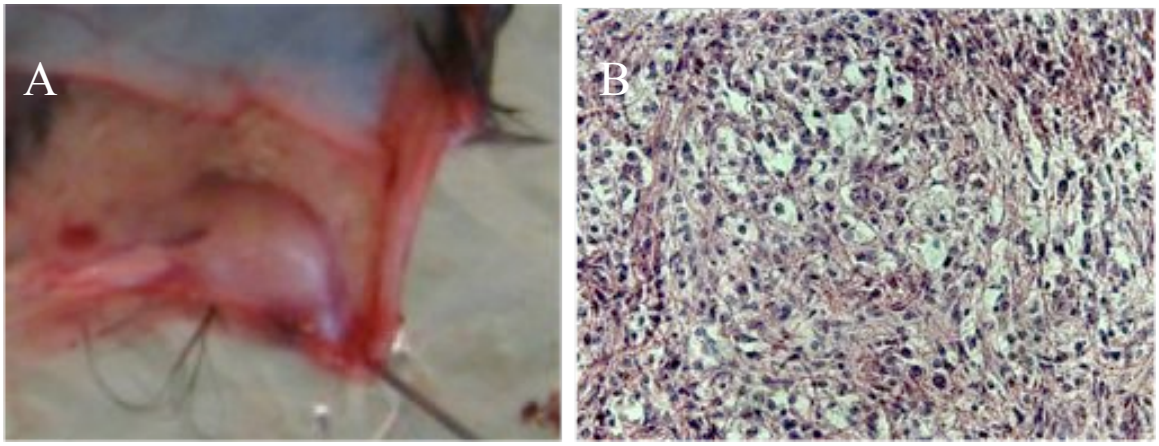


Figure 3.1 TAT-Cre-induced dermal tumors. A) Gross necroscopy of TAT-Cre-induced dermal tumors. B) H&E stained section of A with large, bloated, clear cytoplasm.

the cutaneous melanocyte population, 4'OH tamoxifen was administered to the ears of Rosa$^{EA1}$;Tyr-CreERT2 1 mice. Administration of 4'OH tamoxifen has proven the most efficient way of inducing the highest rates of recombination within the cutaneous layers of the mouse (Bosenberg et al., 2006). This did not lead to tumor formation or hyperpigmentation of the melanocyte population at 8 months post administration. These mice will be followed out to greater time spans, but it is already apparent that the epidermal melanocytes are not as efficient at transformation as the mesenchymal lineage.

Global Expression of *EWS-ATF1* Under the Control of the Tyrosinase Promoter in Adult Mice Leads to Aberrant Growth of Adipose Tissue but Lack Tumorigenesis

Although the cutaneous expression of *EWS-ATF1* did not lead to tumor formation, we wanted to rule out the possibility of a "misplaced" melanocyte as the cell of origin for dermal clear cell sarcoma. To achieve expression of *EWS-ATF1* in melanocytes outside of the epidermal niche, we induced global recombination using several different schemes of tamoxifen administration. We first administered tamoxifen to Rosa$^{EA1}$;TYR-CreERT2 mice at 6 months postnatally through intraperitoneal injections (IP). Tamoxifen was administered through IP injections to induce global recombination under the tyrosinase promoter. Traditionally, this technique is not used when trying to reach the epidermal melanocytes but as the goal was to initiate recombination in any subdermal melanocyte cells, this was ideal.

Expression of *EWS-ATF1* through the tyrosinase promoter after 6 months of age led to rapid onset of obesity. These mice exhibited aberrant growth of adipose tissue

within the fat pads and extending into areas normally devoid of adipocytes. Recent evidence has shown that adipose tissue may produce pigment transiently. This would indicate that there may be a low expression of tyrosinase in adipose tissue (Randhawa et al., 2009). This may explain the phenotype seen in Rosa$^{EA1}$;Tyr-CreERT2. Necroscopy done on this subset of mice showed fat pads containing otherwise normal adipose tissue. Abnormal looking adipose growths protruded from the sternum and within the rib cage. H&E histology showed aggressive invasion of the adipose into the musculature. Other than its invasive nature, the adipose appeared benign (Figure 3.2). Twelve to 14 months after recombination was induced, there was no sign of tumor formation in the dermis or elsewhere.

Global Expression of *EWS-ATF1* in Adolescent Mice Leads to Occasional Tumor Formation

Mice were also administered tamoxifen at 3 months of age through IP injections. The second subset of mice where *EWS-ATF1* was expressed prior to 3 months of age, the mice began to overgroom themselves and show irritation with their skin at approximately 1 year after the injections. On closer examination, the mice showed tumor formation. Most mice exhibited only one tumor each. The dermal tumors extracted from the Rosa$^{EA1}$;TyrCreERT2- mice expressed the EWS-ATF1 fusion as seen through the GFP reporter (Figure 3.3).

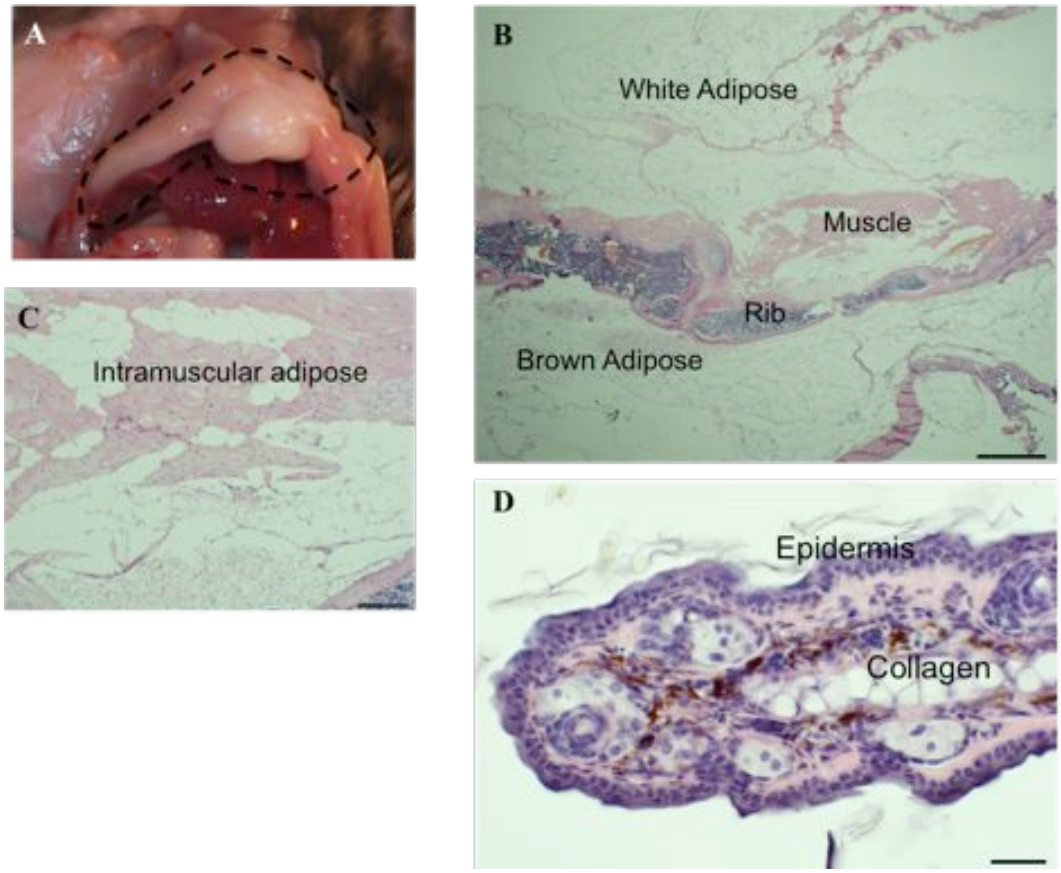


Figure 3.2 Aberrant adipose growth in TyrCreER;RosaEA1 mice injected after 6 months of age. A) necroscopy photo of mouse ribcage with excessive adipose tissue. B) HE section of rib with excessive adipose tissue. C) Magnification of adipose within muscle. D) Section of mouse ear from obese mice showing a slight but insignificant proliferation of the melanocytes.

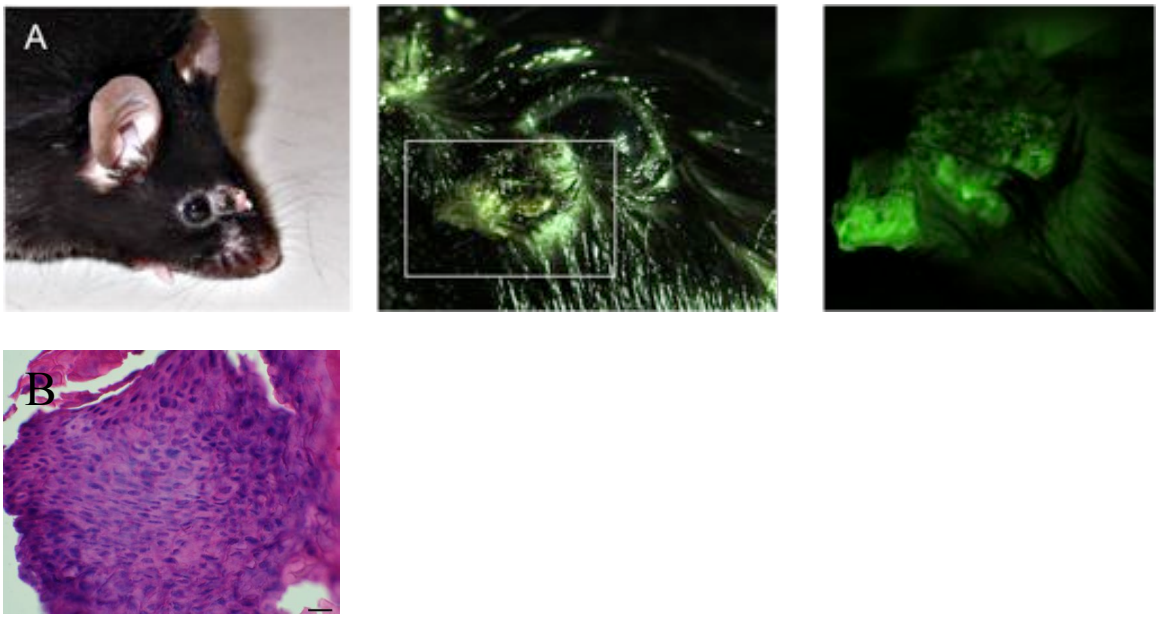


Figure 3.3 Tumors arise in the cutaneous layers of TyrCreER;RosaEA1 mice 1 year post injection. A) tumor arising near eye of mouse expresses GFP reporter. B) H&E stain of tumor arising near the eye.

## Melanoblasts Are a Potential Cell of Origin for Dermal Clear Cell Sarcoma

Due to the striking contrast in latency tumor formation between the $Rosa^{EA1}$;TyrCreERT2 mice and the TAT-Cre-induced mice, we hypothesized there may be an alternative more efficient source of dermal clear cell sarcoma. We reviewed the tissue-specific Cre lines that formed dermal tumors and investigated the potential cells in which these tumors arose. While Prx1CreER; $Rosa^{EA1}$ mice formed dermal tumors, they did not resemble clear cell sarcoma (Figure 3.4). Bmi1IresCreER; $Rosa^{EA1}$ mice formed dermal tumors that did resemble clear cell sarcoma in morphology and immunohistochemistry. Reports have surfaced that claimed Bmi1 expression within human dermal melanoblasts (Yu et al., 2010) and we decided to explore this link in mice.

When a Cre antibody is used to identify cells expressing Bmi1 in the Bmi1IresCreER mouse line, we see expression clearly in the basement membrane of the epidermis. These cells co-label with melanoblast markers MITF and KIT. Therefore, this indicates that the Bmi1 dermal tumors arise from the melanoblast lineage. Combining this with the data from the tyrosinase experiments, it suggests the tumors are arising in the melanoblast lineage versus the more differentiated melanocytes.

# Experimental Procedures

## Animals, Radiograph, Tissue Preparation, and Immunohistochemistry

All mouse experiments were performed in accordance with humane practices, national and international regulations, and with the approval of the University of Utah Institutional Animal Care and Use committee. Radiographs were obtained post

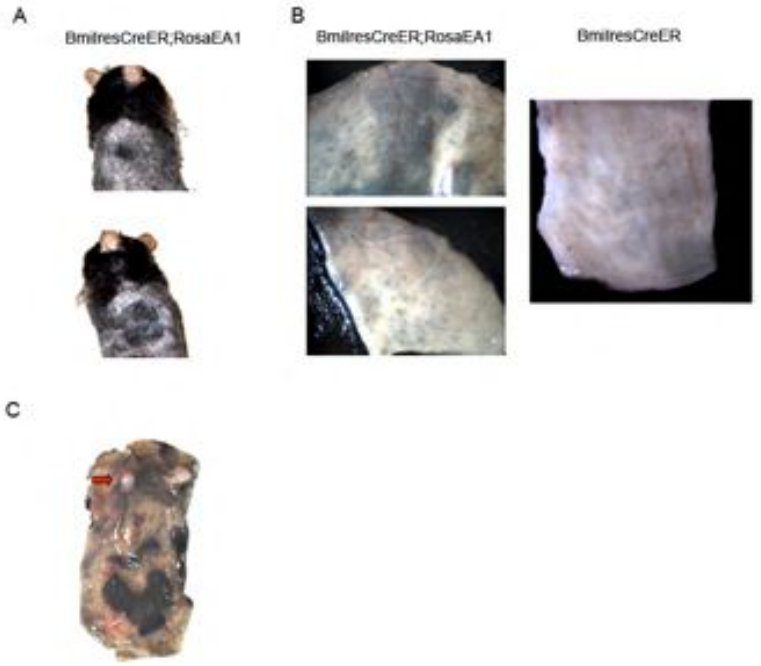


Figure 3.4 Tumors form in the dermis of Bmi1IresCreER;RosaEA1 mice. A)Bmi1IresCreER; RosaEA1 mice showing mole formation on epidermis. B) Mole formation in Bmi1IresCreER;RosaEA1 in the dermis. C) Dermal tumor formation (arrow)

asphyxiation using a Carestream 4000 Pro-Fx instrument (Carestream Molecular Imaging, Woodbridge, Connecticut). Tissues were prepared in 10% formaldehyde overnight in 4 degrees Celsius. They were then sectioned at 5-8 uM and prepared as explained previously.

## Discussion

Our previous model showed multiple potential cells of origin for clear cell sarcoma. Each cell of origin impacted the tumor phenotype in a different way. In this study, we showed that although melanocytes may represent a cell of origin for dermal clear cell sarcoma, the efficiency of transformation is dramatically lower than the less differentiated stem-like cells. The extended latency of tumorigenesis after expression of *EWS-ATF1* implies there are other mutations necessary to initiate transformation. We also showed that global expression of *EWS-ATF1* under the tyrosinase reporter did not lead to tumors in deeper mesenchymal locations. This indicates melanocytes are not the cell of origin for traditional clear cell sarcoma of the tendons and aponeuroses.

While tumors from both the *Bmi1*- and the *Prx1*- postnatal lineages developed within the dermis, the *Prx1*-derived tumors did not fit the histologic appearance of human clear cell sarcoma. The *Bmi1*-derived tumors arising in the dermis did fit the histologic appearance of dermal clear cell sarcoma and arose quicker than tumors arising within tyrosinase expressing cells. *Bmi1* marks a melanoblast population of cells that is slightly less differentiated than melanocytes. Even though the *Bmi1*-derived tumors arose quicker than Tyrosinase-derived tumors, they were lower in frequency than the deeper *Bmi1*-driven mesenchymal clear cells. This reflects the incidence of dermal clear cell sarcoma

portrayed in the literature. Although *Bmi1* dermal tumors arise 1 for every 10 deep tumors, this may reflect the pathology of these tumors that are infrequent subtypes of clear cell sarcoma. While the origin of the melanocytic features of human clear cell sarcoma has been attributed to both cell of origin and transformation by *EWS-ATF1,* this study further supports that the majority of clear cell sarcoma tumors are not arising from deep melanocytic cells.

In summary, we have shown that melanocytes are not a cell of origin for the deep mesenchymal clear cell sarcoma-like tumors and are not efficient cells of origin for the dermal clear cell sarcoma. The long latency between *EWS-ATF1* expression and tumorigenesis leads to the hypothesis that there are additional mutations that are necessary for tumorigenesis and again demonstrates the impact cell of origin has on tumor characteristics.

## References

Antonescu, C.R., Tschernyavsky, S.J., Woodruff, J.M., Jungbluth, A.A., Brennan, M.F., and Ladanyi, M. (2002). Molecular diagnosis of clear cell sarcoma: detection of EWS-ATF1 and MITF-M transcripts and histopathological and ultrastructural analysis of 12 cases. J Mol Diagn *4*, 44-52.

Bosenberg, M., Muthusamy, V., Curley, D.P., Wang, Z., Hobbs, C., Nelson, B., Nogueira, C., Horner, J.W., 2nd, Depinho, R., and Chin, L. (2006). Characterization of melanocyte-specific inducible Cre recombinase transgenic mice. Genesis *44*, 262-267.

Cichorek, M., Wachulska, M., Stasiewicz, A., and Tyminska, A. (2013). Skin melanocytes: biology and development. Postepy Dermatol Alergol *30*, 30-41.

Coindre, J.M., Hostein, I., Terrier, P., Bouvier-Labit, C., Collin, F., Michels, J.J., Trassard, M., Marques, B., Ranchere, D., and Guillou, L. (2006). Diagnosis of clear cell sarcoma by real-time reverse transcriptase-polymerase chain reaction analysis of paraffin embedded tissues: clinicopathologic and molecular analysis of 44 patients from the French sarcoma group. Cancer *107*, 1055-1064.

Davids, L.M., du Toit, E., Kidson, S.H., and Todd, G. (2009). A rare repigmentation

pattern in a vitiligo patient: a clue to an epidermal stem-cell reservoir of melanocytes? Clin Exp Dermatol *34*, 246-248.

Gleason, B.C., Crum, C.P., and Murphy, G.F. (2008). Expression patterns of MITF during human cutaneous embryogenesis: evidence for bulge epithelial expression and persistence of dermal melanoblasts. J Cutan Pathol *35*, 615-622.

Hantschke, M., Mentzel, T., Rutten, A., Palmedo, G., Calonje, E., Lazar, A.J., and Kutzner, H. (2010). Cutaneous clear cell sarcoma: a clinicopathologic, immunohistochemical, and molecular analysis of 12 cases emphasizing its distinction from dermal melanoma. Am J Surg Pathol *34*, 216-222.

Randhawa, M., Huff, T., Valencia, J.C., Younossi, Z., Chandhoke, V., Hearing, V.J., and Baranova, A. (2009). Evidence for the ectopic synthesis of melanin in human adipose tissue. FASEB J *23*, 835-843.

Segal, N.H., Pavlidis, P., Noble, W.S., Antonescu, C.R., Viale, A., Wesley, U.V., Busam, K., Gallardo, H., DeSantis, D., Brennan, M.F*., et al.* (2003). Classification of clear-cell sarcoma as a subtype of melanoma by genomic profiling. J Clin Oncol *21*, 1775-1781.

Straessler, K.M., Jones, K.B., Hu, H., Jin, H., van de Rijn, M., and Capecchi, M.R. (2013). Modeling clear cell sarcomagenesis in the mouse: cell of origin differentiation state impacts tumor characteristics. Cancer Cell *23*, 215-227.

Yamada, K., Ohno, T., Aoki, H., Semi, K., Watanabe, A., Moritake, H., Shiozawa, S., Kunisada, T., Kobayashi, Y., Toguchida, J*., et al.* (2013). EWS/ATF1 expression induces sarcomas from neural crest-derived cells in mice. J Clin Invest *123*, 600-610.

Yu, H., Kumar, S.M., Kossenkov, A.V., Showe, L., and Xu, X. (2010). Stem cells with neural crest characteristics derived from the bulge region of cultured human hair follicles. J Invest Dermatol *130*, 1227-1236.

# CHAPTER 4

# DISCUSSION

## Modeling Clear Cell Sarcoma

The significance of deciphering clear cell sarcomagenesis far exceeds its rare prevalence in the human population. Clear cell sarcoma's manifestation in a relatively young population coupled with its disturbingly low rates of survival make it an important clinical challenge to explore. Because of its lack of genomic instability and relatively young age of onset, clear cell apparently achieves its clinically aggressive phenotype from the formation of single chimeric transcription factor. This presumed dominance of a single genetic perturbation against an otherwise clean genetic background was readily testable using mouse genetics. This inspired our initial pursuit of a genetic model of clear cell sarcoma in the mouse.

Our initial goal of this project was to determine whether the human *EWS-ATF1* was sufficient to induce sarcomagenesis. Previously, others had hypothesized that *EWS-ATF1* was the initiating mutation driving tumor formation in clear cell sarcoma, but strictly speaking, all that could be shown was a consistent association between the two. In mice, it was possible to test the sufficiency of this oncogene. We anticipate three possible responses a cell might have to *EWS-ATF1* expression: apoptosis, transformation, or tolerance. Cell death upon expression of the fusion was seen in both embryonic stages

and specific postnatal lineages (Straessler et al., 2013). Turning on *EWS-ATF1* in a permissive cell type led to tumors forming with 100% efficiency. Other models, such as alveolar rhabdomyosarcoma expressing *PAX3-FKHR* (Keller et al., 2004a), and liposarcoma expressing *FUS-DDT3* (Perez-Mancera et al., 2007), have required secondary mutations in tumor suppressors to form the sarcomas. The speed and efficiency with which sarcomas formed following expression of *EWS-ATF1* without any additional genetic manipulations suggest that it is sufficient for inducing sarcomagenesis.

Clear cell sarcoma provided an ideal opportunity to test our secondary hypothesis as well. Driving tumorigenesis or even sarcomagenesis is distinct in some way from driving the ultimate phenotype of a particular cancer type. We hypothesized that EWS-ATF1 would also do this. Visvader et al. proposed the generalizable theorem that specific oncogenes when expressed within a progenitor cell will drive the tumor phenotype (Visvader, 2011). This model implies that the diversity between tumor subtypes lies in the oncogenes driving the tumors as opposed to the cell from which the tumor arises. Previous mouse models of Ewing sarcoma have demonstrated that simply driving expression of a pathognomonic fusion protein is not always sufficient to shape tumor phenotype (Lin et al., 2008). Expression of the *EWS-FLI* in a progenitor population led to undifferentiated sarcomas rather than driving a Ewing sarcoma phenotype. This was not the case with the *EWS-ATF1* clear cell model. *EWS-ATF1* proved capable of reprograming a cell to resemble melanocytes of a separate lineage. It was previously shown that EWS-ATF1 can bind the mMITF promoter and induce expression in the tumor cell lines (Davis et al., 2006); however, this is the first time that it is shown *in vivo* that expression of *EWS-ATF1* can take an undifferentiated cell and direct the cell to express melanocyte specific markers (Straessler et al., 2013). Therefore, *EWS-ATF1* can

in fact reprogram a cell to influence the tumor phenotype. Although this fits well with the oncogene model, there remains a strong role for cell of origin with *EWS-ATF1*-driven tumors.

We next demonstrated that differentiation state of the cell of origin influences permissibility to tumor formation. Mesenchymal stem cells were permissive to forming clear cell sarcoma with the full melanocytic profile. Slightly more differentiated cells from the *Prx1*-lineage also formed tumors, but they did not always express the melanocyte markers. Committed cells such as the myoblast *myf5cre*-lineage, or the satellite *Pax7CreER*-lineage did not form tumors and toxicity from the fusion was seen. This implies that there are intrinsic characteristics of the cell of origin that directly affect the tumor phenotype even with an oncogene such as *EWS-ATF1* that strongly drives a distinct differentiation pathway. Similar results are achieved when *EWS-ATF1* is expressed in the melanocytic lineage. Experiments revealed that the melanoblast progenitor pool was more permissive to tumor formation than its committed daughter cells. Not only does the oncogene drive a specific set of genes molding the tumors final outcome, but the tumors must arise in a cell type that is permissive, most likely cells that have not epigenetically silenced the genes that shape the tumor phenotype. Clear cell sarcoma is one of the models that have shown there is a place for both the oncogene and cell of origin in shaping tumor.

The work within this thesis has demonstrated that *EWS-ATF1* in clear cell sarcoma is a causal genetic perturbation that shapes the distinct phenotype. The next obvious goal would be to determine the role of *EWS-ATF1* in more benign tumors such as HCCC and AFH. These tumors express *EWS-ATF1* but do not mimic the gene

expression profile of clear cell sarcoma. It is reasonable to hypothesize that while EWS-ATF1 may drive tumorigenesis, the cell of origin distinguishes the phenotypic differences between these tumor types. As seen within Appendix A, there are abnormal growths and tumors that arise within Prx1CreER;RosaEA1 mice that are not classic-histology clear cell sarcomas. This preliminary research indicates that there are differentiated cells that are capable of forming different sarcomas in the presence of *EWS-ATF1* in the mouse model. We know that Prx1 in the adult is not restricted to the progenitor cells and can in fact be expressed in several committed cells throughout the body. More research needs to be done to identify the cells of origin for AFH and HCCC along with other EWS-ATF1-driven tumors. It will be interesting ultimately to determine the role each cell of origin has on the tumor behavior and patient outcome.

## Morphology versus Genetics

Screening for the EWS-ATF1 transcript has assisted in the diagnosis of clear cell sarcoma in anatomical locations in which clear cell has a low frequency such as the dermis and gastrointestinal tract (Hantschke et al., 2010; Lyle et al., 2008). Because specificity of the *EWS-ATF1* transcript has expanded to include AFH and HCCC, it becomes more difficult to diagnose these specific tumors that express the fusion gene and show conflicting morphological characteristics. The question is how to handle both the diagnostic process and the treatment of tumors when their morphology and genetics do not match previously described entities. A great example of how this can become a diagnostic conundrum can be seen repeatedly when reviewing the *EWS-ATF1* or clear cell sarcoma literature. A recent example would be of an angiosarcoma of the paratoid

gland found to harbor a t(12;22). This tumor was initially diagnosed as metastatic melanoma. It was reclassified as clear cell sarcoma when the *EWS-ATF1* fusion gene was detected. However, when taking a closer look, they noticed vascular differentiation (Gru et al., 2013). The question arose of whether this was a clear cell sarcoma or an angiosarcoma. While the tumor's histopathology and location suggested angiosarcoma, its genetics indicated clear cell sarcoma. The important question lies in which is more important in diagnosing tumors, genetics or pathology. This becomes very important when deciding on therapy and prognosis of the patient. The same question has been asked of *EWS-ATF1*-expressing tumors that resemble psammomatous melanotic schwannoma (Sengoz et al., 2006), polyphenotypic round cell sarcoma (Folpe, 2006), clear cell ondontogenic carcinoma (Bilodeau et al., 2013) and myoepithelial tumors (Flucke et al., 2012). Ultimately, this mouse model may be used to differentiate the importance both the oncogenes and cell of origin has on tumor behavior and biology.

## Targeted Therapeutics Using Mouse Sarcoma Models

Several mouse genetic models of translocation-associated sarcomas have been described over the last decade, including models of myxoid liposarcoma (Perez-Losada et al., 2000), alveolar rhabdomyosarcoma (Keller et al., 2004b), synovial sarcoma (Haldar et al., 2007; Haldar et al., 2009; Haldar et al., 2008), and clear cell sarcoma (Straessler et al., 2013; Yamada et al., 2013). These mice form tumors that resemble the human tumors with striking fidelity. A great deal has been learned about cell of origin and tumor formation from these models. The ultimate goal of each mouse model, however, is to improve upon the treatment options available to patients. All of these tumors are rare but aggressive. The ability to gather enough patients to study and perform drug trials is not

likely. These sarcoma mouse models provide a method of studying the disease and drug efficacy in controlled preclinical trials.

Targeting Fusion Proteins

Clear cell sarcoma is a difficult entity to treat, as it is resistant both to standard chemotherapies and radiotherapy, leaving wide surgical excision as the main course of action. This is a common theme seen in many sarcoma types leaving high rates of relapse and metastasis. A common goal in cancer research is to develop targeted therapies that will enhance efficacy and have fewer side effects than the current cytotoxic regiments.

The translocation-based tumors provide a perfect molecular target for future therapeutics. Not only have these fusions proven to be instrumental in the initiation of sarcomas, there is evidence that they are also involved in tumor maintenance as well. This is termed "oncogene addiction" and cell culture experiments have demonstrated that knockdown of these chimeric proteins leads to cell death. This was demonstrated clearly with Ewing sarcoma that is dependent on its EWS-FLI1 fusion for survival (Smith et al., 2006). Recently, mouse models have supported these data, showing that removal of the chimeric gene from tumors leads to cytoreduction in synovial sarcoma (unpublished) and clear cell sarcoma (Yamada et al., 2013). This has strengthened the hypothesis that targeting the fusion protein would provide an efficient and effective therapy.

There are several ways of designing targeted molecular therapies. The first is to find inhibitors of the fusion protein. This approach was taken recently with the EWS-FLI1 fusion protein present in Ewing Sarcoma. Sankar et al. showed a novel LSD1 inhibitor was capable of blocking the function of EWS-FLI1 and reversing the transcriptional changes induced by expression of the fusion protein (Sankar et al., 2013).

This particular inhibitor targets the EWS portion of the fusion showing extreme promise in treatment of other sarcomas due to the redundancy of EWSR1 as a fusion partner in several tumors, including clear cell sarcoma.

The second promising approach is immune-based therapies. In this method, the immune system is used to target different antigens present in the tumor that are absent in normal tissue. The fusion protein provides a perfect target that is not present in healthy tissue. Exposing the immune system to the fusion peptide so it recognizes it as an antigen can prime the immune system to attack tumorigenic cells. This has been done with the SS18-SSX fusion (Sato et al., 2002) with moderate success.

Lastly, it has already been shown that decreasing expression of the fusion protein will lead to tumor cell death. Many labs have shown that by decreasing the expression of the fusion *in vitro,* using antise DNA oligonucleotides and siRNA, they have induced cell death, but delivery of these agents *in vivo* has proven difficult. As gene targeting develops, it will become more and more practical to target these fusion genes and inhibit synthesis of the mRNA all together. Though we have seen these approaches used *in vitro* to extend the technology *in vivo,* based therapies will require development of greatly improved delivery techniques.

Although none of these techniques are clinic-ready, what is obvious is that the fusion proteins hold great potential as molecular targets and merit additional therapeutic development.

## Concluding Remarks

Not only did expression of *EWS-ATF1* transform cells without other genetic manipulations, but also it achieved this transformation so efficiently and aggressively that

neoplasms were visible in only a few weeks. This speed of tumorigenesis has not been observed in other mouse sarcoma models. Few tumor suppressor knockouts or oncogene inductions yield nearly the oncogenic power of *EWS-ATF1* as a single genetic factor. It was also extremely surprising to see the strength in regard to fashioning the final tumor phenotype. The tumors that developed faithfully recapitulated their human counterparts histologically and molecularly, when the expression was induced in appropriate cells of origin. This mouse model has been validated and can now be used to investigate novel therapeutics.

## References

Bilodeau, E.A., Weinreb, I., Antonescu, C.R., Zhang, L., Dacic, S., Muller, S., Barker, B., and Seethala, R.R. (2013). Clear cell odontogenic carcinomas show EWSR1 rearrangements: a novel finding and a biological link to salivary clear cell carcinomas. Am J Surg Pathol *37*, 1001-1005.

Davis, I.J., Kim, J.J., Ozsolak, F., Widlund, H.R., Rozenblatt-Rosen, O., Granter, S.R., Du, J., Fletcher, J.A., Denny, C.T., Lessnick, S.L.*, et al.* (2006). Oncogenic MITF dysregulation in clear cell sarcoma: defining the MiT family of human cancers. Cancer Cell *9*, 473-484.

Flucke, U., Mentzel, T., Verdijk, M.A., Slootweg, P.J., Creyt, D.H., Suurmeijer, A.J., and Tops, B.B. (2012). EWSR1-ATF1 chimeric transcript in a myoepithelial tumor of soft-tissue: a case report. Hum Pathol *43*, 764-768.

Folpe, A.L. (2006). Association of the t(12;22)(q13;q12) EWS/ATF1 rearrangement with polyphenotypic round cell sarcoma of bone: a case report. Am J Surg Pathol *30*, 1057-1058; author reply 1058-1059.

Gru, A.A., Becker, N., and Pfeifer, J.D. (2013). Angiosarcoma of the parotid gland with a t(12;22) translocation creating a EWSR1-ATF1 fusion: a diagnostic dilemma. J Clin Pathol *66*, 452-454.

Haldar, M., Hancock, J.D., Coffin, C.M., Lessnick, S.L., and Capecchi, M.R. (2007). A conditional mouse model of synovial sarcoma: insights into a myogenic origin. Cancer Cell *11*, 375-388.

Haldar, M., Hedberg, M.L., Hockin, M.F., and Capecchi, M.R. (2009). A CreER-based random induction strategy for modeling translocation-associated sarcomas in mice. Cancer Res *69*, 3657-3664.

Haldar, M., Randall, R.L., and Capecchi, M.R. (2008). Synovial sarcoma: from genetics to genetic-based animal modeling. Clin Orthop Relat Res *466*, 2156-2167.

Hantschke, M., Mentzel, T., Rutten, A., Palmedo, G., Calonje, E., Lazar, A.J., and Kutzner, H. (2010). Cutaneous clear cell sarcoma: a clinicopathologic, immunohistochemical, and molecular analysis of 12 cases emphasizing its distinction from dermal melanoma. Am J Surg Pathol *34*, 216-222.

Keller, C., Arenkiel, B.R., Coffin, C.M., El-Bardeesy, N., DePinho, R.A., and Capecchi, M.R. (2004a). Alveolar rhabdomyosarcomas in conditional Pax3:Fkhr mice: cooperativity of Ink4a/ARF and Trp53 loss of function. Genes Dev *18*, 2614-2626.

Keller, C., Hansen, M.S., Coffin, C.M., and Capecchi, M.R. (2004b). Pax3:Fkhr interferes with embryonic Pax3 and Pax7 function: implications for alveolar rhabdomyosarcoma cell of origin. Genes Dev *18*, 2608-2613.

Lin, P.P., Pandey, M.K., Jin, F., Xiong, S., Deavers, M., Parant, J.M., and Lozano, G. (2008). EWS-FLI1 induces developmental abnormalities and accelerates sarcoma formation in a transgenic mouse model. Cancer Res *68*, 8968-8975.

Lyle, P.L., Amato, C.M., Fitzpatrick, J.E., and Robinson, W.A. (2008). Gastrointestinal melanoma or clear cell sarcoma? Molecular evaluation of 7 cases previously diagnosed as malignant melanoma. Am J Surg Pathol *32*, 858-866.

Perez-Losada, J., Pintado, B., Gutierrez-Adan, A., Flores, T., Banares-Gonzalez, B., del Campo, J.C., Martin-Martin, J.F., Battaner, E., and Sanchez-Garcia, I. (2000). The chimeric FUS/TLS-CHOP fusion protein specifically induces liposarcomas in transgenic mice. Oncogene *19*, 2413-2422.

Perez-Mancera, P.A., Vicente-Duenas, C., Gonzalez-Herrero, I., Sanchez-Martin, M., Flores-Corral, T., and Sanchez-Garcia, I. (2007). Fat-specific FUS-DDIT3-transgenic mice establish PPARgamma inactivation is required to liposarcoma development. Carcinogenesis *28*, 2069-2073.

Sankar, S., Bell, R., Steph, B., Zhuo, R., Sharma, S., Bearss, D.J., and Lessnick, S.L. (2013). Mechanism and relevance of EWS/FLI-mediated transcriptional repression in Ewing sarcoma. Oncogene *32*, 5089-5100.

Sato, Y., Nabeta, Y., Tsukahara, T., Hirohashi, Y., Syunsui, R., Maeda, A., Sahara, H., Ikeda, H., Torigoe, T., Ichimiya, S.*, et al.* (2002). Detection and induction of CTLs specific for SYT-SSX-derived peptides in HLA-A24(+) patients with synovial sarcoma. J Immunol *169*, 1611-1618.

Sengoz, A., Tasdemiroglu, E., and Togay, H. (2006). Is clear cell sarcoma a malignant form of psammomatous melanotic schwannoma? Case report. Neurosurg Focus *21*, E11.

Smith, R., Owen, L.A., Trem, D.J., Wong, J.S., Whangbo, J.S., Golub, T.R., and Lessnick, S.L. (2006). Expression profiling of EWS/FLI identifies NKX2.2 as a critical target gene in Ewing's sarcoma. Cancer Cell *9*, 405-416.

Straessler, K.M., Jones, K.B., Hu, H., Jin, H., van de Rijn, M., and Capecchi, M.R. (2013). Modeling clear cell sarcomagenesis in the mouse: cell of origin differentiation state impacts tumor characteristics. Cancer Cell *23*, 215-227.

Visvader, J.E. (2011). Cells of origin in cancer. Nature *469*, 314-322.

Yamada, K., Ohno, T., Aoki, H., Semi, K., Watanabe, A., Moritake, H., Shiozawa, S., Kunisada, T., Kobayashi, Y., Toguchida, J.*, et al.* (2013). EWS/ATF1 expression induces sarcomas from neural crest-derived cells in mice. J Clin Invest *123*, 600-610.

# APPENDIX A

## MULTIPLE TUMOR SUBTYPES IN PRX1-LINEAGE WHEN DRIVEN BY EWS-ATF1 EXPRESSION

### Introduction

The past 5 years have seen a rapid expansion of tumor types driven by *EWS-ATF1*. Not all of these tumors mirror the clear cell sarcoma in histology or immunohistochemistry and EWS-ATF1 may in fact be a more promiscuous driver of tumorigenesis than previously hypothesized. Tumors expressing EWS-ATF1 range from relatively benign Angiomatoid fibrous histiocytoma found in multiple unusual anatomic locations (Chen et al., 2011; Mangham et al., 2010; Thway et al., 2012) to the hyalinizing clear cell carcinoma of the salivary gland (Weinreb, 2013), which has a distinct tissue compartment and potential cell of origin.

While searching for the cell of origin for clear cell sarcoma, it became clear that *EWS-ATF1* could drive multiple tumor subtypes in the mouse as seen in the human literature. These results were seen with the mouse model expressing *EWS-ATF1* under a ubiquitous promoter. When the fusion gene was expressed globally using the RosaCreER/EA1 mice tumors, appeared in multiple tissue compartments and had a range of morphologies (Figure 5.1). Specifically, when driving *EWS-ATF1* in the *Prx1*-lineage, there were multiple tumor types that did not resemble clear cell sarcoma. One such tum

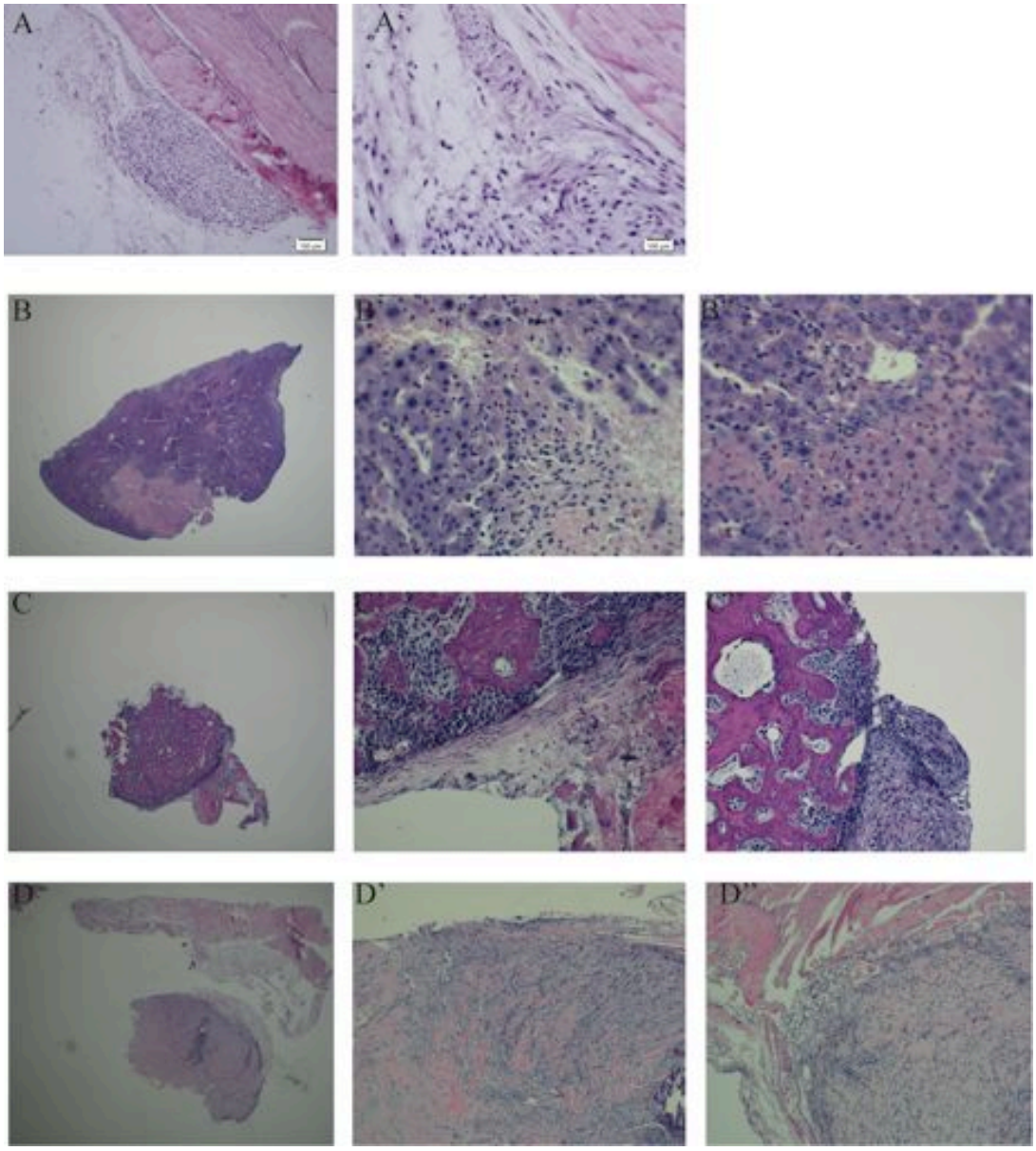


Figure 5.1 *Prx1*-derived tumors A) arising in the limb from a nerve. B) arising in the liver C&D) tumor arising in the hindlimb. ‘ and ‘’ represent magnified images of the original.

identified itself as a synovial sarcoma on a genome-wide gene expression profile (Straessler et al. 2013). Prx1, although shown to be expressed in the mesenchymal progenitor cell population, can also be seen in several more differentiated cell types throughout the body. Specifically, we find tumors arising within the dermis that do not resemble CCS (Figure 5.2). Below is a representation of the tumor subtypes found in the Prx1CreER;Rosa$^{EA1}$ mice.

## Materials and Methods

### Mice

Prx1CreER mouse has been previously described along with the Rosa$^{EA1}$ line. All mouse experiments were performed in accordance with humane practices, national and international regulations, and with the approval of the University of Utah Institutional board. Tamoxifen was prepared at 20mg/ml stock and administered at 9 mg per 40 grams body weight.

### Tissue Preparation

Tissues were prepared in 10% formaldehyde overnight in 4 degrees Celsius. They were then sectioned at 3-8 uM and prepared as explained previously.

## Results

Prx1CreER;RosaEA1 mice were given tamoxifen at 4 weeks postnatal and their littermates were left untreated. The mice that were administered tamoxifen developed on average 10 tumors per mouse and the majority of these tumors resembled clear cell sarcoma by 10 weeks postnatal. A small subset of these tumors did not resemble the

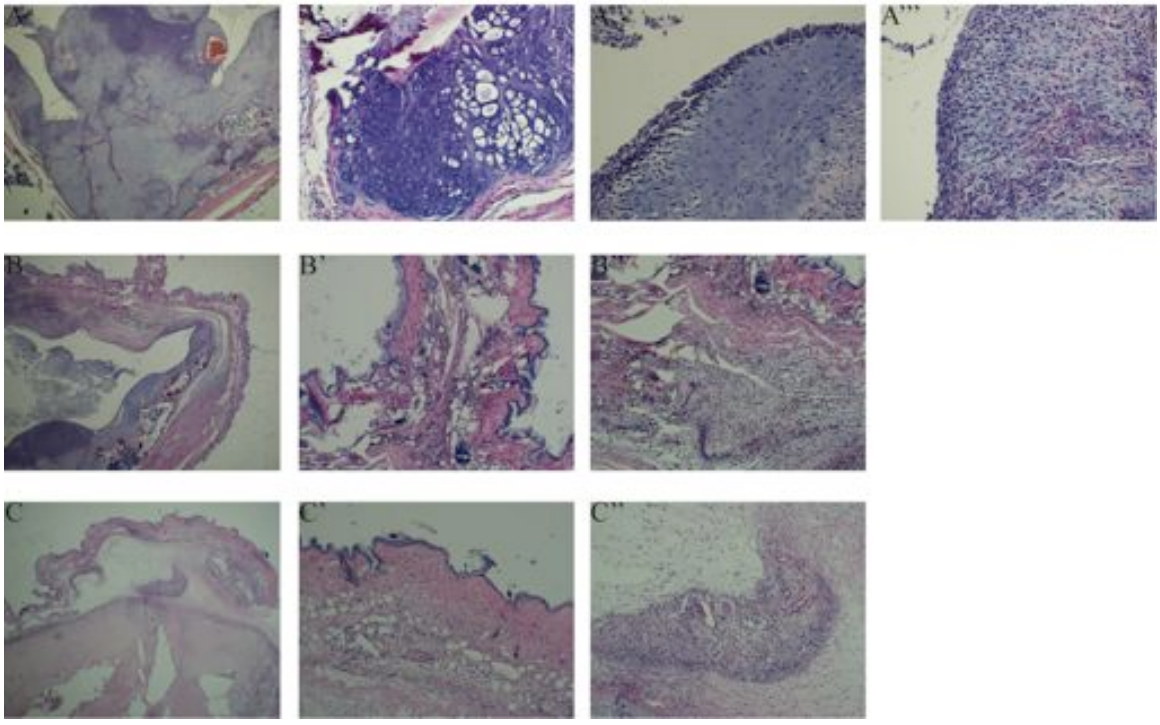


Figure 5.2 *Prx1*-driven tumors arising in the dermis. ‘ and ‘ ‘ represent amplified images of the original tumor. A) Tumor A was taken from the abdomen of a female PRX1CreER;EA1 mouse. B) was a tumor located adjacent to A. C) Tumor C was excised from the abdomen of a female mouse.

histology typical of clear cell. Littermate controls that did not receive tamoxifen formed tumors closer to 6 months of age. The uninjected mice formed fewer tumors but the majority of these tumors, contrary to the injected mice, did not resemble the clear cell morphology. This situation mirrors what is seen when tamoxifen is given and withheld from the notoriously leaky RosaCreER line (Straessler et al., 2013). Although previous lineage studies have failed to reveal leakiness in the Prx1CreER mice, this tumor model proves otherwise. This again highlights the potency of *EWS-ATF1* when presented to permissive cells types.

## References

Chen, G., Folpe, A.L., Colby, T.V., Sittampalam, K., Patey, M., Chen, M.G., and Chan, J.K. (2011). Angiomatoid fibrous histiocytoma: unusual sites and unusual morphology. Mod Pathol *24*, 1560-1570.

Mangham, D.C., Williams, A., Lalam, R.K., Brundler, M.A., Leahy, M.G., and Cool, W.P. (2010). Angiomatoid fibrous histiocytoma of bone: a calcifying sclerosing variant mimicking osteosarcoma. Am J Surg Pathol *34*, 279-285.

Straessler, K.M., Jones, K.B., Hu, H., Jin, H., van de Rijn, M., and Capecchi, M.R. (2013). Modeling clear cell sarcomagenesis in the mouse: cell of origin differentiation state impacts tumor characteristics. Cancer Cell *23*, 215-227.

Thway, K., Nicholson, A.G., Wallace, W.A., Al-Nafussi, A., Pilling, J., and Fisher, C. (2012). Endobronchial pulmonary angiomatoid fibrous histiocytoma: two cases with EWSR1-CREB1 and EWSR1-ATF1 fusions. Am J Surg Pathol *36*, 883-888.

Weinreb, I. (2013). Translocation-associated salivary gland tumors: a review and update. Adv Anat Pathol *20*, 367-377.